CONTRAST OPTIMIZED OF FLUID-ATTENUATED INVERSION RECOVERY (FLAIR) PULSE SEQUENCE TECHNIQUE IN MRI

CPT. PATHCHRAPORN SAENGRUANG-ORN

A THESIS SUBMITTED IN PARTIAL FULFILLMENT
OF THE REQUIREMENTS FOR
THE DEGREE OF MASTER OF SCIENCE
(MEDICAL PHYSICS)
FACULTY OF GRADUATE STUDIES
MAHIDOL UNIVERSITY

2000

ISBN 974-664-223-5

Thesis

entitled

CONTRAST OPTIMIZATION OF FLUID-ATTENUATED INVERSION RECOVERY (FLAIR) PULSE SEQUENCE TECHNIQUE IN MRI

Pathchraporn Saengruang-Orn

Cpt. Pathchraporn Saengruang-Orn
Candidate

Pairash Sai

Asst. Prof. Pairash Saiviroonporn, Ph.D.
Major-advisor

Kitima Thammarak

Asst. Prof. Kitima Thammarak, M.D.
Co-advisor

Kamolwan Jungmeechoke

Kamolwan Choegmeechoke, M.D.
Co-advisor

Liangchai Limlomwongse

Prof. Liangchai Limlomwongse,Ph.D.
Dean
Faculty of Graduate Studies

Vipa Boonkitticharoen

Assoc. Prof. Vipa Boonkitticharoen, Ph.D.
Chairman
Master of Science Programme
In Medical Physics
Faculty of Medicine,
Ramathibodi Hospital.

Thesis

entitled

CONTRAST OPTIMIZATION OF FLUID-ATTENUATED INVERSION RECOVERY (FLAIR) PULSE SEQUENCE TECHNIQUE IN MRI

was submitted to the Faculty of Graduate Studied, Mahidol University
for the degree of Master of Science (Medical Physics)

on
August 16 , 2000

Pathchraporn Saengruang-Orn
Cpt. Pathchraporn Saengruang-Orn
Candidate

Pairash Sai
Asst. Prof. Pairash Saiviroonporn, Ph.D.
Chairman

Vipa Boonkitticharoen, Ph.D.
Member

Kitima Thammarak
Asst. Prof. Kitima Thammarak, M.D.
Member

M. Mongkolsuk
Manus Mongkolsuk, M.Sc.
Member

Kamolwan Choegmeechoke
Kamolwan Choegmeechoke, M.D.
Member

Liangchai Limlomwongse,Ph.D.
Dean
Faculty of Graduate Studies
Mahidol University

Prakit Vathesatogkit
Prof. Prakit Vathesatogkit, M.D.
A.B.I.M.
Dean
Faculty of Medicines,
Ramathibodi Hospital
Mahidol University

ACKNOWLEDGMENT

I would like to express my sincere gratitude and deep appreciation to Dr. Pairash Saiviroonporn my major advisor for his guidance, invaluable advice, supervision and encouragement throughout. He was never lacking in kindness and support. I am equally grateful to Dr. Kitima Thammarak and Dr. Kamolwan Choegmeechoke my co-advisors for their constructive comments, supervision and encouragement. They were always nice and friendly.

I also express my appreciation to the examination committee, Dr. Vipa Boonkitticharoen and Associate Professor Manus Mongkolsuk. I would like to thank Ms. Somporn Krasaesub who taught me about SPSS program for window.

I wish to thank, SM1 Suwan Lagdang and SM1 Watanachai Julasak, the technicians of magnetic resonance imaging at Royal Thai Army hospital for their co-operation and generous assistance. I also thank Mr. Somrak Chaipipat, the MR engineer GE Medical System, who help me in MRI data.

I am particularly indebted to the school of Medical Physics for my academic knowledge and all staff members for their good collaboration.

Finally, I thank my family, my husband and son, for their encouragement throughout. Word can not describe all they have done for me.

Pathchraporn Saengruang-Orn

4136156 RAMP/M : MAJOR : MEDICAL PHYSICS : M.Sc.(MEDICAL PHYSICS)
KEY WORD : FLUID-ATTENUATED INVERSION RECOVERY PULSE SEQUENCE / T_1 RELAXATION TIME / BRAIN MRI
PATHCHRAPORN SAENGRUANG-ORN : CONTRAST OPTIMIZATION OF FLUID-ATTENUATED INVERSION RECOVERY (FLAIR) PULSE SEQUENCE IN MRI. THESIS ADVISOR : PAIRASH SAIVIROONPORN,Ph.D., KITIMA THAMMARAK, M.D., KAMOLWAN CHOEGMEECHOKE, M.D.,
149 p. ISBN 974-664-223-5

Fast fluid-attenuated inversion recovery (FLAIR) pulse sequence, is a powerful method for detecting intracranial lesions especially those located near ventricles. This method generates a T_2 -weighted image nulling the cerebrospinal fluid (CSF), thus creating a distinct image of the lesion. The purpose of this study was to determine the optimal TI values of fast FLAIR technique in order to suppress signal CSF so as to obtain a good periventricular image.

Seventeen patients (age 40-86 years), were sampled for this investigation on the basis of their periventricular lesions appearing as bright images by both fast FLAIR and T_2 -weighted fast spin echo (FSE) imaging techniques. A total of 41 lesions were examined by the magnetic resonance imaging (MRI) unit for brain investigation (1.5 Tesla imager). T_2 -weighted FSE image was the standard of reference. The patients were scanned by fast FLAIR pulse sequencing of varying TI (2000, 2100, 2200, 2300, and 2400 msec). Signal intensity (SI) values for CSF, white matter (WM) and the lesion were averaged from data acquired from 5 images and subsequently used for determining signal to noise ratio (SNR), contrast to noise ratio (CNR), and contrast ratio (CR).

The fast FLAIR with TI 2100 msec was found to yield minimal SNR_{CSF} , maximal $CNR_{lesion,CSF}$ and maximal $CR_{lesion,CSF}$. Statistically, the $CNR_{lesion,CSF}$ and $CR_{lesion,CSF}$ were superior to those obtained from T_2 -weighted FSE imaging (p-value < 0.0005). When the comparison was made between the lesion and WM, $CNR_{lesion,WM}$ and $CR_{lesion,WM}$ were at maximum TI of 2400 msec. However, the $CNR_{lesion,WM}$ image was less distinct than those obtained by the standard approach (p-value < 0.005). In conclusion TI of 2100 msec is the optimal value for fast FLAIR imaging of the periventricular lesions.

4136156 RAMP/M : สาขาวิชา : ฟิสิกส์การแพทย์ : วท.ม. (ฟิสิกส์การแพทย์)

พัชราภรณ์ แสงเรืองอ่อน : การศึกษาปัจจัยกำหนดการแยกความเปรียบต่างของขบวนการสร้างภาพคลื่นสนามแม่เหล็ก โดยวิธีให้ลำดับคลื่นวิทยุแบบ ฟลูอิด-แอทเทนนูเอเต็ด อินเวอร์ชั่น รีคัฟเวอรี่ (CONTRAST OPIMIZATION OF FLUID - ATTENUATED INVERSION RECOVERY (FLAIR) PULSE SEQUENCE IN MRI) คณะกรรมการควบคุมวิทยานิพนธ์: ไพรัช สายวิรุณพร วศด., กิติมา ธรรมรักษ์ พบ., กมลวรรณ จึงมีโชค พบ., 146 หน้า ISBN 974-664-223-5

ปัจจุบันเราให้ความสนใจกับการสร้างภาพด้วยคลื่นสนามแม่เหล็ก โดยการให้ลำดับคลื่นวิทยุแบบ fast fluid-attenuated inversion recovery (FLAIR) pulse sequence ในการวินิจฉัยโรคทางสมองโดยเฉพาะเมื่อมีรอยโรคอยู่ใกล้หรือล้อมรอบน้ำหล่อเลี้ยงสมอง (CSF) ที่อยู่ในโพรงสมอง ในการให้ลำดับคลื่นวิทยุแบบนี้ จะให้ภาพเป็น T_2-weighted image ขณะเดียวกันสามารถทำให้สัญญาณที่ได้จาก CSF เป็นศูนย์ ทำให้เห็นขอบเขตของรอยโรคที่อยู่ใกล้หรือล้อมรอบน้ำหล่อเลี้ยงสมองที่อยู่ในโพรงสมองได้ดียิ่งขึ้น การศึกษานี้เพื่อหาค่า TI ที่เหมาะสม เพื่อสามารถแยกความเปรียบต่างระหว่างรอยโรคที่อยู่ล้อมรอบน้ำหล่อเลี้ยงสมองกับน้ำหล่อเลี้ยงสมองในโพรงสมองได้ดีที่สุด

กลุ่มตัวอย่างเป็นคนไข้ที่มาตรวจสมองด้วยคลื่นสนามแม่เหล็ก 1.5 เทสลา ที่ร.พ. พระมงกุฎเกล้าซึ่งมีรอยโรคปรากฏเป็นขาวทั้งใน fast FLAIR images และ T_2-weighted fast spin echo (FSE) images อยู่ล้อมรอบ CSF มีอายุตั้งแต่ 40-86 ปี จำนวน 17 ราย มีจำนวนรอยโรคทั้งหมด 41 รอยโรค ผู้ป่วยทุกรายได้รับการตรวจสมองด้วย fast FLAIR pulse sequence ที่ใช้ค่า TI ต่างกัน 5 ค่า (TI 2000, 2100, 2200, 2300 และ2400 msec) และ T_2-weighted FSE pulse sequence เพื่อวัดค่าเฉลี่ยความเข้มของสัญญาณ (SI) ของ lesions, CSF, white matter (WM) ข้อมูลที่ได้นำมาหาค่า signal to noise ratio (SNR) ของทั้ง 3 เนื้อเยื่อ, contrast to noise ratio (CNR)และ contrast ratio (CR) ของ lesion กับ CSF และ WM ปรากฏว่า fast FLAIR pulse sequence ที่ TI 2100 msecให้ SNR_{CSF} ต่ำที่สุด ค่า TI นี้แตกต่างจากค่า TI ที่ประมาณได้ทางคณิตศาสตร์ เพื่อให้ได้ SI ของ CSF เป็นศูนย์ เท่ากับ 4.4%. โดย $CNR_{lesion,CSF}$ และ $CR_{lesion,CSF}$ ให้ค่าสูงสุดที่ TI 2100 msec ซึ่งค่าเหล่านี้สูงกว่าเมื่อเทียบกับ T_2-weighted FSE sequence (P-value < 0.0005). $CNR_{lesion,WM}$ และ $CR_{lesion,WM}$ ให้ค่าสูงสุดที่ TI 2400 msec โดย $CNR_{lesion,WM}$ ของ fast FLAIR ที่ TI 2400 msec มีค่าน้อยกว่าเมื่อเทียบกับ T_2-weighted FSE pulse sequence (P-value< 0.005). ดังนั้น fast FLAIR pulse sequence ที่ TI 2100 msec ให้ contrast optimized ระหว่าง Periventricular lesion กับ CSF ดีที่สุด และดีกว่า เมื่อเทียบกับ T_2-weighted FSE pulse sequence.

CONTENTS

LIST OF TABLES

LIST OF FIGURES

LIST OF FIGURES (Continued)

LIST OF FIGURES (Continued)

Page

LIST OF FIGURES (Continued)

Page

LIST OF ABBREVIATIONS

Abbreviation	Term
B_0	The external magnetic field
BW	Bandwidth
CNR	Contrast to noise ratio
CR	Contrast ratio
CSF	Cerebrospinal fluid
E_1	Lower energy state
E_2	Upper energy state
FID	Free induction decay
Fig.	Figure
FLAIR	Fluid-attenuated inversion recovery
FOV	Field of view
IR	Inversion recovery
L	Left
M_0	Net magnetization
MHz	Mega-Hertz
min	Minute (s)
ml	Milliliter (s)
MR	Magnetic Resonance
MRI	Magnetic Resonance Imaging

LIST OF ABBREVIATIONS (Continued)

Abbreviation	Term
msec	Millisecond (s)
M_{x-y}	Longitudinal magnetization
M_z	Transverse magnetization
NEX	Number of acquisition or excitations
R	Right
RF	Radio-frequency
ROI	Region of interest
S	Spin quantum number
S.D	Standard deviation
SE	Spin echo
SI	Signal intensity
SNR	Signal-to-noise ratio
T	Tesla
T_1	Longitudinal relaxation time
T_2	Transverse relaxation time
TI	Inversion time
TE	Echo time
TR	Repetition time
WM	White matter

CHAPTER I

INTRODUCTION

Previously, conventional T_2 - weighted spin - echo (SE) magnetic resonance (MR) imaging has been a mainstay of evaluation many pathologic processes of the brain such as multiple sclerosis, infarct etc.(1). Most of these pathologic processes increase the T_2 relaxation times of the affected tissue, causing the lesion to have signal intensities intermediate CSF and normal gray or white matter on T_2 - weighted images (1,2). Therefore T_2 - weighted images may be difficult to make diagnosis (3) when these lesions have side touching to the CSF border.

Recently, we are interested in fluid - attenuated inversion recovery (FLAIR) pulse sequence because the FLAIR sequence is a magnetic resonance imaging (MRI) sequence designed to produce a strongly T_2 - weighted images while CSF signal is suppressed (2). We apply a 180^0 inversion - recovery pulse and chose an inversion time (TI) to allow the longitudinal magnetization of CSF to return to the null point before spin echo imaging(4). At this point, all other brain tissues have made almost complete recovery of longitudinal magnetization toward equilibrium. Also, the use of a long repetition time (TR) permits tissues with even very long T_1 relaxation time to completely recover. This minimizes T_1 differences of non-CSF tissues, thus producing heavy T_2 -weighting given the relatively long echo time of the sequence. The CSF signal is completely suppressed, and pathologic lesions, with their typical T_2

prolongation in the brain adjacent to CSF interfaces, become easily discerned in comparison with conventional T_2-weighted imaging (2).

The basis of the FLAIR method is to select the TI time so that the signal from CSF is nulled. It relies upon the known lengthy T_1 relaxation time of CSF according to the equation (1) :

$$TI_{null\ of\ CSF} = T_{1\ of\ CSF} \{ \ln 2 - \ln (1 + e^{-(TR)/T_1} \} \quad (1)$$

Where, $TI_{null\ of\ CSF}$ defined TI that make CSF is nulled.

TR is repetition time.

$T_{1\ of\ CSF}$ is the longitudinal relaxation time of CSF.

Using this equation, $TI_{null\ of\ CSF}$ was calculated as a function of TR. from equation (1) that in the limit of infinite TR, the maximum $TI_{null\ of\ CSF}$ is $TI_{null\ of\ CSF}$ X ln 2 (6). Thus $TI_{null\ of\ CSF}$ required to known $T_{1\ of\ CSF}$ to predicted contrast performance.

However, the major disadvantage of conventional FLAIR sequence is a very long acquisition time (7) caused by the long TI and TR that required both null CSF and adequate non - CSF tissues signal recovery before readout (1). One solution to improve the imaging efficiency of FLAIR is the use of the newer "FAST" or "TURBO" spin echo sequences based on the rapid acquisition with relaxation enhancement (RARE) technique (2),

This study measured $T_{1\ of\ CSF}$ from 14 healthy volunteers with inversion - recovery (IR) technique, because this method is the most precise and accurate (8). The volunteers were performed with TR of 11,000 msec, and three different TI values

of 1500, 2000, 2600 msec. The SI of CSF was measured on each of three IR images. The acquired data from measurement is plotted between SI values with difference TI and determinate $T_{1\ of\ CSF}$ by using the SPSS program for window. Then using T_1 of CSF calculate interval of TI value to get the signal from CSF to be null in the equation (1).

Therefore we got the optimum TI values to performed fast FLAIR imaging from 17 periventricular lesion patients that these lesions show bright in both fast FLAIR images and T_2-weighted fast spin echo (FSE) images. Using fast FLAIR pulse sequence in different TI and T_2-weighted FSE pulse sequence scanned all the patients. Then we measured the mean SI of the lesions, CSFand WM. The data was calculated for SNR of individual type of tissues, CNR and CR of the lesion to CSF and normal adjacent WM. To evaluate optimum of TI value with fast FLAIR pulse sequence, to suppress CSF with good periventricular lesions to CSF contrast, and camparison with T_2-weighted FSE pulse sequence.

CHAPTER II

OBJECTIVES

Main objective

To determine the optimum TI value with fast FLAIR pulse sequence, to suppress CSF with good periventricular lesions to CSF contrast.

Sub-objective

1. To determine the values of T_1 of CSF in lateral ventricles from healthy volunteers.

2. To compare fast FLAIR pulse sequence with optimum TI to suppress CSF with that of a T_2-weighted FSE pulse sequence in the evaluation of periventricular lesion that have side touching the CSF border of lateral ventricles.

CHAPTER III

THEORY

The cerebrospinal fluid spaces

Cerebrospinal fluid (CSF) in the cranial cavity appears within the ventricular system, cisternal spaces and the interstitium of the brain parenchyma. Function of CSF is an intermediary pathway between the neural tissue and vascular capillaries, providing nutrients and metabolites to the brain parenchyma. The choroid plexus in the ventricular cavity and the ventricular ependyma produces CSF. The largest volume of choroid plexus is located along the ependymal surfaces of the atrial walls of the lateral ventricles, while the rest is in the roof of the third ventricle, and along the posterior inferior surface of the fourth ventricle (Figure 1). CSF is produced continuously at rate of 25 ml/h (0.35-0.40 ml/min) (11). In the normal state, the total CSF volume at any time is 120 to 135 ml. Of this amount, 25 to 35 ml is within the ventricular space and the remaining is in the subarachnoid cisterns, with a small amount within the interstitial spaces of the brain parenchyma. CSF flows from the interstitial space to the ventricles and then to the subarachnoid cisterns by transmitted force from vascular pulsation (Figure 1). During its passage and turnover within the interstitial spaces, it allows the exchange of metabolites and nutrients.

CSF within the ventricles and the subarachnoid space has constant motion. On MRI, its signal characteristics depend on several factors.

1) The image acquisition time (TR/TE).

The longer acquisition time commonly causes loss of CSF signal. This is called CSF flow void sign therefore when evaluating long TR sequence MRI flow-related artifacts in the CSF spaces should be kept in mind.

2) Nature flow factor.

There is disturbance of CSF flow at narrow segments of CSF pathway such as the aqueduct of Sylvius, the foramen of Monro, these regions show varying CSF signal intensity depend on flow dynamics. The usual signal intensity of CSF is hypointense on T_1 weighted image and hyperintense on T_2 weighted image.

3) The relaxation time of the CSF and its constituents.

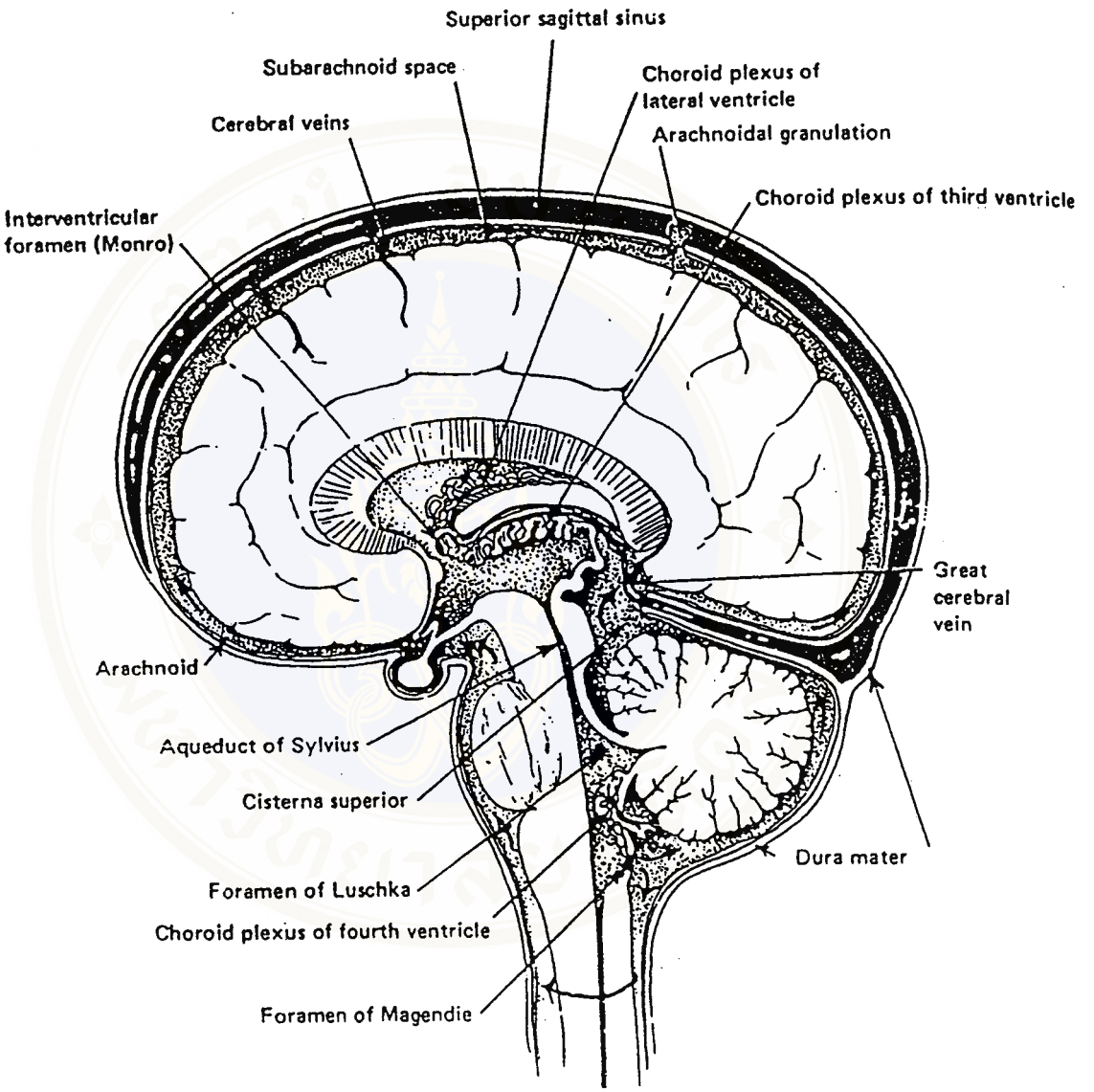

Figure 1. Midsagittal section of the brain demonstrating the choroid plexus of lateral ventricles; third ventricle and fourth ventricle including direction of CSF flow from the interstitium space to the ventricles and to the subarachnoid cisterns (10).

Basic principle of magnetic resonance.

1. Atomic structure.

Atom composes of a core-nucleus and surrounding cloud of electrons. The nucleus consists of positive electrical charge called proton and neutral electrical charge called neutron (11). When a proton as charged sphere, spinning it represents a current flowing in a loop around the axis of rotation, thereby generating an electromagnetic field (12) (Figure 2). We can think the proton as a "bar magnet".

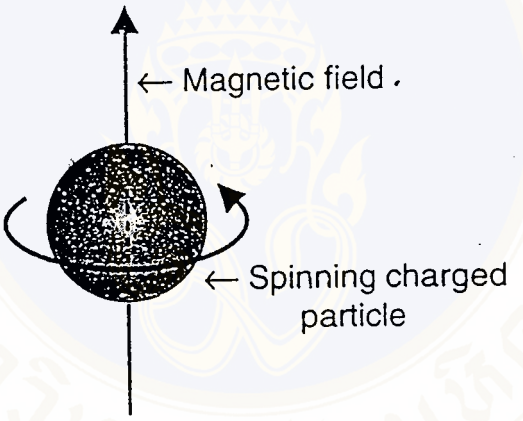

Figure 2. A spinning charged particle generates a magnetic field (13).

2. MR active nuclei.

MR active nuclei are nuclei that have odd number of protons or neutrons. That means there is one proton or neutron unpaired.The unpair proton points either north or south and has a net magnetic field or "magnetic dipole moment", its

symbol is μ (Figure 3). But the nuclei that have even number of protons and neutrons, they will pair that means every spin with magnetic field pointing up, will have a paired spin with magnetic field pointing down. So the magnetic field of even nuclei will cancel and net magnetic field is zero. However in MRI, we are interested in hydrogen nucleus which has a single positive charged proton due to its natural abundance (approximately 60% of the body is water (H_2O)) and relative sensitivity (Table I).

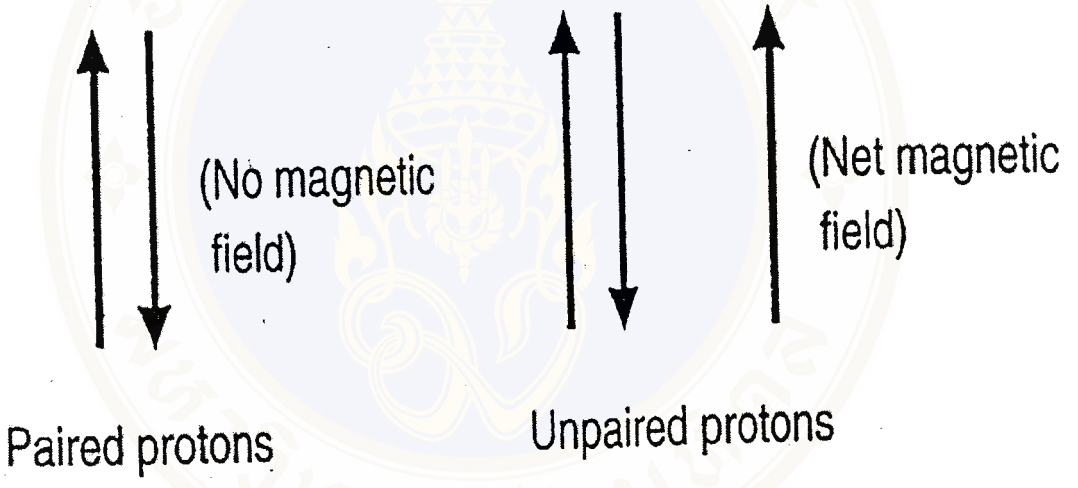

Figure 3. A. The magnetic fields of paired protons with cancel each other out, giving no net magnetic field.

B. Show that unpaired proton gives a net magnetic field (13).

Table I. Show magnetic properties of medically important nuclei (14).

Nucleus	Spin Quantum Number (S)	Gyromagnetic Ratio (MHz/T)	Natural Abundance (%)	Relative Sensitivity
^{1}H	1/2	42.58	99.98	1
^{13}C	1/2	10.71	1.11	$1.7 X10^{-4}$
^{19}F	1/2	40.05	100	0.83
^{23}Na	3/2	11.26	100	$9.2 X10^{-2}$
^{31}P	1/2	17.23	100	$6.6 X10^{-2}$

3. MR active nuclei in the absence of an external field B_0.

MR active nuclei in the absence of B_0 will be randomly oriented, giving zero magnetization of the material (Figure 4).

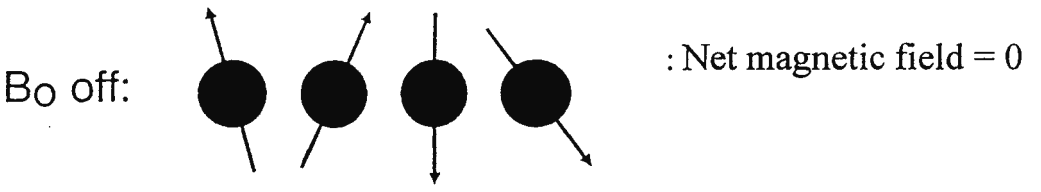

Figure 4. In the absence of B_0, their net magnetic field will be zero (13).

4. MR active nuclei in the presence of B_0.

MR active nuclei in the presence of an external field B_0 tends to align with the applied field, but they don't all align up in the same direction. Estimate half point north and half point south. Over time, more spins align with the applied field, generating net magnetization (Figure 5).

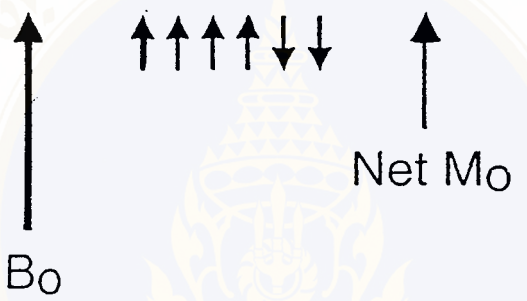

Figure 5. In the presence of B_0, protons will produce net magnetization (13).

From laws of quantum mechanics nuclei align at one angle to the direction of the field have specific energy levels related to property called " spin quantum number S "(13). The hydrogen nucleus has a spin quantum number S of 1/2 (Table I). The number of energy states of nucleus is determined by the equation: (13)

number of energy states of nucleus = $2S + 1$ (2)

For a proton with a spin S = 1/2

So number of energy states of hydrogen nucleus $= 2(1/2) + 1 = 2$

Therefore, a hydrogen proton has two energy states. The energy difference between these two states (ΔE) is calculated by:

$$\Delta E = E_2 - E_1 = (2\mu)(B_0) \quad (3)$$

where, μ is the magnetic dipole moment.

B_0 is the external magnetic field.

At upper energy state (E_2), the spin direction is antiparallel to the external magnetic field direction (spin down) while at the lower energy state (E_1), the spin will parallel to the external magnetic field direction (spin up).

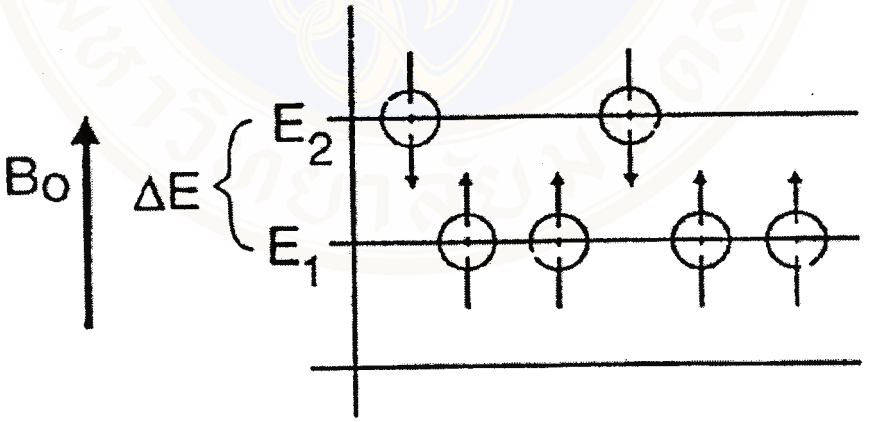

Figure 6. In a magnetic field B_0, protons are at two energy states; in the upper energy state they are antiparallel to B_0, but in the lower energy state they parallel to it (13).

5. Precession.

Precession is motion of proton that rotates around the axis of the apply external magnetic field B_0 with constant angular precession frequency (ω_0) (Figure 7).

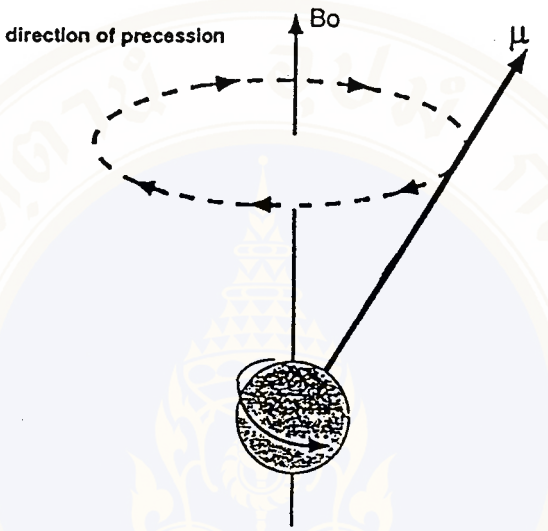

Figure 7. A spinning proton with magnetic moment μ under the effect of an external magnetic field B_0 will precess around axis of B_0 with constant angular precession frequency (ω_0) (16).

6. Larmor equation.

Larmor equation is equation that represents the rate of the proton's, precession around an external magnetic field B_0, expressing as:

$$\omega_0 = \gamma B_0 \qquad (4)$$

where, ω_0 is the angular precession frequency, called the larmor precession frequency (in Mhz or radians/second).

γ is the gyromagnetic ratio which is specific for the nucleus (in MHz/Tesla) (Table I).

B_0 is the strength of external magnetic field (in Tesla).

7. Net magnetization and it's component.

Net magnetization is a sum of the contributions of all the magnetic moments of the individual proton. Net magnetization composes of two components are the longitudinal and the transverse magnetization.

The longitudinal component is the projection of the net magnetization along the direction of the external magnetic field. The transverse component is the projection of the net magnetization onto the plane perpendicular to the direction of B_0 (Figure 8).

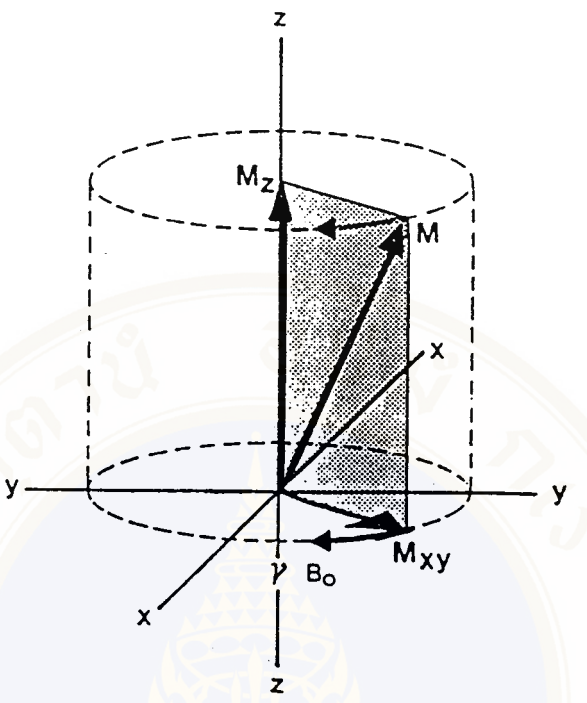

Figure 8. The net magnetization vector can be broken down into two components: longitudinal magnetization (M_z), along the direction of the magnetic field, and transverse magnetization (M_{x-y}), in the plane perpendicular to the field (17).

8. Radio frequency (RF) pulse.

Radio frequency (RF) pulse is in radio frequency range of the electromagnetic spectrum. When the patient is in the magnet, RF pulse is applied along the x axis perpendicular to the axis of B_0 to flip the longitudinal magnetization 90^0 into the the x-y plane. If all of the vectors flip into the x-y plane, the magnitude of M_{xy} equals the magnitude of M_0. This is called a 90^0 flip, and the pulse that gives the 90^0 flip is called 90^0 RF pulse (Figure 9). When all vectors flip into the x-y plane, this transverse magnetization will precess in phase around the axis of B_0 at the

Larmor frequency. Similarly, when we apply a 180^0 RF pulse, the longitudinal magnetization vector is inverted to - M_z.

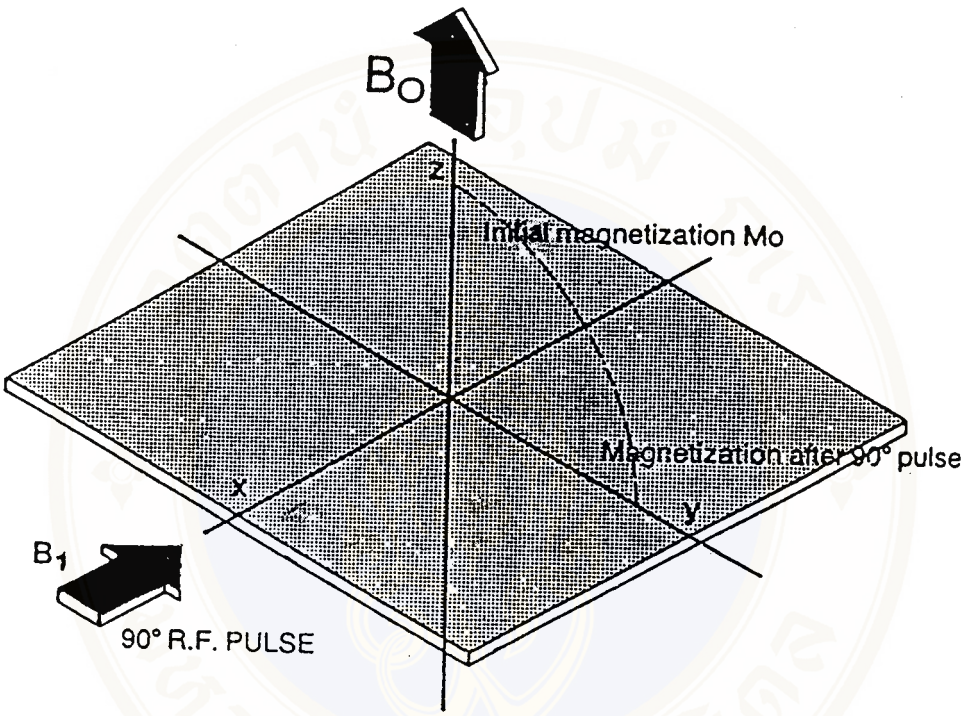

Figure 9. When the whole magnetization vector is flipped into the x-y plane, it is called a 90^0 flip (17).

9. Resonance.

Resonance is a phenomenon occurring when the frequency of the applied RF pulse matches the proton ω_0 allowing the proton to receive some energy from RF pulse. If the RF frequency does not match the ω_0 of the proton, the system won't resonate and can not receive energy from RF pulse.

When system resonates with 90^0 RF pulse, the protons flip into the x-y plane and are in phase because the protons don't point in random directions. This creates M_{xy}.

10. Relaxation of the magnetization.

Relaxation of the magnetization is the process that nuclei return to equilibrium state after the RF pulse is turned off, by emitting electromagnetic radiation that was received from RF pulse and transferring it to the surroundings (lattice) or between themselves.

Relaxation of longitudinal component is referred to as T_1 relaxation time. It is measured by the time that the longitudinal component returns to 63 % of its original state (M_z) after the RF pulse is turned off (17) (Figure 10). The M_z component will start to grow at a rate characterized by T_1 relaxation time, and can be described mathematically as:

$$M_z(t) = M_0 (1- e^{-t/T_1}) \qquad (5)$$

Where $M_z(t)$ is the longitudinal magnetization component at time (t).

M_0 is the equilibrium longitudinal magnetization.

t is the time after the RF pulse.

T_1 is the T_1 relaxation time constant that is an exponential time constant that is related to the period required for longitudinal component to recover 63% of its equilibrium alignment (86 % after 2 X T_1, 95% after 3X T_1, and 98.5% after 4X T_1).

T_1 relaxation time is commonly referred to as spin-lattice relaxation, because the emitting energy will be transferred to their environment (lattice). T_1 relaxation time of proton is different in different tissues in the body, depend on the efficient transfer of energy to the surrounding lattice and strength of the external magnetic field.

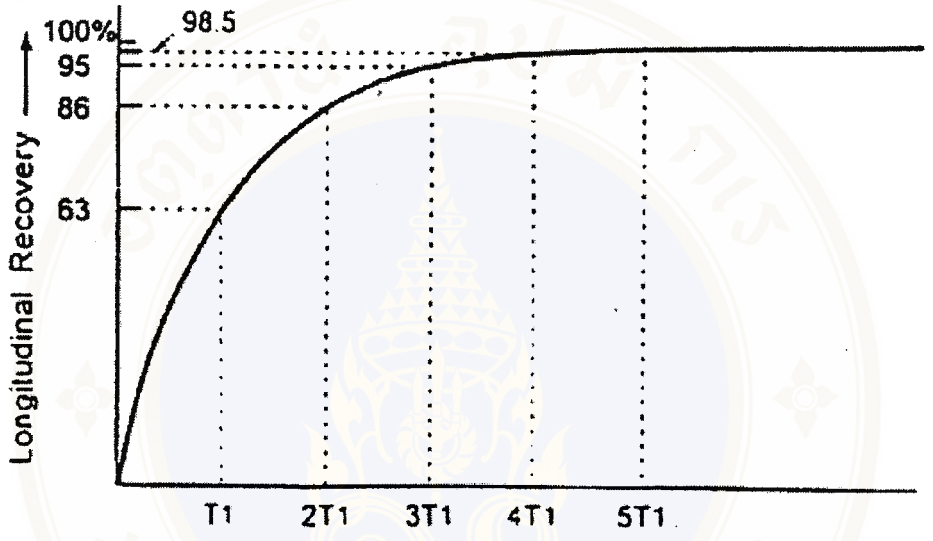

Figure 10. A typically T_1 relaxation curves (16).

Efficient transfer of energy to the surrounding lattice depends on molecular motion and the presence of macromolecules. The most efficient energy transfer occurs when the natural motional frequencies (translation, rotation, and vibration) of the proton are at the Larmor frequency. Hydrogen protons in fat (medium-sized molecule) have natural motional frequencies that are almost equal to the Larmor frequencies for hydrogen. The efficiency of energy transfer from the protons to the lattice is increased, thus decreasing T_1. But Hydrogen proton in the small molecules and large molecules has natural motional frequencies that are difference from the Larmor

frequencies for hydrogen. So the efficiency of energy transfer from the protons to the lattice is decreasing, thus increasing T_1 (Figure 11).

The presence of macromolecule, when water molecules is bound to a hydrophilic macromolecule such as a protein. These bound water molecules lose some of the freedom in their motion. As a result, the natural motional frequencies of the water molecules get closer to the Larmor frequency, thus yielding a more efficient energy transfer. The net result is shortening in the T_1 relaxation time.

T_1 relaxation time also depends on the external magnetic field strength. It tends to increase at stronger field strength (Table II), because in the stronger magnetic field there will be more protons aligning with it. Thus these protons have more energy to give to the lattice, and take longer time in transferring energy to their environment, resulting in longer T_1 relaxation time.

Relaxation time of the transverse component is referred to as T_2 relaxation time. T_2 relaxation time is a measure of the time that the transverse component has decayed to 37 % of its original value after the apply of the 90^0 RF pulse(Figure 12), and is commonly called spin-spin relaxation time. The transverse vector M_{x-y} decays at the rate characterized by T_2 relaxation time: (13)

$$M_{x-y}(t) = M_0 e^{-t/T_2} \qquad (6)$$

Where, $M_{x-y}(t)$ is the transverse magnetization component at the time (t)

M_0 is the transverse magnetization component at the time t = 0, immediately after the RF pulse is turned off. It will be equal to the value of M_z just prior to the RF excitation pulse.

t is the time after the RF pulse is turned off.

T_2 is the T_2 relaxation time constant that is an exponential time constant of transverse component

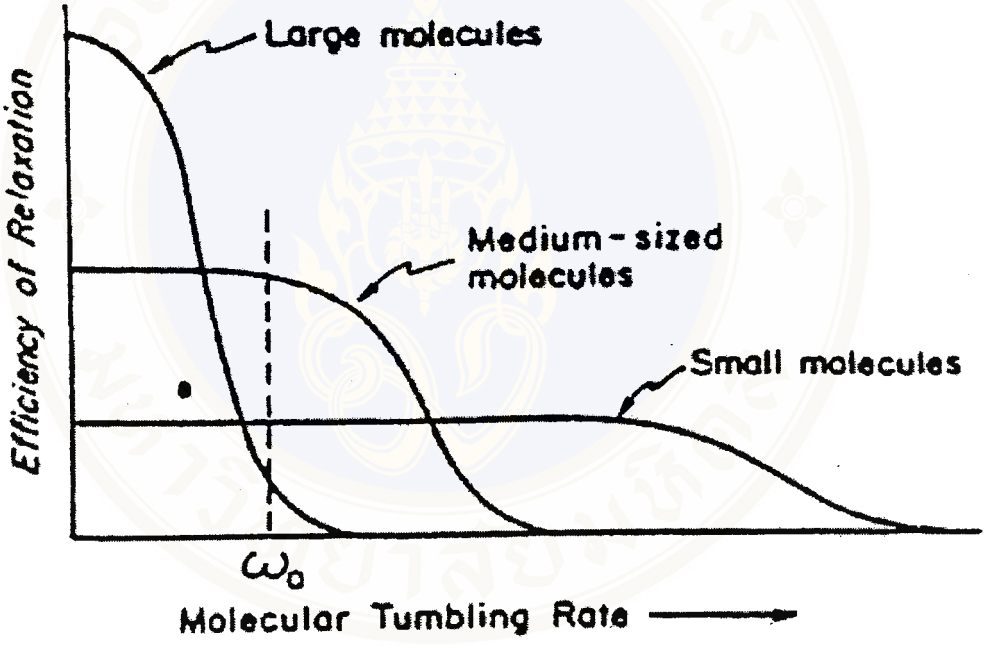

Figure 11. Show relaxation efficiency versus molecular size that spin-lattice relaxation efficiency is the best for substances with frequency of molecular nears larmor frequency ω_0 (17).

Table II. T_1 and T_2 values for human tissue (12).

TISSUES	T_1 at 1.5 Tesla (msec)	T_1 at 0.5 Tesla (msec)	T_2 (msec)
Fat	260	215	84
Liver	490	323	43
Kidney	650	449	58
Spleen	780	554	62
White matter	790	539	92
Lung	830	600	79
Skeletal muscle	870	666	47
Gray matter	920	656	101
Cerebrospinal fluid	>4000	>4000	>2000

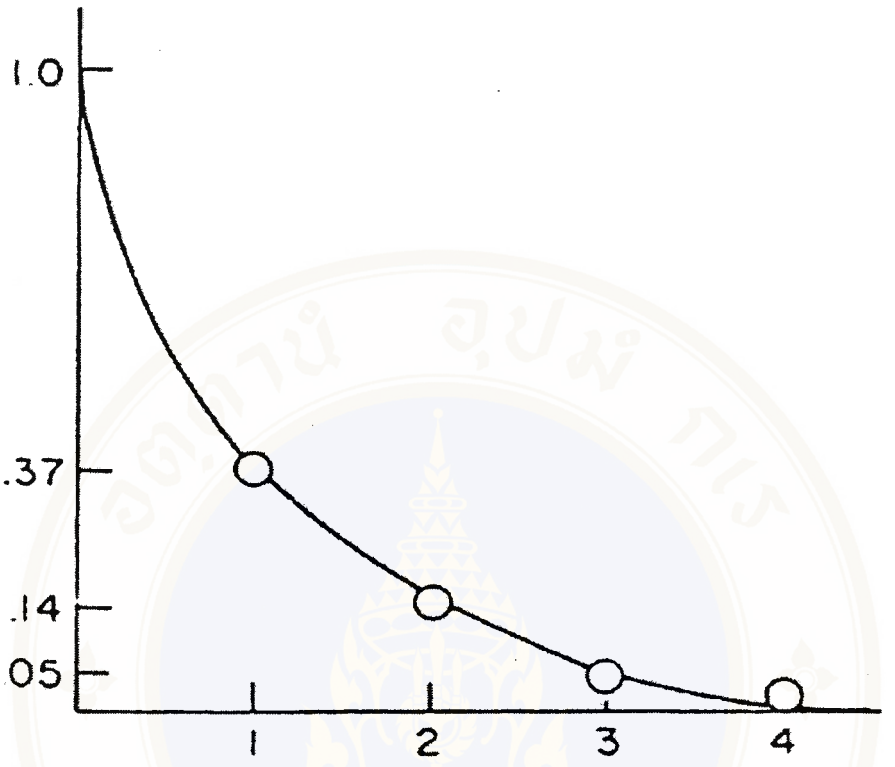

Figure 12. Curve showing decay of the transverse magnetization. At the time = T_2 the magnetization has decayed to 37% of its initial value (17).

The mechanism that causes the decay of the transverse magnetization is the dephasing of the spin. Dephasing is the result of interaction between spins and external magnetic field inhomogeneities. An interaction between individual spins is called spin-spin interaction, which is inherent property of every tissue and is measured by T_2 relaxation time. External magnetic field inhomogeneities cause protons in different positions to precess at different frequencies because each spin is exposed to a slightly different magnetic field strength.

11. Free induction decay

Free induction decay is decay of oscillating signal, that generated by oscillating spins of the net magnetization in transverse plane after turn off the RF pulse which it is induced by a current in a receiver coil. This decaying oscillating signal is described mathematically as:

$$M_{x\text{-}y}(t) = M_0 e^{-t/T_2^*} (\cos \omega_0 t) \quad (7)$$

Where, $M_{x\text{-}y}(t)$ is the transverse magnetization component at the time (t).

M_0 is the transverse magnetization component at the time t = 0, immediately after the RF pulse is turned off.

e^{-t/T_2^*} is the decay signal with the time constant of T_2^*.

$\cos \omega_0 t$ is the formula for an oscillating wave, at a Larmor frequency of excited ω_0.

Therefore, the general form of the signal come from an oscillating signal which varies as $\cos \omega_0 t$ and a decaying signal which decays with time constant T_2^* as given by the exponential e^{-t/T_2^*} (Figure 13).

The free induction decay signal has the following characteristics:

- The free induction decay signal oscillates with component at the Larmor frequencies of the excitation.

- The free induction decay signal has an initial transverse magnitude related to the density of initial longitudinal magnitude before flipped into transverse plan.

- The free induction decay signal decreases in an amplitude with time, as a function of the transverse relaxation process.

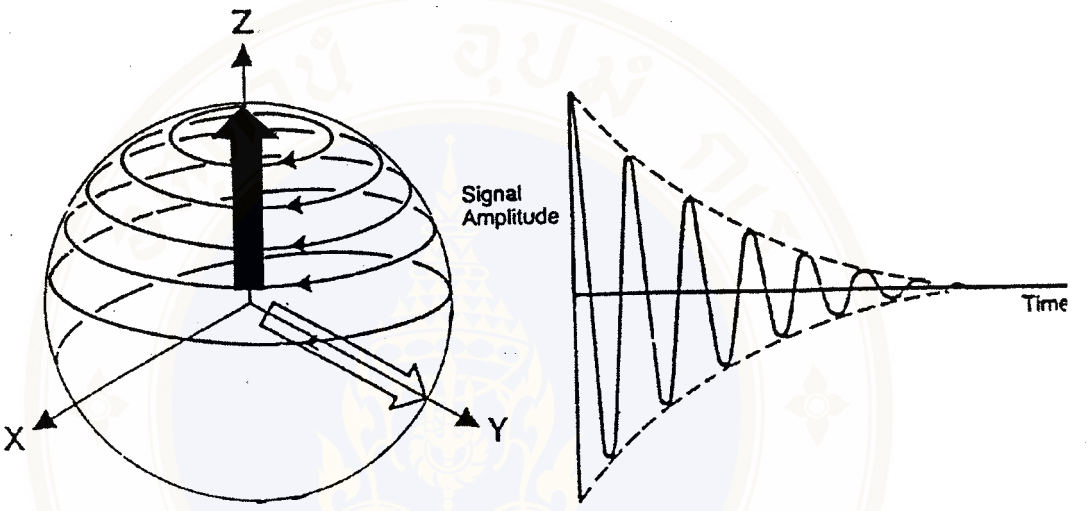

Figure 13. Show Free induction decay after a 90^0 RF pulse. When the all vector flips into the x-y plane, this transverse magnetization will precess in phase around the axis of the external magnetic field (B_0) at the Larmor frequency (17). Then when we turn off 90^0 RF pulse signal, this transverse magnetization will dephase with time at rate define as T_2^* (17).

12. Fourier transform.

Fourier transform is an analytical algorithm, which converts the received signal into one, which can be displayed on a monitor, having attributed frequency values to the amplitude variations. An image is formed because the computer is enabled to related values of signal strength (hydrogen density) to specific spatial locations.

13. Spin echo (SE) pulse sequence.

13.1 Spin echo (SE) pulse sequence consists of a 90^0 excitation pulse followed by 180^0 RF rephasing or refocusing pulse after time τ, to eliminate the dephasing effects caused by external magnetic field inhomogeneities by maximizing spin rephasing at the time 2τ .We call 2τ " the echo time" (TE) at this time maximal SI will be obtained. The 90^0 excitation pulse and 180^0 RF rephasing pulse is repeated after an interval called repetition time (TR) (Figure 14).

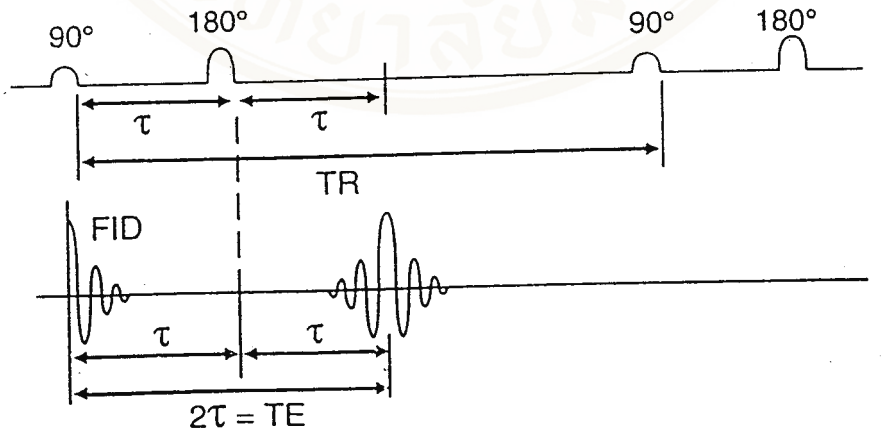

Figure 14. Show a diagram of a spin echo pulse sequence. A 180^0 rephasing pulse is applied after 90^0 excitation pulse at time τ (13).

13.2 Tissue contrast in spin echo pulse sequence depends on TR and TE; there are three types of tissue contrast:

13.2.1. Proton density weighted imaging.

Proton density weighted imaging represent a tissue contrast that is produced as a result of variations in the amount of mobile hydrogen nuclei. This can be done by using a long TR (1500-3000 msec) and short TE (10-40 msec). The long TR lets the tissue get full longitudinal magnetization. The short TE permits minimal loss of transverse signal due to T_2 relaxation time. Therefore this sequence needs the long TR to reduce T_1 effect and the short TE to reduce T_2 effect.

13.2.2. T_1 weighted imaging

T_1 weighted imaging represent tissue contrast that is produced by considering the variations in longitudinal relaxation rate. This is obtained by using a short TR (300-800 msec) and short TE (10-40 msec) (Figure 15). The short TR causes tissues with a short T_1, such as fat, to fully recover along the longitudinal direction and tissues with a long T_1, such as CSF, to only partially recover. The short TE reduces T_2 effect and short TR increases T_1 effect.

13.2.3. T_2 weighted imaging

T_2 weighted imaging represents a tissue contrasts that is produced by considering the variations in transverse relaxation rate. This is done by using a long TR (1500-3000 msec) and long TE (50-100 msec) (18). The long TR causes all tissues to fully recover along the longitudinal direction and long TE controls loss of transverse signal due to T_2 relaxation time. Long TR reduces T_1 effect and long TE highlights T_2 effect. It is very important to remember that many pathologies such

as tumor, infarction have long T_2 but not equal to CSF. T_2 weighted imaging is very good in producing very bright signal from these pathologies (Figure 16). But there may be some difficulties in differentiating pathologies from CSF especially when they are close to each other.

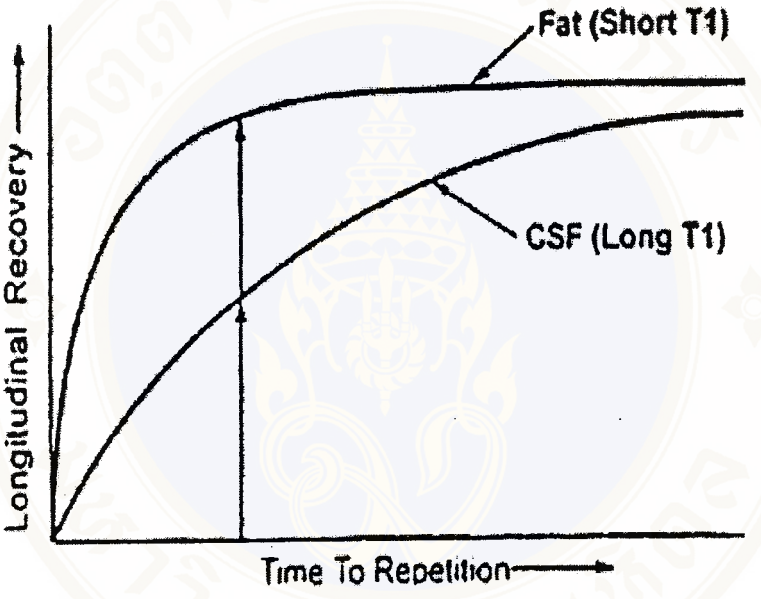

Figure 15. Show tissue contrast with short TR and short TE that short TR enhances the T_1 contrast (16).

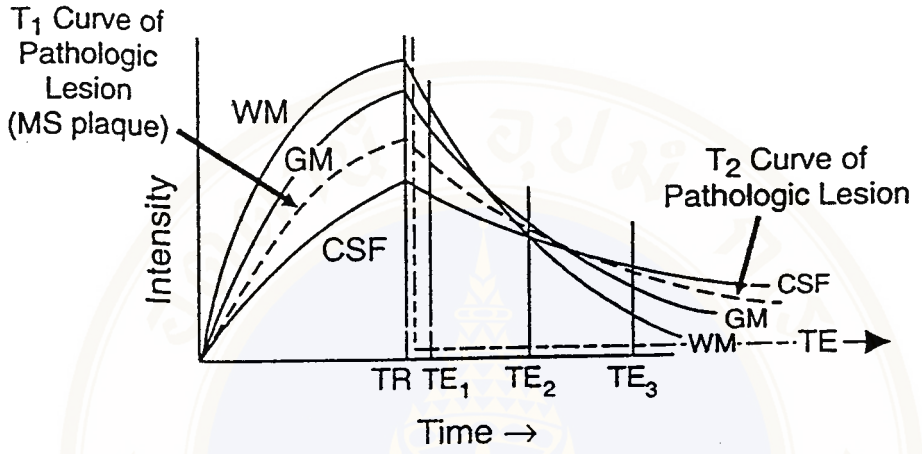

Figure 16. Show T_1 and T_2 curves of CSF, white matter, gray matter and lesion. The long TR allows tissues to reach full longitudinal magnetization that reduces T_1 effects. The long TE allows controlled loss of transverse signal due to T_2 relaxation and increases the signal intensity differences between these tissues (13).

Inversion Recovery (IR) pulse sequence

Inversion Recovery (IR) pulse sequences consists of 180^0 inversion RF pulse, followed by the spin echo pulse sequence for signal detection. First, we apply 180^0 RF pulse to invert the longitudinal magnetization from the +Z direction to -Z direction (Figure 17) that allows tissue to relax over twice the dynamic range of spin echo technique. Then, when the 180^0 inversion RF pulse is removed, the magnetization returns toward its equilibrium state in the +Z direction. Because the

echo technique. Then, when the 180^0 inversion RF pulse is removed, the magnetization returns toward its equilibrium state in the +Z direction. Because the receiver's antennae (RF coil) can detect magnetization only in perpendicular plan to the main magnetic field, so after 180^0 inversion RF pulse we apply 90^0 RF pulse at a time called "inversion time" (Figure 18).

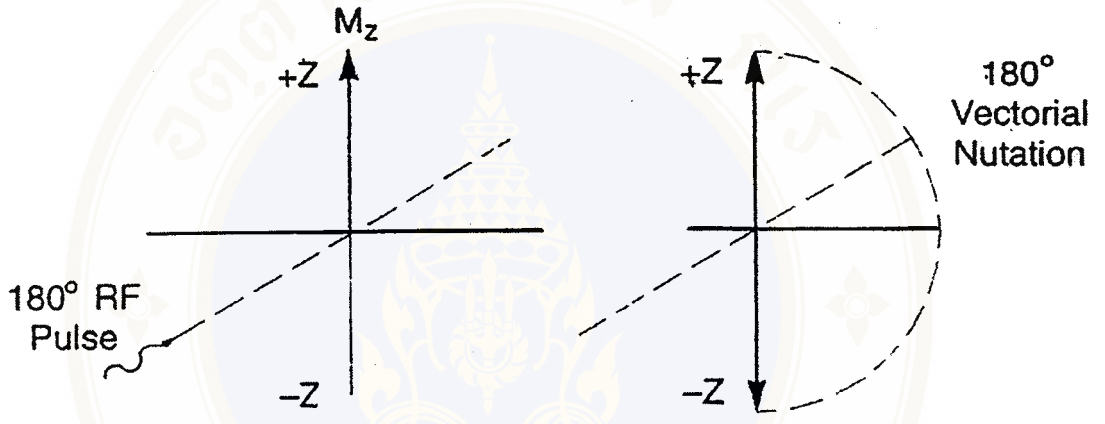

Figure 17. Show the effect of the 180^0 inversion RF pulse on longitudinal magnetization, that the magnetization is moved from the +Z into -Z direction (19).

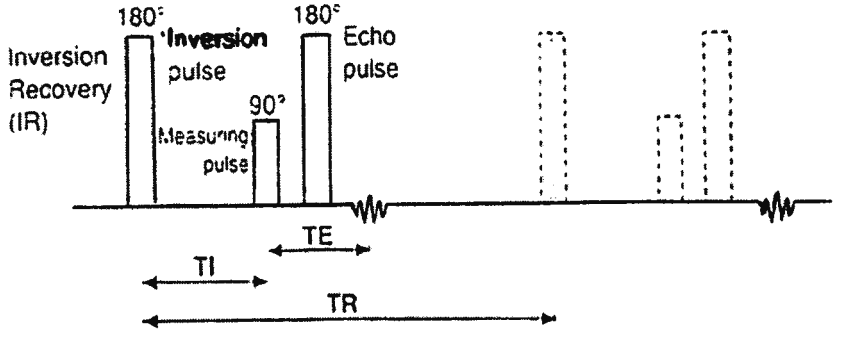

Figure 18. This figure shows diagram of inversion recovery pulse sequence. First, the magnetization is inverted with 180^0 inversion RF pulse. After interval TI, a 90^0 RF

measurement pulses is applied to rotate the magnetization into the transverse plane, for detection (19).

This 90^0 RF pulses flips the partially recovered spins into the transverse plane, so that a signal may be detected. This signal amplitude (S) is given by:

$$S_{IR} = K\rho e^{-TE/T_2}(1-2e^{-TI/T_1} + 2\,e^{-(TR+TI)/T_1} - e^{-TR/T_1}) \quad (8)$$

Where K is the system-related scale factor.

ρ is the proton density.

However, TR is common very much larger than TI, to yield the simplified expression:

$$S_{IR} = K\rho e^{-TE/T_2}(1-2e^{-TI/T_1} + e^{-TR/T_1}) \quad (9)$$

The advantages of inversion recovery (IR) pulse sequences:

1. IR pulse sequence is a good method to demonstrate T_1 difference between tissues. Although T_1 difference is narrow, the contrast is high due to the effect of 180^0 inverting pulse, which allows tissue to relax twice the dynamic range of spin echo technique. T_1 contrast can be varied by selection of the optimal value of TI. Figure 19 shows curves of the longitudinal magnetization recovery of tissues with a short T_1 (curve S) and long T_1 (curve L) after apply 180^0 inverting pulse. To produce maximum T_1 enhancement of the image contrast, it is necessary to apply the 90^0 excitating pulse at time = optimum TI that is the maximum difference between the value of the recovered magnetization of one tissue and that of the other tissue.

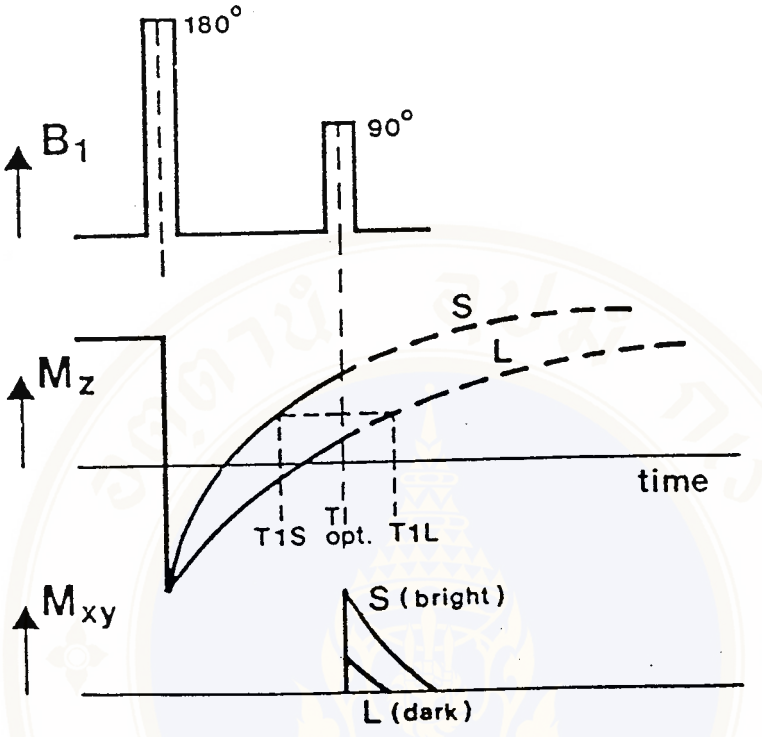

Figure 19. The curves marked S and L represent the behavior of M_z after inversion in tissue with a short and a long T_1 respectively. Ideally, the timing (TI) of the 90^0 RF pulses is set for maximum separation in the curves. The amplitude of the response signal is related to the valued of $M_{x\text{-}y}$ (17).

Therefore IR image need long TR for the longitudinal magnetization of each tissues recovered fully before to the next 90^0 excitating pulse. If the TR is short relative to T_1, the longitudinal magnetization will recovers partially before the next inversion pulse, so the contrast is less. However the level of T_1 contrast obtained with IR images also depends on whether the images are sensitive to the phase of the MR

signal. Most MR systems generate IR images by using phase insensitive images (magnitude image). On these magnitude images, information about whether the longitudinal component of M_z is positive or negative is lost. As a result, M_z can vary between 0 to 1. Some system actually produces phase sensitive images, which can depict whether M_z is positive or negative. As a result, M_z can vary from -1 to 0 to 1; that is, the dynamic range for T_1 contrast is doubled (Figure 20).

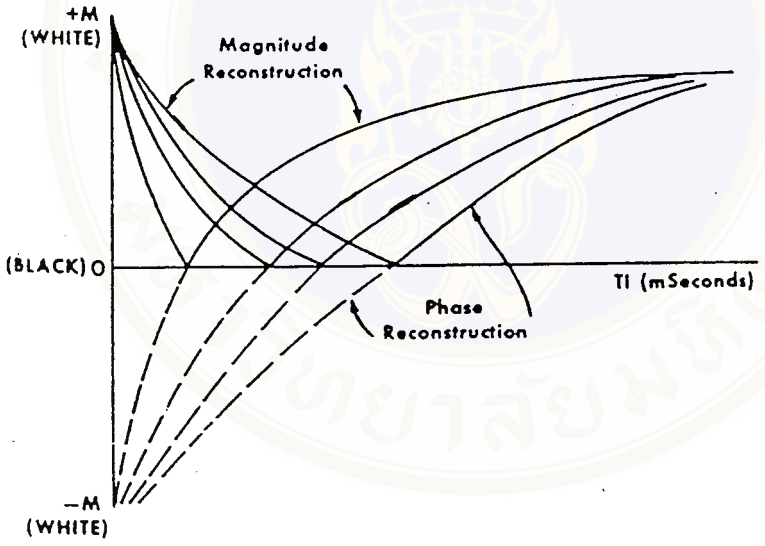

Figure 20. Show the magnitude and phase sensitive reconstruction of IR images. The magnitude reconstruction gives us only positive signals, so the curves are reflected above the zero line, this result may loss of contrast. But phase sensitive reconstruction retains sign of magnetization and may result in improved tissue contrast (17).

2. A second utility of IR sequences is suppression of some tissues that we need. When the inversion pulse is removed, the magnetization returns toward its equilibrium state in the +Z direction. At some point, the magnetization will pass from the -Z direction to the +Z direction. When this crossover occurs, there is no longitudinal magnetization. This point is referred to as the null point (Figure 21).

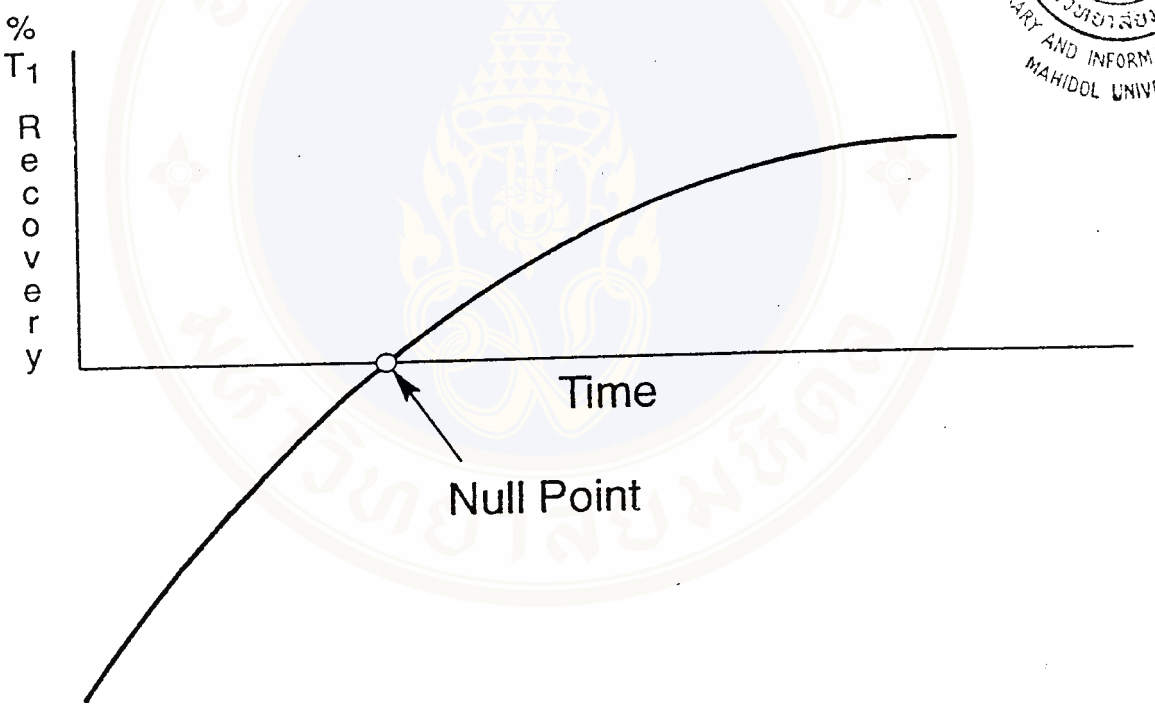

Figure 21. Show the null points which the signal crosses the zero line . At this point, the signal intensity is zero (18).

The null point can be used to create signal voids for various tissues. We can use the Equation (9) for TI(null) at which point the signal intensity is zero, from the equation (9) express as:

$$S_{IR} = K\rho e^{-TE/T_2}(1-2e^{-TI/T_1} + e^{-TR/T_1})$$

then, $$S_{IR} = 0 = (1-2e^{-TI/T_1} + e^{-TR/T_1})$$

When, the limit of infinite TR, then $e^{-TRT_1} \cong 0$, the solution to TI(null) is: (6)

$$TI_{null} \cong (\ln 2)\, T_1$$

or $$TI_{null} \cong 0.693\, T_1 \qquad (10)$$

Where, TI_{null} is the inversion time that, gives signal voids for tissues we need to suppress, and T_1 is T_1 relaxation time of suppressing tissues.

So, if the selected TI matches exactly with the time at which null point occurs, a signal void for that particular tissue will occur. This is because at the null point there is no longitudinal magnetization for 90^0 RF pulse to flip into the transverse plane, so no signal can be created. Here is an example; if we want to suppress fat tissue which has T_1 approximately 250 msec at 1.5 Tesla, TI must be 0.693 x 250 = 173.25 msec. Because we can suppress fat in an IR image, by using short TI, this technique is called Short-TI inversion recovery (STIR) (Figure 22).

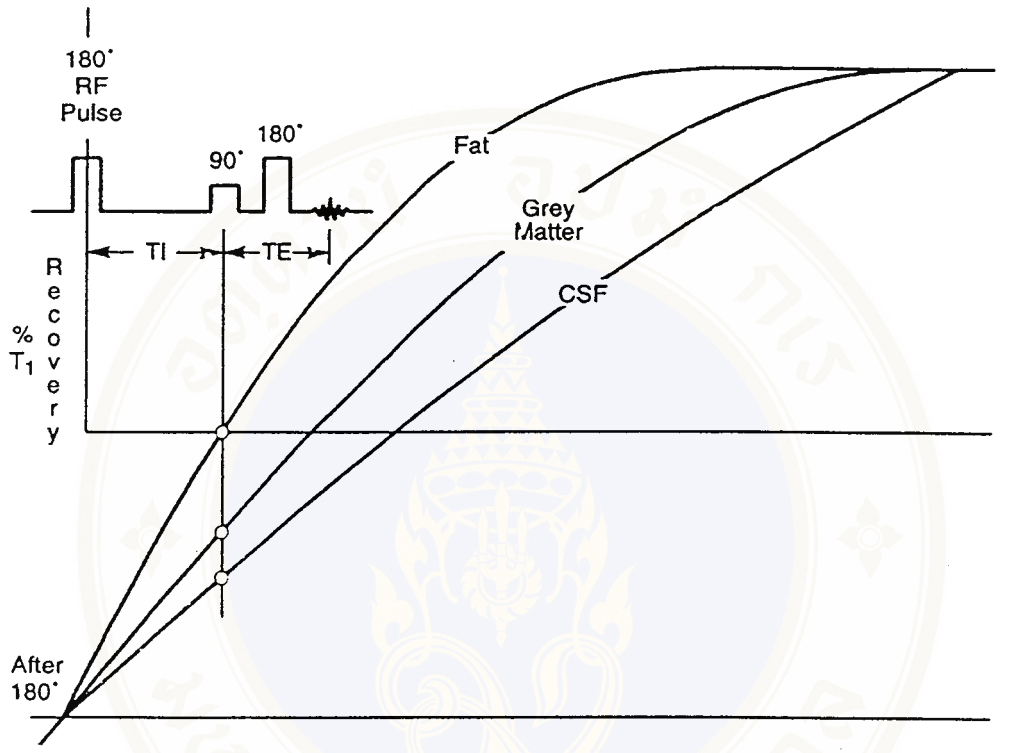

Figure 22. Showing if TI is selected to match exactly with the time at null point of fat, fat can be suppressed (13).

3. IR pulse sequence provides heavily T_1 weighted images with long TR, allowing more imaging volume to be covered; as shown by equation of number of slices:

$$\text{number of slices} \cong \text{TR/TE} \quad (11)$$

In contrast to T_1 weighted images of spin echo pulse sequence, short TR is used, limiting the number of slices.

The disadvantage of IR pulse sequences:

The disadvantage of IR sequences is a very long acquisition time due to long TR for the longitudinal magnetization of each tissue to recover fully. Therefore, technique is developed by combining a fast spin-echo sequence with an inversion-recovery sequence (fast IR pulse sequence), to reduce the scanning time.

Fluid-Attenuated Inversion Recovery (FLAIR) pulse sequence.

Fluid-Attenuated Inversion Recovery (FLAIR) pulse sequence is a magnetic resonance imaging (MRI) sequence designed to produce a heavily T_2-weighed image while suppressing the CSF signal. From the fundamental of an inversion recovery sequence, CSF suppression is achieved by using a 180^0 inversion recovery with an TI chosen to null the signal from CSF. We can desire TI depending on the T_1 relaxation time of the CSF and TR chosen. Assuming the interval of T_1 relaxation time for the CSF is 3050-3400 msec. We can designed interval of TI for suppressing CSF by calculation from the equation (10) expressing as:

$$TI_{null\ of\ CSF} \cong 0.693\ T_{1\ of\ CSF}$$

Therefore, interval of TI for suppressing signal of CSF is 2100 to 2400 msec. That means; when we apply 180^0 inverting RF pulse to invert the longitudinal

magnetization from the +Z direction to -Z direction, followed by exciting RF pulse at these TI, it allows the longitudinal magnetization of CSF return to the null point before spin echo imaging. At this point, all other brain tissues have almost complete recovery of longitudinal magnetization toward equilibrium (Figure 23).

So, this is result of FLAIR must used long TR, which it permits tissues with very long T_1 relaxation time to completely recovery of magnetization before the next excitation, which long TR will result in better signal to noise ratio and increased contrast to noise ratio between the lesion, gray matter and white matter, and long TR also decrease T_1 effect of non-CSF tissues, thus producing heavy T_2- weighted imaging that relative with long echo time of the FLAIR sequence.

The CSF signal is completely suppressed, and pathologic lesion, which typical, have increased T_2 relaxation time in the brain, specially it adjacent to CSF interfaces, become easily to distinguish lesions from CSF interfaces when comparison with T_2- weighted spin echo.

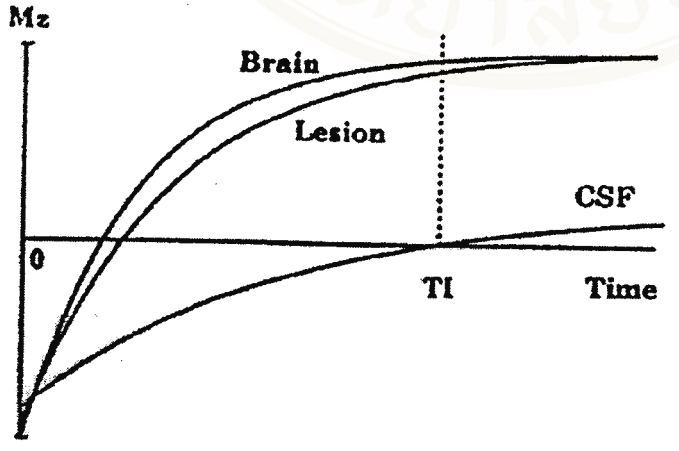

Figure 23. Showing the T_1 recovery curves after inversion of 180^0 RF pulse. TI is set so that CSF is nulled (20).

The advantage of FLAIR pulse sequence.

1. The FLAIR pulse sequence requires long TR. The inversion null time of CSF is also long enough that almost all other tissues will have fully recovery. So that the sequence is suitable for "proton density" and "T_2 weighted " clinical imaging of other tissues.

2. The FLAIR pulse sequence can effectively eliminate the bright "ghost" artifacts from pulsatile CSF motion, significantly increasing the diagnostic quality of clinical imaging of the central nervous system.

3. Finally, suppression of the bright CSF signal improves the dynamic range, thus it permits greater lesion conspicuity, specifically at brain-CSF interfaces and periventricular lesion.

The disadvantage of the FLIR pulse sequence.

The important disadvantage of conventional FLAIR sequences is a very long acquisition time, because of using long TR. Therefore we combine conventional FLAIR pulse sequences with fast-spin echo technique, calling fast FLAIR pulse sequences, for decreased acquisition time.

Image assessment

1. Signal to noise ratio (SNR)

Signal to noise ratio (SNR) is a term used to describe the relative contributions to a detected signal made by the true signal and random superimposing signals (noise). Noise composes of two types.The first, noise that result from variations in the

signal created by moving objects in the body. The second type of noise is inherent in the system.

Factors which affect SNR

1. The magnetic field.

The increased strength of the magnetic field increases the detected signal.

2. Voxel volume.

SNR may be improved by increasing the volume, because larger voxel volume will increase the number of proton spin to contribute to the signal intensity (Figure 24). The voxel volume is defined as: (13)

$$\text{Voxel volume} = \Delta x \,.\, \Delta y \,.\, \Delta z \qquad (12)$$

Where Δx is the pixel size in the x direction.

Δy is the pixel size in the y direction.

Δz is the slice thickness.

3. Slice thickness.

SNR is improved by increasing the slice thickness because increasing the slice thickness increases the signal volume per image, resulting in a higher ratio. But a partial volume effect may degrade the image.

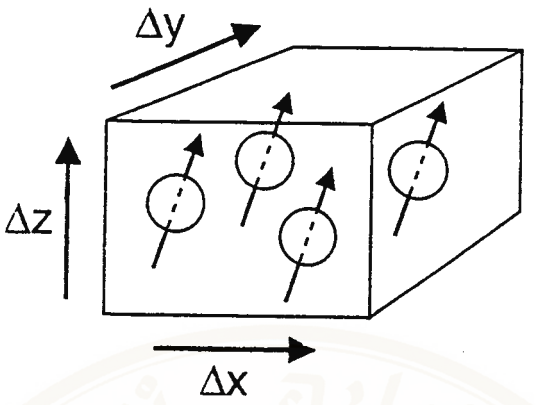

Figure 24. Voxel is a three-dimensional volume element with dimensions Δx , Δy and Δz. The more spins in a voxel, the more signal. Therefore, increasing voxel size increases SNR (13).

4. Repetition time (TR).

The increasing repetition time improves SNR by increasing the time that longitudinal magnetization is permitted to recover for all tissues. More signal will be obtainable to be flipped to the transverse plane during subsequent RF pulses.

5. Echo time (TE).

The increasing TE decreases SNR by allowing more time for tissue vectors to dephase; resulting in signal loss.

6. Number of acquisitions or excitations (NEX).

The number of acquisitions or excitations (NEX) represents the number of times that we collect data for a given phase encode value and average the information to represent one image. Signal increases linearity with increasing NEX but

noise is random. If we double NEX, the signal doubles and noise increases by $\sqrt{2}$, thus SNR increases by factor of $\sqrt{2}$. This calculates to an increase in SNR of about 41 percent. But doubling the acquisitions also doubles scan time, which may result in more artifact noise due to patient's movement.

7. Bandwidth (BW).

The bandwidth is a range within a band of frequencies that a MRI system is tuned to receive frequencies. The received bandwidth of an image determines the number of frequencies encompassed in the image. The increasing BW will include more noise, and SNR decreases. Therefore, the decreasing BW will allow less noise, and the SNR increased SNR.

8. Field of view (FOV).

Field of view is the area of the anatomy being image, it is determined by:

$$FOV = (\text{pixel size}) \times (\text{number of pixels}) \qquad (13)$$

When FOV is decreased while maintaining the number of pixels, the pixel size becomes very small. Therefore, there is less signal per unit volume, and decreased SNR.

9. Spatial resolution

Spatial resolution (pixel size) is the smallest distance that we can distinguish between two points on an image. The high resolution image is obtained with small voxels. When we look at the Equation (13), if we maintain the

FOV and increase number of pixels, the size of pixel is decreased, giving decreased SNR. Therefore high resolution image usually gives poor SNR.

10. Artifact reduction techniques.

The elimination or reduction of artifacts will improve the image quality. Artifact reduction techniques are able to minimize flow (CSF and blood), breathing and other artifacts; such as flow compensation techniques. Flow compensation techniques use gradients to minimize motion artifacts created by the flow of slow moving blood and CSF. This technique can improve image quality by affecting the SNR of the image.

One method of measuring the signal to noise ratio consists of determining the ratio of mean signal intensity in the anatomic region of interest (ROI), divided by the standard deviation from a region outside the image boundaries that free of ghost artifacts (SD_{air}), (8,21).

2. Contrast ratio (CR)

Contrast ratio is ratio of signal difference between two tissues or regions to the sum of both signals, expressing as:

$$CR_{tissue(1,2)} = (S_{tissue(1)} - S_{tissue(2)}) / (S_{tissue(1)} + S_{tissue(2)}) \qquad (14)$$

Where, $CR_{tissue(1,2)}$ is contrast ratio between $tissue_{1,2}$ and S = signal intensity of individual types of tissue, assessed by region of interest measurement.

3. Contrast to noise ratio (CNR)

CNR is ratio of signal difference between two tissues to the standard deviation of the background air (noise) measured in areas free of ghost artifacts (SD_{air}), expressing as:

$$CNR_{tissue(1,2)} = (S_{tissue(1)} - S_{tissue(2)}) / SD_{air} \quad (15)$$

CNR is one measurement of image quality. CNR is useful for comparing performance of different pulse sequences in to lesion detection. While contrast considers only the relative signal differences. From the equation (15), CNR considers the relative signal differences with standard deviation of the noise (SD_{air}), if the images have high contrast with very high noise, then images may show low CNR (Figure 25).

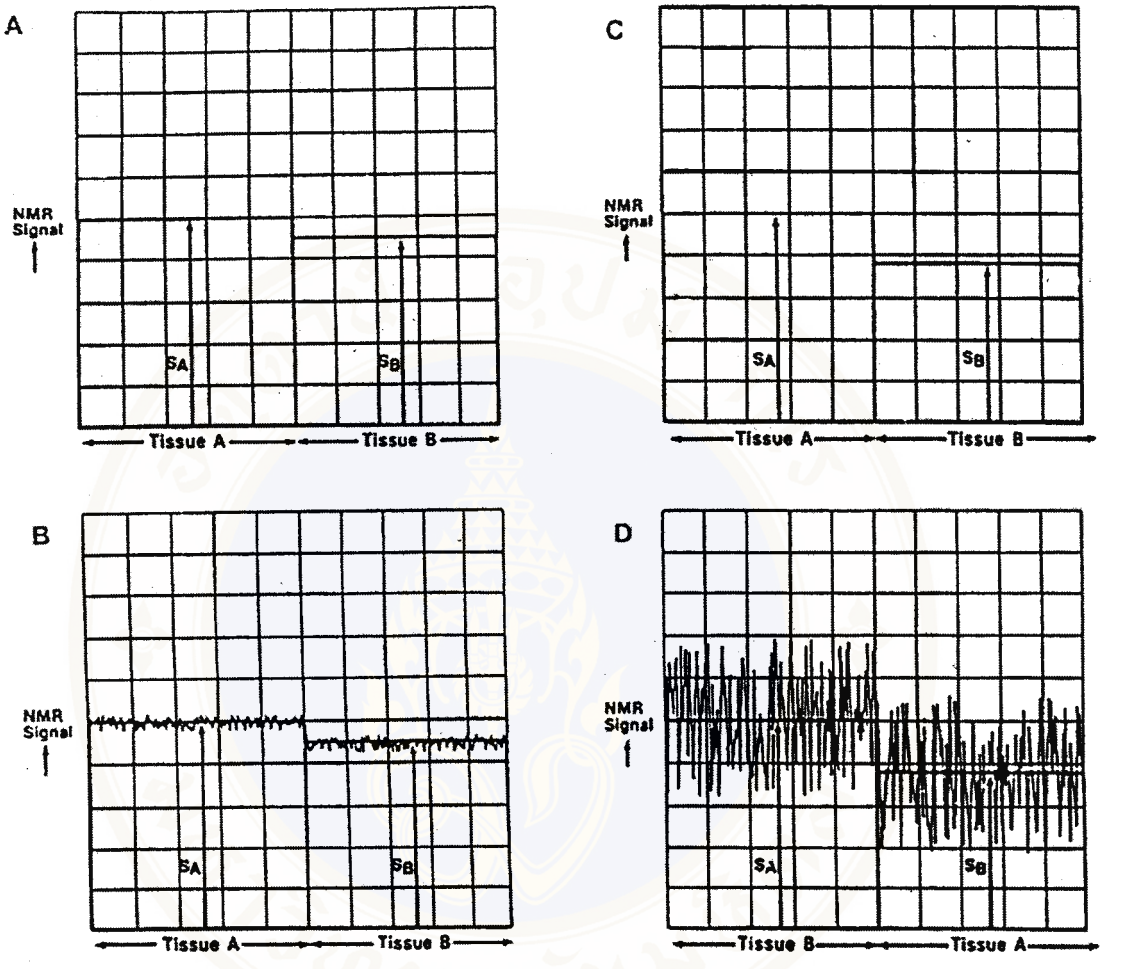

Figure 25. (A) and (C) show different contrast for two anatomic structures that (C) gives higher contrast. (B) and (C) show different contrast to noise ratio that (D) has higher constant than (B) but it gives lower contrast to noise ratio because of its higher noise level (21).

CHAPTER IV

MATERIALS AND METHODS

4.1 The measurement of T_1 values of CSF.

4.1.1 Materials

4.1.1.1 Magnetic resonance unit

The magnetic resonance unit used in this study is a 1.5 Tesla superconductive magnet, manufactured by General Electric, Milwaukee, USA, model Signa Horizon (High speed) 1.5T with 5.8 software version (Figure 26).

Figure 26. The magnetic resonance unit used in the study.

4.1.1.2 Coil

Head coil is used for T_1 measurement of CSF. This coil is a one-piece device that both transmits and receives RF signals (Figure 27).

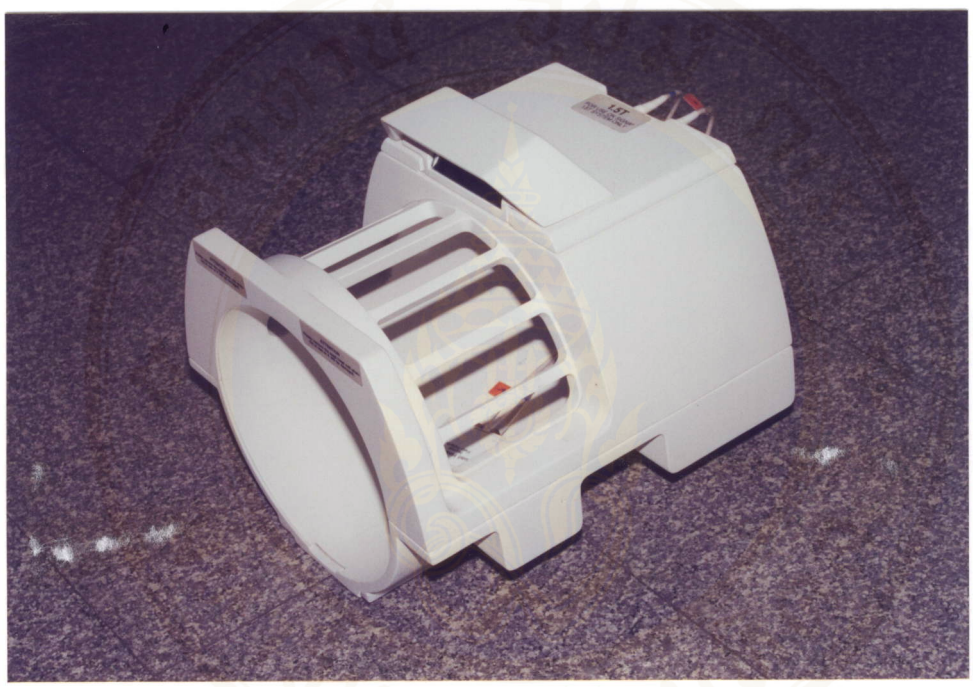

Figure 27. The head coil.

4.1.1.3 Film.

Films used in this study are Konica's, LP 670-E. It is used for archiving the image of CSF in lateral ventricles for T_1 measurement.

4.1.1.4 Region of interest (ROI).

A ROI is a user-defined area on an acquired image used to measure SI and display statistical analysis. This key is found on top level display.

4.1.1.5 Sampling unit.

T_1 relaxation time of CSF was measured in 20 healthy volunteers. The volunteer subjects (10 men, 10 women) ranged from 19 to 50 years in age (mean, 32.9 ± 10.3). They are all Thais.

4.1.2 Methods.

4.1.2.1 Imaging techniques.

All healthy volunteers had MR imaging at 1.5 T as follows:

4.1.2.1.1 Sagittal T_1-weighted scout location sequence.

Scanning parameters for sagittal T_1-weighted sequence were as follows: TR/TE/NEX = 300/8/1; imaging matrix = 256x192; FOV = 20x20; section thickness = 5 mm; and an acquisition time = 1 minute 4 seconds.

4.1.2.1.2 Axial IR sequence.

Sagittal T_1-weighted scout image was used to select the axial IR images level that best demonstrates the lateral ventricles. Scanning parameters for axial IR image were as follows: TR/TE/NEX =11,000/20/0.5; matrix = 256 x 128; thickness = 5 mm; giving a voxel size of 0.78 x 1.56 x 5 mm^3 at a field of

view 20 x 20 cm. Three different TI values: 1500, 2000, 2600 msec are used. Total imaging time for the IR sequence was 46 minutes 12 seconds.

4.1.2.2 Measurement of SI

SI was measured on each of three IR images with automated "Evaluated" features of the standard console. Two rectangles were placed within right and left anterior horns of lateral ventricles on the image which has minimized partial-volume contributions from choroid plexus, and then the rectangles were placed precisely at the same positions on other two images (Figure 28).

ROI were routinely selected first on the 1500 msec TI image, on which contrast is clearest. The window and center setting were set as low as possible, so that the image appeared uniformly white; the center value was then increased until the ventricles became dark, and the ROI was placed in a uniformly dark area.

4.1.2.3 Calculation of T_1

The values of SI acquired from the measurement described above were plotted versus TI by using the program package SPSS (ver.M, release 9.1 G). These curves were estimated by using logarithmic model that showed regrowth curve with increased TI. We can determine TI (null) by using constants that acquired from this program in the equation (16):

$$Y\ (SI) = B \ln TI + C \qquad (16)$$

Where B and C are constant values. We know TI (null), then we can solve the equation mathematically for T_1 value by using the equation (10) expressing as:

$$TI_{null\ of\ CSF} \cong 0.693\ T_{1\ of\ CSF}$$

We can also determine T_1 value by using curve with the point at which the SI is zero. The time at this null point is denoted TI (null), then we can solve T_1 values by using the equation (10) too. In this study we used former method. The example for T_1 calculation was showed in Appendix A.

Figure 28. Showing the positions of the right and left anterior horns of lateral ventricles where T_1 valued were calculated.

4.1.2.4 Statistical Analysis

T_1 measurement was obtained in both sides of lateral ventricles (L/R ratio), to verify precision of the measurement technique within a single volunteer. Ratios of T_1 measurements (left-to-right sided) were calculated in each subject (8).

Level of confidence and power of test can represent the statistical accuracy of T1 measurements.

4.2 Contrast optimization of fast FLAIR pulse sequence.

4.2.1 Materials

4.2.1.1 Magnetic resonance unit, Coil, Flim, and ROI are the same in the topic 4.1.1

4.2.1.2 Patients.

We studied 17 patients perventricular lesions (7 men and 10 women; ranging of age = 40 to 86 years old, mean age, 56 years) who were referred for MR brain imaging at Thai army hospital. The lesions selected for this study show hypersignal intensity both in T_2-weighted and fast FLAIR sequences; and touch CSF border, the total number of the lesions was 41.

4.2.2 Methods.

All the patients had MR imaging at 1.5 T as follow :

4.2.2.1 Imaging techniques.

4.2.2.1.1 Sagittal T_1-weighted scout location sequence.

Scanning parameters for sagittal T_1-weighted sequences were as follows: TR/TE/NEX = 640/8/3; imaging matrix = 256x256; FOV = 22x22; section thickness = 5 mm; and an acquisition time of 2 minutes 47 seconds.

4.2.2.1.2 Axial fast FLAIR sequences.

The axial images that best depicted the periventricular lesions were selected. Scanning parameters for axial fast FLAIR images were as follows: TR/TE /NEX = 11000/148/1 with ETL of 20; signal BW of ± 32 Khz; imaging matrix = 256 x 192; section thickness = 5 mm; giving a voxel size 0.78 x 1.33 x 5 mm^3 at a field of view 20 x 20 cm. To use five different TI values: 2000, 2100, 2200, 2300, and 2400 msec and total imaging time for the five IR series was 9 minutes 17 seconds.

4.2.2.1.3 Axial T_2-weighted FSE sequence.

Scanning parameters for axial T_2-weighted FSE images were as follows: TR/TE/NEX = 4000/101/3 with ETL of 20; signal BW of ± 32 Khz; imaging matrix = 256 x 256; section thickness, 5 mm; giving a voxel size 0.78 x 0.78 x 5 mm^3 at a field of view 20 x 20 cm and total imaging time was 3 minutes 4 seconds.

4.2.2.2 Measurement of SI

SI was measured on each of five fast FLAIR images and T_2-weighted FSE images with automated "Evaluate" features of the standard console. A rectangle was placed within a particular anatomic structure on one image such as periventricular lesions, CSF in lateral ventricle and WM that have side touching the periventricular lesions (Figure 29). The rectangle was then placed on precisely the same position on the remaining images.

To measure SI in the periventricular lesions and CSF, ROI were routinely selected on the 2100 msec TI image, on which contrast is clearest. The other images in this series were then examined to confirm that a single tissue type was included within the ROI. To measure SI in WM, the ROI was first placed on the 2200 msec TI image, on which contrast is clearest.

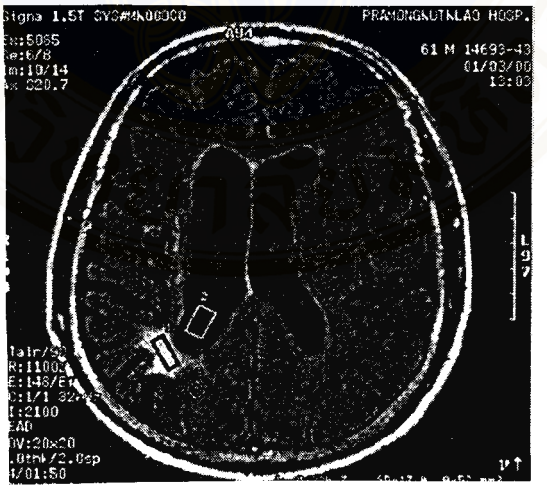

Figure 29. Showing the measurement of SI of CSF, periventricular lesion, and WM in fast FLAIR axial image of 61 years old male.

4.2.2.3 Measurement of standard deviation (SD) of background air

The SD of the mean SI of background air was used to estimate noise. This SD was measured in areas free of ghost artifacts (SD_{air}), and then the rectangle was placed on precisely the same volume of background air on each the other images.

4.2.2.4 The precision of random sampling for SI measurement.

To determine variation in random sampling for SI measurement, we measured SI in three different area within each lesion, CSF, and WM (Figure 30). The coefficient of variation (SD divided by the mean) of SI in three different areas within each lesion, CSF, and WM represents to the precision of random sampling.

4.2.2.5 Objective image assessment.

For objective image assessment, SNR of the individual type tissues, CR and CNR of periventricular lesions to normal adjacent WM and CSF, were determined by following the equations(17), (14) and (15), respectively.

$$SNR_{tissue} = S_{tissue} / SD_{air} \quad (17)$$

$$CR_{tissue(1,2)} = (S_{tissue(1)} - S_{tissue(2)}) / (S_{tissue(1)} + S_{tissue(2)}) \quad (14)$$

$$CNR_{tissue(1,2)} = (S_{tissue(1)} - S_{tissue(2)}) / SD_{air} \quad (15)$$

Where SNR is signal to noise ratio.

CR is contrast ratio.

CNR is contrast to noise ratio.

S is signal intensity.

Then SNR, CR, and CNR were compared among all of the five different TI images to determined the TI that cause optimal CSF suppression.

The CR and CNR of the fast FLAIR images with the optimal inversion for CSF suppression with good lesions to CSF contrast obtained from our study and those of the fast FLAIR images with TR/TI 11000/2200 msec as recommended by Signa Horizon 1.5 Tesla protocal guide for optimal CSF suppression with good gray to white matter contrast (23) were compared by using a paired one-tailed *t* test (P-value < 0.05). Research of John N.Rydberg (5) recommended TR/TI exceeding 11000/2600 to provide 90% lesion (multiple sclerosis) to white matter contrast. So comparison between CR, CNR of images with TI 2400 msec and optimal TI for CSF suppression obtained from our study was done by using a paired one-tailed *t* test (P-value < 0.05). TI 2400 msec was used instead of TI 2600 because it is the maximal value in our study.

Last, the SNR, CR and CNR of the fast FLAIR images with optimal TI for CSF suppression and those of T_2-weighted FSE images were compared by using a paried one-tailed *t* test (p-value < 0.05).

A.

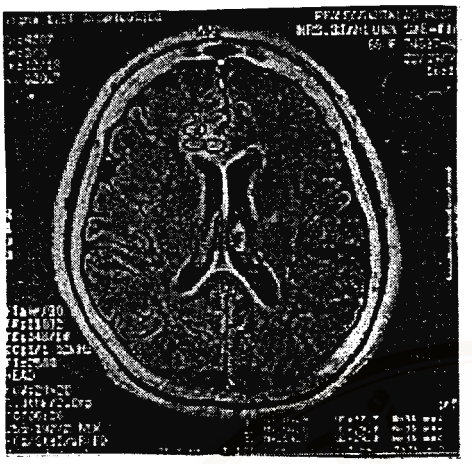

C.

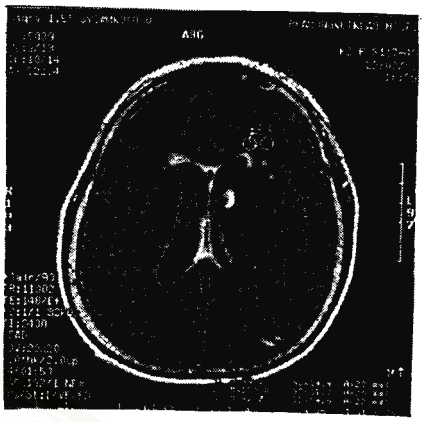

B.

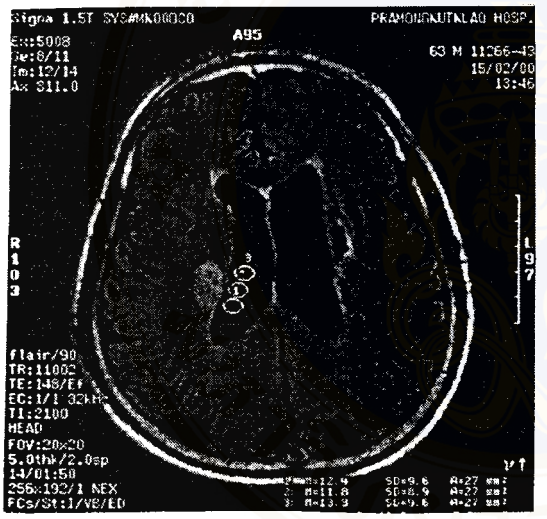

Figure 30. Showing the position of the random sampling to measure SI of each tissues in fast FLAIR images. (A) the position of the lesion which was measured by random sampling in three different areas. (B,C) the position of CSF and WM was measured by random sampling in three different areas, respectively.

CHAPTER V

RESULTS

5.1. T_1 values of CSF in lateral ventricles.

T_1 value of CSF was measured in 20 healthy volunteers with IR technique. The volunteers subjects (10 men, 10 women) ranged in age from 19 to 50 years (mean, 32.9±10.3). They are Thais. The volunteers were performed with TR of 11,000 msec, and three different TI values of 1500, 2000, 2600 msec. The SI of CSF was measured on each of three IR images. The acquired data from measurement is plotted between SI values with difference TI and determinate T_1 of CSF by using the SPSS program for window. When we know T_1 value of CSF, we can calculate interval of TI value to get the signal from CSF to be null in the equation (1).

T_1 values of CSF were averaged from 14 healthy volunteers because lateral ventricles of six volunteer subjects are too small to measure the SI, which calculation of T_1 represent in Appendix A. T_1 value of CSF are shown in Table III, these data are normal distribution with 95% confidence level.The mean T_1 value of CSF (± S.D) in 14 volunteer subjects is 3225.7 ± 173.8 msec (3051.9 to 3399.5 msec), the coefficient of variance is 5.39%. The statistical accuracy of these data is 95% confidence level and 90% power of test, that maximum allowable error between this statistical sample value and the population value is 5% of mean statistical sample value.

Table III. T_1 of CSF in healthy volunteers

No.	AGE	SEX	T_1 of Lt. Ant. horn (msec.)	T_1 of Rt. Ant. horn (msec.)	L / R ratio	T_1 (msec)
1	19	M	3339.3	3166.9	1.054	3253.1
2	22	F	3301.1	3420.7	0.965	3360.9
3	22	M	3198.4	3023.4	1.058	3110.9
4	22	M	3339.3	3141.1	1.063	3240.2
5	23	M	2853.5	2817.0	1.013	2835.2
6	23	M	3324.5	3281.4	1.013	3302.9
7	26	F	3352.3	3249.0	1.032	3300.7
8	34	F	3418.7	3298.5	1.036	3358.6
9	40	M	2903.0	3107.3	0.934	3005.2
10	42	M	3256.8	3170.7	1.027	3213.8
11	43	F	3423.8	3211.2	1.066	3317.5
12	43	M	3419.7	3567.1	0.959	3493.4
13	47	F	3072.4	2991.5	1.027	3031.9
14	50	M	3436.5	3233.2	1.063	3334.8
		Mean			1.022	3225.7
		Standard deviation			0.042	173.8
		Variance				30189.1
		Coefficient of variance				5.39%

The ratio of T_1 CSF value in the left and right anterior horn of lateral ventricles (L/R ratio) is measured by the precision of the T_1 measurement technique. This ratio is 1.022 ± 0.042. It is not significantly different from 1.000 indicating symmetrical of right to left hemisphere identity, suggesting that within - volunteer precision was excellent.

The result obtained in the our research, comparing the previous research, R. Grant Steen and Suzanne A. Gronemeyer (8). From previous research (8), T_1 values of CSF were measured in 26 healthy volunteers, (14 men, 12 women) ranged in age from 18.2 to 59.6 years (mean 34.6 years ±9.8). T_1 of CSF from previous research were avearged from 20 volunteers because six subjects had ventricles too small for measurement of SI. These data are listed in Table IV and summarized in Figure 31.

Table IV. Mean T_1 relaxation time of CSF (± S.D) of our and previous research (8).

Research	Mean T_1 (msec)	CV (%)	Range (msec)
Our research	3,226 ± 174	5.4	2,835-3,494
Previous research	4,282 ± 1,552	36.2	2,495-7,791

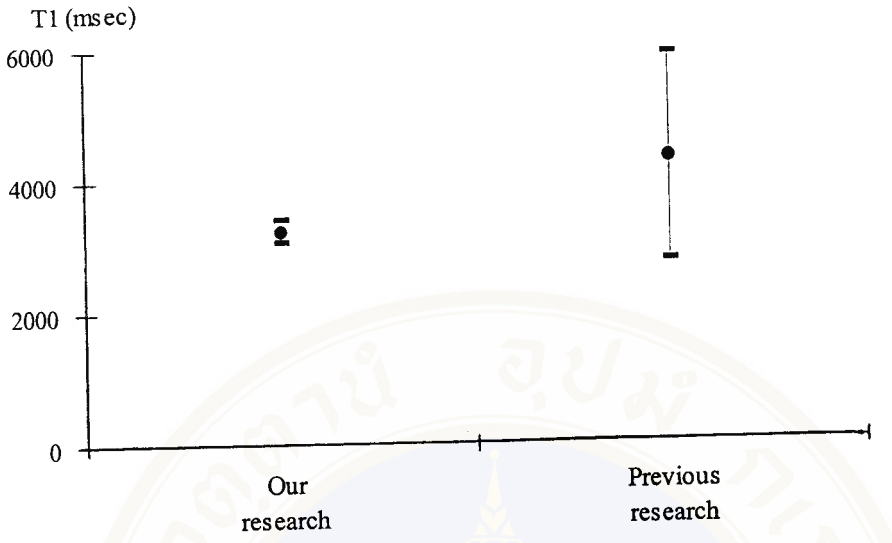

Figure 31. Showing the mean (± S.D) of T_1 of CSF obtained in our research, is in interval of the mean (± S.D)T_1 of CSF obtained in previous research.

5.2 Image assessments of fast FLAIR pulse sequence in various TI

5.2.1 SNR

The data measurements of SI of individual type tissue are shown in Appendix D. The SI of each tissues is calculated for SNR. The precision of the random sampling for SI measurement data are shown in Appendix C. These data of SNR of individual types of tissue in various TI of fast FLAIR pulse sequence show in Appendix E. The SNR of individual types of tissue in various TI of fast FLAIR pulse sequence are normal distribution with 95% confidence level. The mean SNR of individual types of tissue (± S.D) versus various TI is plotted in Figure 32-34.

5.2.1.1 The mean SNR of the lesions versus various TI of FLAIR pulse sequence is shown in Figure 32. The mean SNR of the lesion were obtained from 41 lesions, those increased with TI. From the data, the fast FLAIR pulse sequence with a

lesions, those increased with TI. From the data, the fast FLAIR pulse sequence with a TI of 2000 msec, give minimum average SNR of the lesion. While the fast FLAIR pulse sequence with a TI of 2400 msec, give maximum average SNR of the lesion.

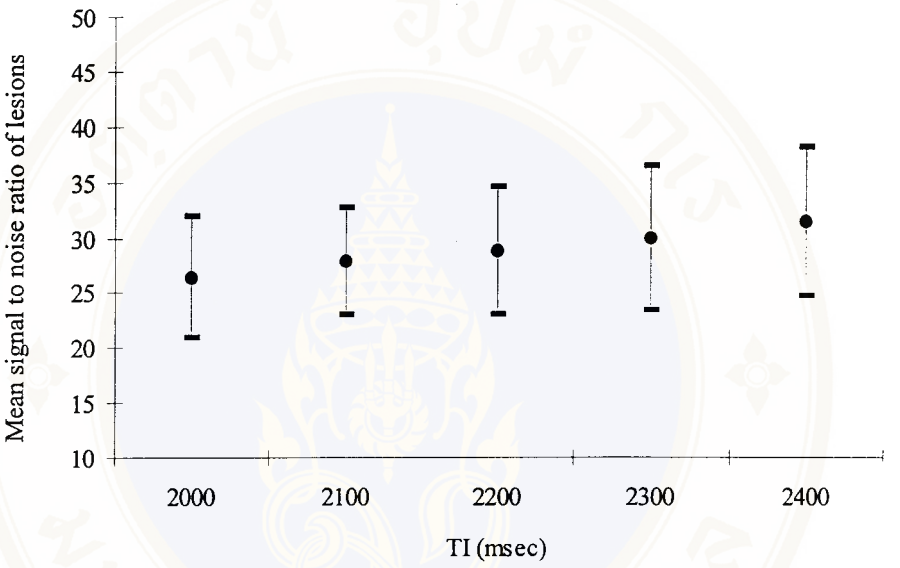

Figure 32. Plot of the mean SNR of the lesions (± SD) versus different TI. The mean SNR of the lesions increased with TI.

5.2.1.2 The mean SNR of CSF versus various TI of the fast FLAIR pulse sequence is shown in Figure 33. The mean SNR of CSF were obtained from 41 CSF areas. The fast FLAIR pulse sequence with a TI of 2100 msec, give minimum mean SNR of CSF. The fast FLAIR pulse sequence with TI higher than 2100 msec is increasing the value of mean SNR of CSF depend on the value of TI that is maximum at 2400 msec. We calculated TI values that nulls the CSF signal from the equation (10), expressing as:

at 2400 msec. We calculated TI values that nulls the CSF signal from the equation (10), expressing as:

$$TI_{(null)} \cong 0.693\ T_1$$

This performance is consistent with a mean T_1 of healthy volunteer from this experiment (3225.7 msec). Therefore TI that nulls the CSF signal that calculate from the equation (10) is 0.693 x 3225.7 msec = 2235 msec. But TI of CSF that gives near zero or minimum of SNR_{CSF} from this experiment of FLAIR pulse sequence in different TI, is TI of 2100 msec. It values difference from the null TI of CSF in calculation from the equation (10)approximate 4%.

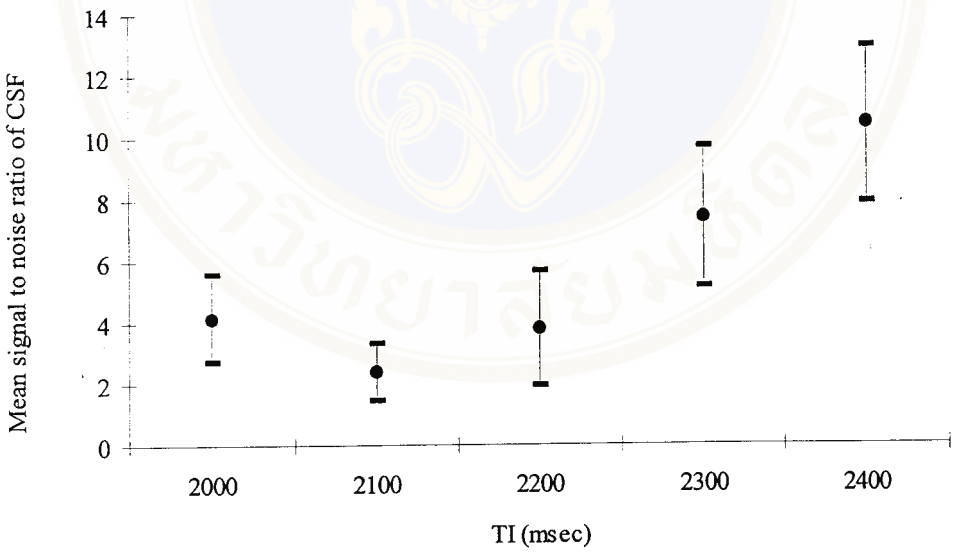

Figure 33. Plot of the mean SNR of CSF (± SD) versus different TI. The fast FLAIR pulse sequence with a TI of 2100 msec, give minimum mean SNR of CSF. The fast FLAIR pulse sequence with TI higher than 2100 msec, these values increased with TI that is maximum at TI 2400 msec.

FLAIR pulse sequence with TI higher than 2100 msec, these values increased with TI that is maximum at TI 2400 msec.

5.2.1.3 The mean SNR of WM versus various TI of the fast FLAIR pulse sequence is shown in Figure 34. The mean SNR of WM were obtained from 36 WM areas. They increased with TI. From the data, the fast FLAIR pulse sequence with a TI of 2000 msec, give minimum average SNR of the WM. While the fast FLAIR pulse sequence with a TI of 2400 msec, give maximum mean SNR of the WM.

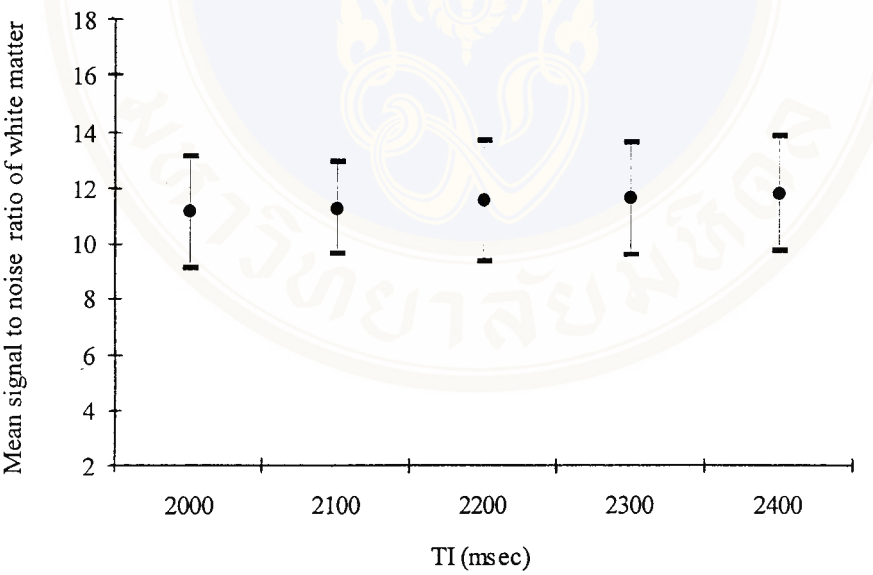

Figure 34. Plot of the mean SNR of WM (± SD) versus different TI. The mean SNR of WM increased with TI. These means that, for the fast FLAIR pulse sequence with a TI of 2000 msec, give minimum mean SNR of WM. While the fast FLAIR pulse sequence with a TI of 2400 msec, give maximum mean SNR of WM.

The difference of the SNR in the lesion, CSF, and WM in various TI is shown in Figure 35. The fast FLAIR pulse sequence of TI 2100 msec gives the maximum difference of SNR between the lesions and CSF, while TI of 2400 msec gives the minimum. Unlike the difference of SNR between lesion and WM, the difference of SNR between the lesion and WM is maximum in TI 2400 msec, and minimum in TI 2000 msec.

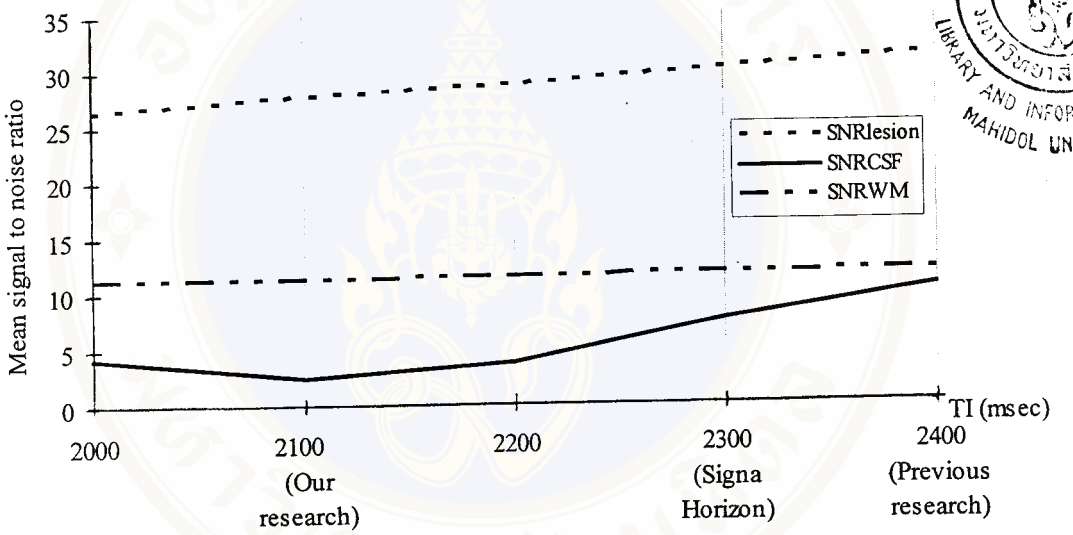

Figure 35. Plot of the difference of the SNR in the lesion, CSF, and WM in different TI.

5.2.2 CNR

5.2.2.1 The CNR of the lesions to CSF are shown in Appendix E. These data are normal distribution with 95% confidence level. The mean CNR of lesions to CSF (± S.D) versus various TI of the fast FLAIR pulse sequence were obtained from 41 CNR of lesions to CSF, that are shown in the Figure 36. The fast FLAIR pulse sequence provided the highest CNR of lesions to CSF in TI 2100 msec, and the lowest CNR of lesions to CSF in TI 2400 msec. This means that, the fast FLAIR pulse sequence with a TI of 2100 msec gives the maximum increasing lesion conspicuity in the periventricular region. This result is similar to the different SNR between the lesions and CSF.

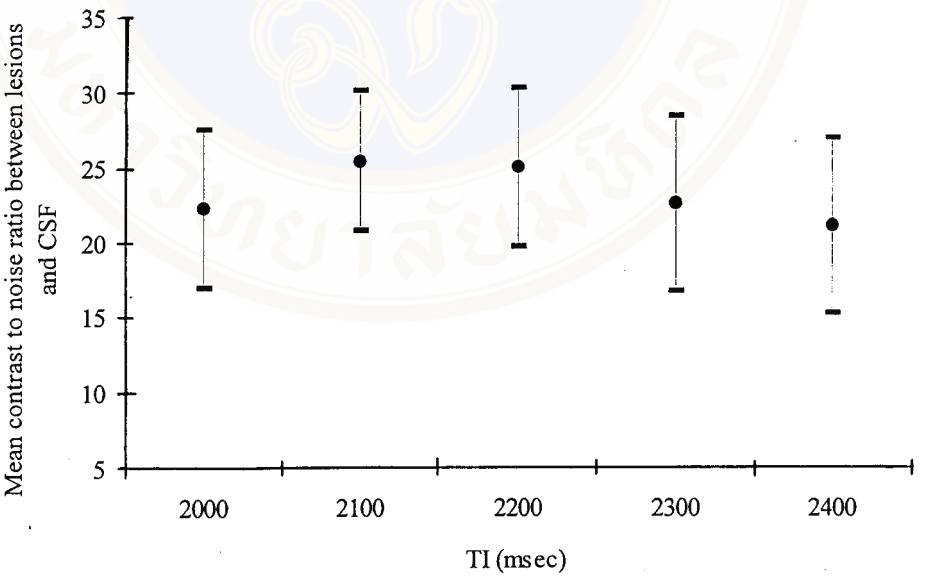

Figure 36. Plot of the mean CNR between the lesions and CSF versus different TI.

5.2.2.2 The CNR of the lesions to WM are shown in Appendix E. These data are normal distribution with 95% confidence level. The mean CNR of lesions to WM (± S.D) versus various TI of the fast FLAIR pulse sequence were obtained from 36 CNR of lesions to WM, that are shown in the Figure 37. The fast FLAIR pulse sequence with TI 2400 msec provided the highest CNR of lesions to WM and the lowest CNR of lesions to WM in TI 2000 msec. This result is similar to the different SNR between the lesions and WM.

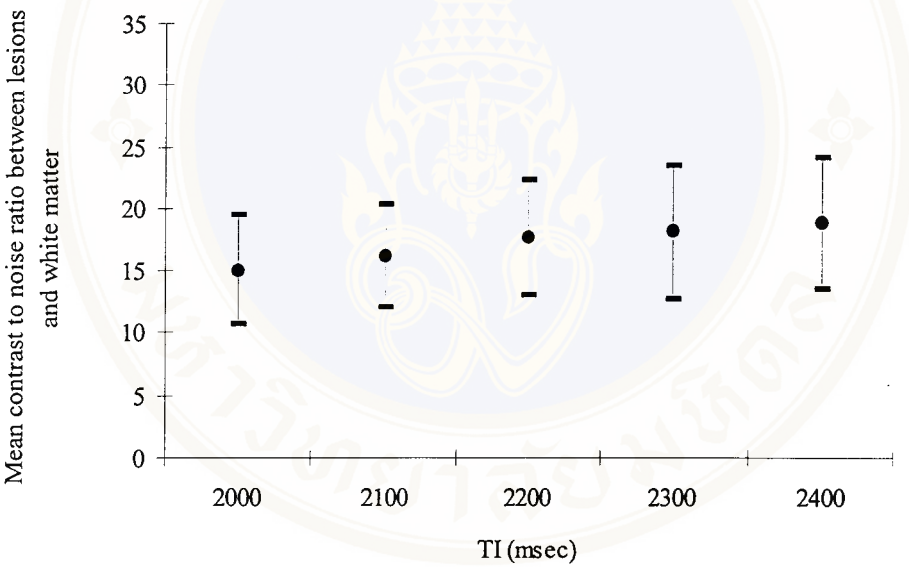

Figure 37. Plot of the mean CNR between the lesions and WM versus different TI. The fast FLAIR pulse sequence of TI 2400 msec provided the highest CNR of the lesions to WM, and the lowest CNR of the lesions to WM in TI 2000 msec.

5.2.3 CR

5.2.3.1 The CR of the lesions to CSF is shown in Appendix E. These data are normal distribution with 95% confidence level. The mean CR of the lesions to CSF (± S.D) versus various TI of the fast FLAIR pulse sequence were obtained from 41 CR of the lesions to CSF, that are shown in Figure 38. The fast FLAIR pulse sequence with TI 2100 msec provided the highest CR of the lesions to CSF, and the lowest CR of the lesions to CSF in TI 2400 msec. The result is similar to the CNR of the lesion and CSF.

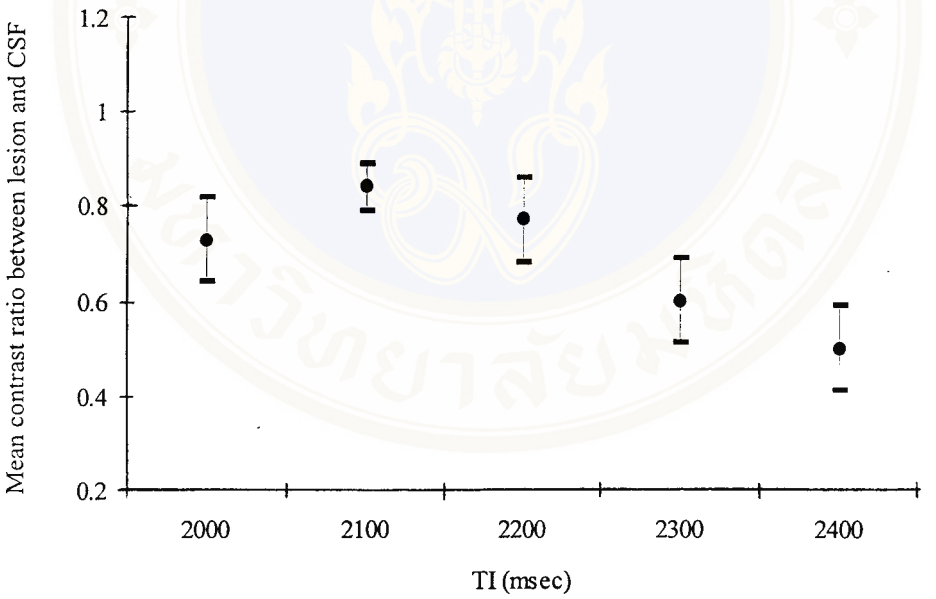

Figure 38. Plot of the mean CR between the lesions and CSF versus different TI. The fast FLAIR pulse sequence of TI 2100 msec provided maximum the mean CR of the lesions to CSF, and minimum the mean CR of the lesions in TI 2400 msec.

5.2.3.2 The CR of the lesions to WM is shown in Appendix E. These data are normal distribution with 95% confidence level. The mean CR of the lesions to WM (± S.D) versus various TI of the fast FLAIR pulse sequence were obtained from 36 CR of the lesions to WM, that are shown in Figure 39. The fast FLAIR pulse sequence of TI 2400 msec provided the highest CR of the lesions to WM, and the lowest CR of the lesions to WM in TI 2000 msec. The result is similar to the CNR between the lesions and WM.

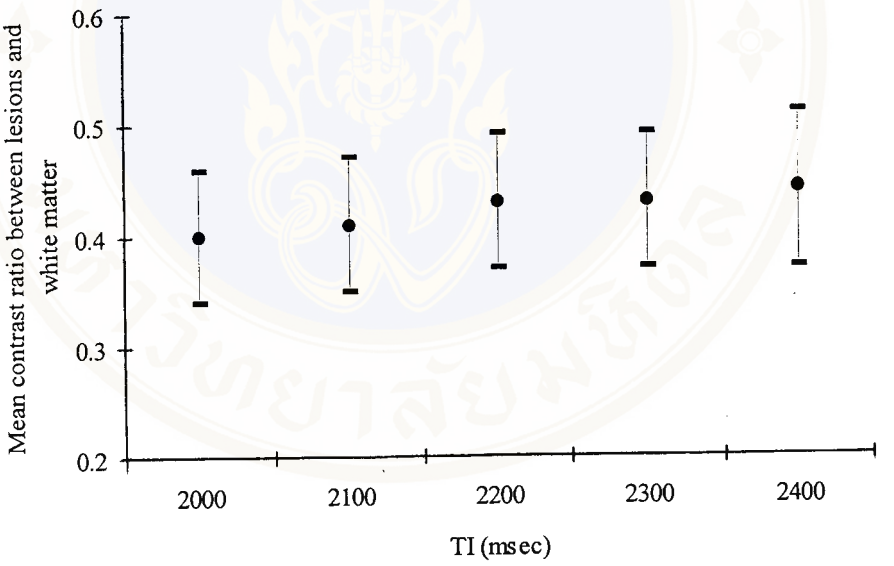

Figure 39. Plot of the mean CR between the lesions and WM versus different TI. The fast FLAIR pulse sequence of TI 2400 msec provided the highest CR of the lesions to WM and the lowest CR of the lesions to WM in TI 2000 msec.

Images of fast FLAIR pulse sequence in difference TI from one patient studies with periventricular lesion are shown in Figure 40(A-E). The Figure 40B shows that the fast FLAIR image with TI 2100 msec gives the best contrast enhancement of the lesion to interfaces of CSF. The Figure 40 E shows that the fast FLAIR image with TI 2400 msec gives poor contrast enhancement of the lesion to interfaces of CSF.

The optimization of contrast is considered to the fast FLAIR pulse sequence, specifically the contrast of the periventricular lesions to CSF. Our research show that fast FLAIR images with TI 2100 msec provides the better CR and CNR of the periventricular lesions to CSF than fast FLAIR images with TI 2000, 2200, 2300, and 2400 msec.

A.

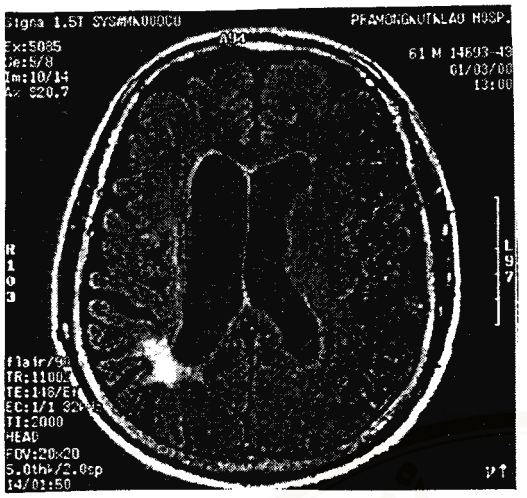

D.

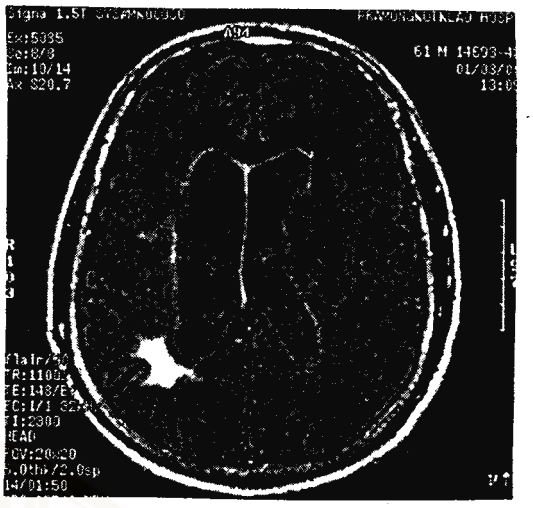

B.

E.

C.

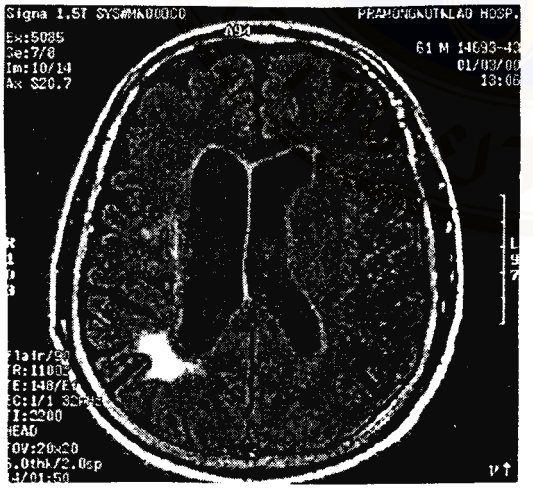

Figure 40. Periventricular lesion in a 61-years-old patient. (A) the fast FLAIR images with TI2000 msec, (B) the fast FLAIR images with TI 2100 msec gives the best contrast enhancement of the lesion to interfaces of CSF, (C,D) the fast FLAIR images with TI 2200, 2300 msec, (E) the fast FLAIR images with TI 2400 msec gives poor contrast enhancement of the lesion to interfaces of CSF.

5.3 Image assessments of T_2-weighted FSE images.

5.3.1 SNR

The SNR of individual type tissue for T_2-weighted FSE techniques are normal distribution with 95% confidence level. These data represent in Appendix F .

5.3.2 CNR and CR.

The CNR and CR of the lesions to CSF and WM for T_2-weighted FSE pulse sequence are normal distribution with 95% confidence level. These data represent in Appendix F.

5.4 Comparing of the SNR, CNR and CR on the fast FLAIR images with optimal TI for CSF suppression that obtained by our research, Signa Horizon 1.5 Tesla protocal guide (23), previous research (5) and T_2-weighted FSE images.

Our study shows that the fast FLAIR with optimal TI 2100 mesc provides CSF suppression with good lesion to CSF contrast. The Signa Horizon 1.5 Tesla protocol guide (23) recommend that the fast FLAIR with optimal TI 2200 msec for CSF suppression with good gray to white matter contrast. The previous research (5) recommended TR/TI exceeding 11000/2600 to provide 90% lesion (multiple sclerosis) to WM contrast.

The SNR, CR, and CNR of FLAIR with optimal TI 2100 that obtained by our research were compared with those of FLAIR with optimal TI 2200 as recommended by Signa Horizon (23), FLAIR with optimal TI 2400 (TI 2400 msec was used instead of TI 2600 because it is the maximal value in our study) as recommended by previous research (5), and T_2 -weighted images.

5.4.1 The SNR of the lesions, WM, and CSF.

The mean SNR of individual types tissue (± S.D) for fast FLAIR with TI 2100, 2200, 2400 msec and T_2-weighted FSE images are shown in TableV.

Table V. The SNR (mean ± S.D) of individual types of the fast FLAIR images with TI 2100, 2200, 2400 msec and T_2-weighted FSE images.

SNR of tissues	T_2-weighted FSE	FLAIR FSE with TI 2100 msec (Our research)	FLAIR FSE with TI 2200 msec (Signa)	FLAIR FSE with TI 2400 msec (Previous research)
SNR_{lesion}	39.04±8.43	27.84±4.82	28.77±5.72	31.23±6.65
SNR_{WM}	14.44±1.97	11.28±1.68	11.51±2.15	11.78±2.07
SNR_{CSF}	60.28±7.41	2.41±0.91	3.80±1.85	10.39±2.51

Note.- FSE indicates fast spin-echo

The fast FLAIR images with optimal TI 2100 msec for CSF suppression that obtained by our research gives the maximum difference of the SNR between the lesions and CSF, while those of T_2 -weighted FSE images is minimum. These result are shown in Figure 41.

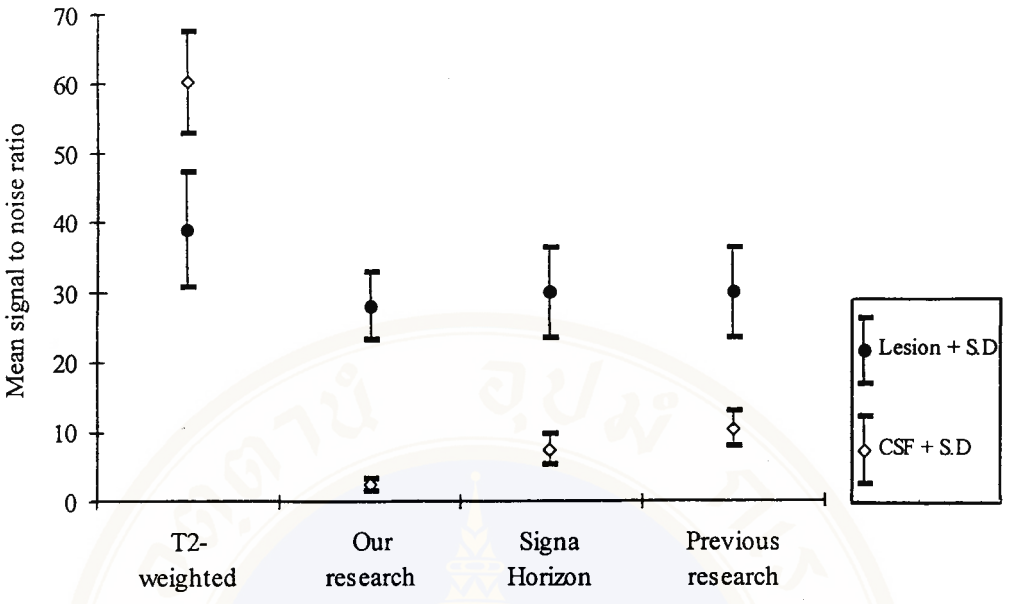

Figure 41. Plot of the mean SNR (± S.D) of the lesions and CSF in different techniques.

5.4.2 The mean CNR of the lesions to CSF.

The mean CNR of lesions to CSF of the fast FLAIR images with optimal TI 2100 msec for CSF suppression that obtained by our research was greater than those of the fast FLAIR images with TI 2200 msec as recommended by Signa horizon (23) for CSF suppression, but this difference was not significant (p-value > 0.05).

The CNR of the lesions to CSF of FLAIR with TI 2100 (our research), and FLAIR with TI 2200 (Signa Horizon) were significantly superior to T_2-weighted images (p-value < 0.05). Conversely, FLAIR images with TI 2400 (previous research) is less CNR of the lesions to CSF than T_2-weighted images, but this

difference was not significant (p-value > 0.05). These results are summarized in Table VI and Figure 42.

Table VI. The CR and CNR (mean ± S.D) of the lesion to CSF and WM of the fast FLAIR with TI 2100, 2200, 2400 msec and T_2-weighted FSE images.

	T_2-weighted FSE	FLAIR FSE with TI 2100 msec (This research)	FLAIR FSE with TI 2200 msec (Signa) *	FLAIR FSE with TI 2400 msec
Lesion to CSF				
CR ± SD	0.22 ± 0.09	0.84 ± 0.05	0.77±0.09	0.50±0.09
CNR ± SD	21.24 ± 8.26	25.42 ± 4.68	24.98±5.26	21.01±5.87
Lesion to WM				
CR ± SD	0.44 ± 0.07	0.41 ± 0.06	0.43±0.06	0.44±0.07
CNR ± SD	23.71 ± 7.70	16.17 ± 4.06	17.67±4.62	18.87±5.30

Note.- * Signa indicates Manufacturer recommendation.

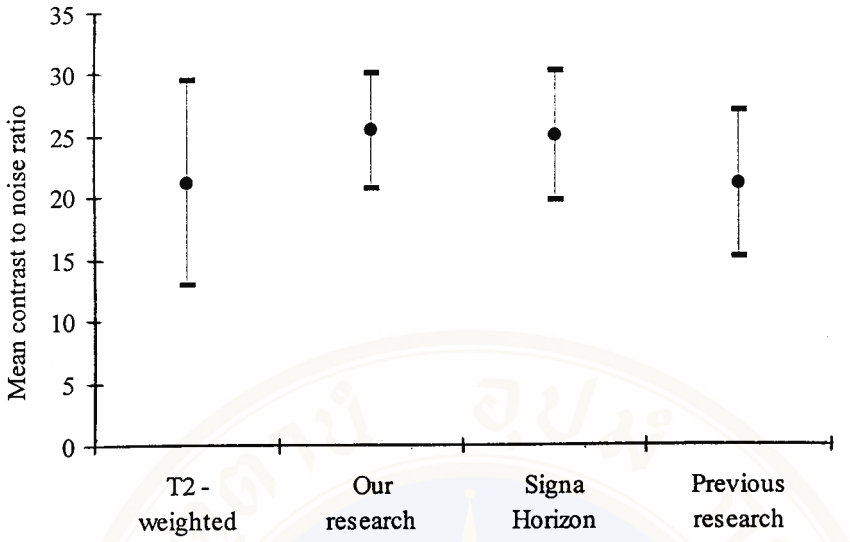

Figure 42. Plot of the mean CNR (±S.D) of the lesions to CSF versus different techniques.

5.4.3 The mean CR of the lesions to CSF.

The mean CR of the lesions to CSF, fast FLAIR images with TI 2100 msec was significantly superior to fast FLAIR images with TI 2200 (p-value < 0.0005).

The mean CR of the lesions to CSF of FLAIR with TI 2100 (our research), FLAIR with TI 2200 (Signa Horizon) were significantly superior to T_2-weighted images (p-value < 0.0005). These results are shown in Table VI and Figure 43.

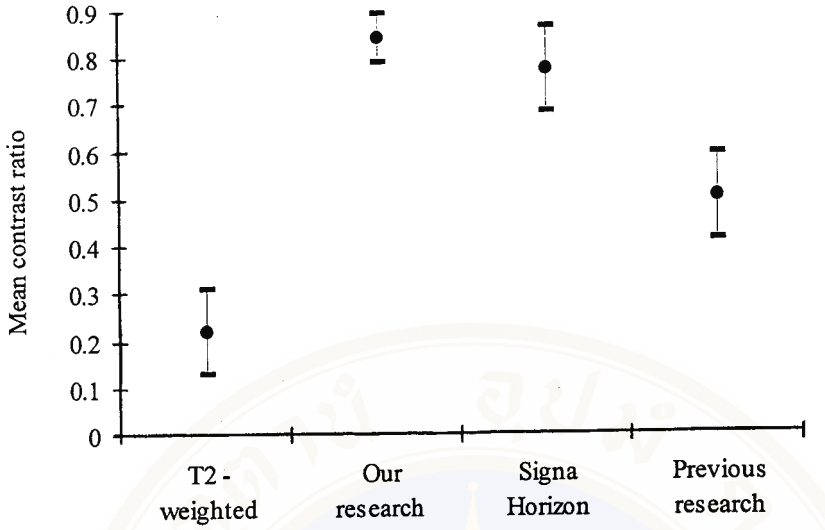

Figure 43. Plot of the mean CR (±S.D) of the lesions to CSF versus different techniques.

5.4.4 The mean CNR of the lesions to WM.

The mean CNR of the lesions to WM of the fast FLAIR images with TI 2200 msec as recommended by Signa Horizon 1.5 Tesla protocol guide (23) for CSF suppression were significantly superior to the fast FLAIR images with TI 2100 msec that obtained by our research for CSF suppression (p-value < 0.0005).

When we consider Figure 37 and 38, CNR and CR between the lesions to WM was increased with TI that those maximum with TI 2400 msec. Then we can estimate values of the CNR and CR between the lesion to WM from these curve that fast FLAIR sequence with TI higher than 2400 msec should increased with along TI. This result is consistent with previous research, John N. Rydberg (5)

recommend that TR/TI times exceeding 11000/2600 msec provide about 90% of the lesion (multiple sclerosis) to WM contrast possible theoretically.

The mean CNR of the lesions to WM of the fast FLAIR images with TI 2400 msec as recommended by previous research (5) were significantly superior to the fast FLAIR images with TI 2100 msec that obtained by our research for CSF suppression (p-value < 0.0005).

The CNR of the lesions to WM of T_2-weighted were significantly superior to the FLAIR with TI 2100 (Our research), FLAIR images with TI 2200 (Signa Horizon), and FLAIR images with TI 2400 (Previous research)(p-value < 0.0005). These result are shown in Fig. 44.

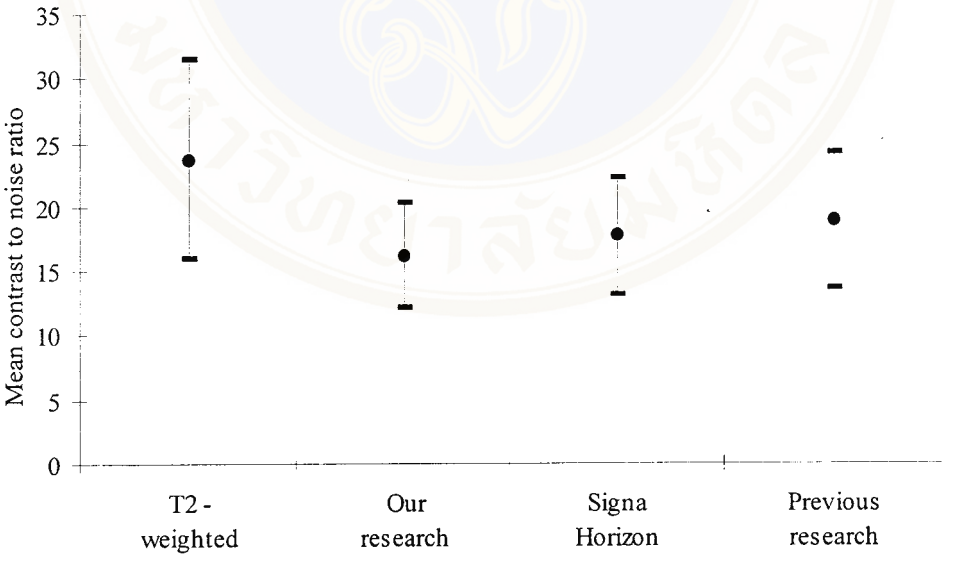

Figure 44. Plot of the mean CNR (±S.D) of the lesions to WM versus different technique.

5.4.5 The mean CR of the lesions to WM.

The mean CR of the lesions to WM, fast FLAIR images with TI 2200and TI 2400 msec was significantly superior to fast FLAIR images with TI 2100 (p-value < 0.005).

The CR of the lesions to WM of T_2-weighted were significantly superior to the FLAIR with TI 2100 (Our research), and FLAIR images with TI 2200 (Signa Horizon) (p-value < 0.005). Comparing FLAIR with TI 2400 (Previous research) and T_2-weighted images, CR of the lesions to WM were similar for both sequences without statistical significance. These result are showed Figure 45.

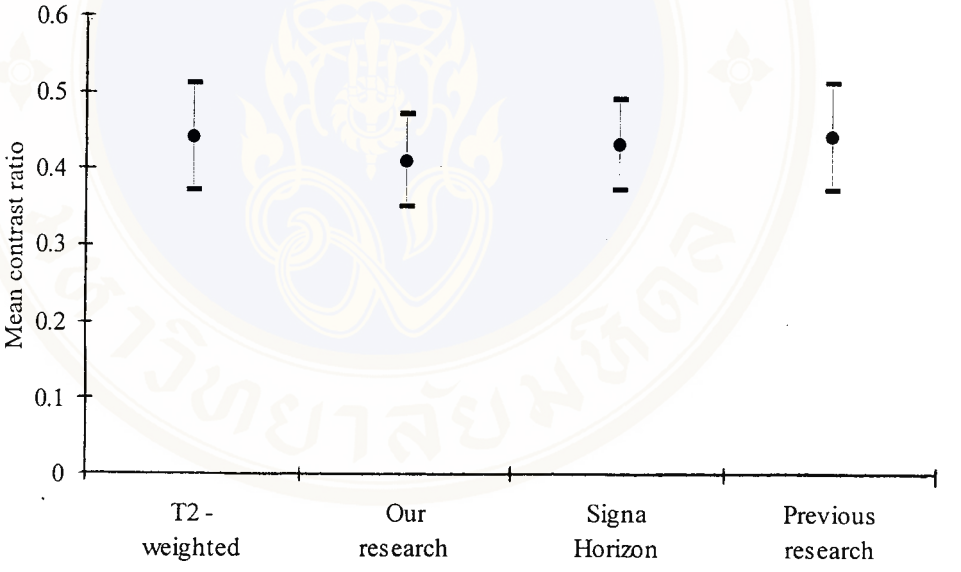

Figure 45. Plot of the mean CR (±S.D) of the lesions to WM versus different technique.

Therefore the fast FLAIR images with TI 2100 msec provides the better optimal TI for CSF suppression with good periventricular lesions to CSF contrast than fast FLAIR with TI 2000 (Signa Horizon), and with TI 2400 msec (Previous research).

In addition to, the fast FLAIR images with optimal TI 2100 msec for CSF suppression with good lesions to CSF contrast improved lesion conspicuity of the periventricular lesions that have side touching the CSF border of lateral ventricles more than T_2-weighted FSE images (Figure 46) .

A.

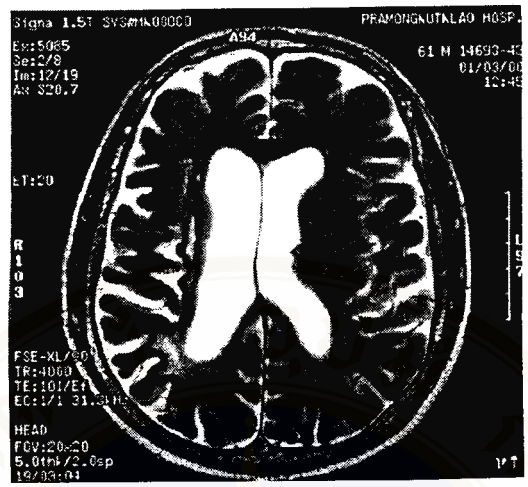

B.

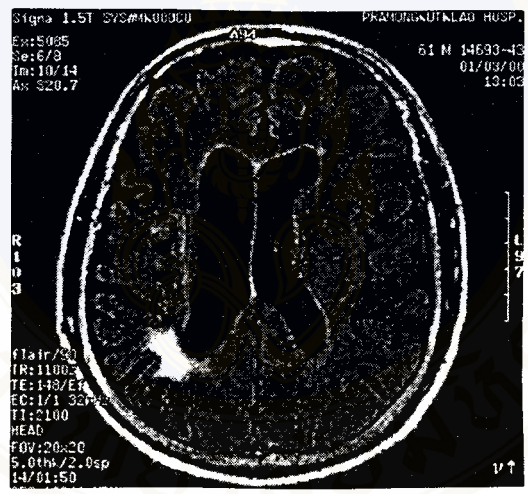

Figure 46. Periventricular lesions in a 61-years-old patient. (A) T_2-weighted FSE axial image (TR/TE = 4000/101) demonstrates a lesion at the periventricular WM of right parietal lobe. (B) fast FLAIR axial image (TR/TE/TI = 11,000/148/2100) shows the same lesion with T_2-weighted image that it clearly visible than T_2-weighted image at the same level.

CHAPTER VI

DISCUSSION

6.1 T_1 values of CSF in lateral ventricles.

Our research showed that the mean (±S.D) of T_1 relaxation time of CSF in lateral ventricles of 14 healthy volunteers is 3,225.7 ± 173.8. However, T_1 of CSF (mean±SD) obtained by previous research (8) was 4,282 ± 1,552 msec. Our result is consistency with previous research, R. Grant Steen and Suzanne A. Gronemeyer (8) that the mean (± S.D) T_1 of CSF obtained in our research is in interval of the mean (± S.D) T_1 of CSF obtained in previous research (8). The mean T_1 of CSF obtained in our research is 24.7 % less than that obtained in previous research (8), perhaps because of difference in the method. Our research, T_1 was calculated by using the equation [10] expressing as:

$$TI_{null} \cong 0.693\ T_1$$

When we know TI(null) of CSF, then we can solve this equation for T_1 value of CSF. We determine TI(null) by using the program SPSS 7.5 for window to estimate the logarithmic curves that were plotted between SI of CSF and different TI. But in the previous research (8), T_1 value was calculated by using the mean SI values of CSF in

different TI that were fitted to the following equation (18), adapted for the SigmaPlot program (Jandel Scientific, San Rafael, Calif) on a MacIntosh Iivx;

$$SI = N(H) [1 + 2e^{-(TR-TE/2)/TI} - e^{-TR/TI} - 2e^{-TI/T_1}] e^{-TE/T_2} \qquad (18)$$

Where N(H) is the spin-density factor, TR is 2,500 msec, TE is 20 msec, and TI is 100, 500, 900, or 2,460 msec.

However, the major disadvantage of the IR technique is that it takes a lot of time, because it is necessary to use several different inversion time, and a long examination caused problems in a clinical setting. Therefore, the next study should improve to decrease the total examination time required for IR measurement of human brain T_1, while maintaining the precision and accuracy inherent in the technique (8).

6.2 Image assessments of fast FLAIR pulse sequence in various TI.

6.2.1 SNR

The mean SNR of the lesion and WM increase with TI that is maximum in fast FLAIR pulse sequence with TI 2400 msec, and minimum with TI 2000 msec. The longer TI allows the longitudinal magnetization of the lesions that are flipped 180^0 to more recover along a T_1 growth curve before applying a 90^0 RF pulse (2). The amount of magnetization flipped into the x-y plane will depend on the amount of the longitudinal magnetization that has recovered during time TI. We measure this flipped magnetization. Therefore, at this point we get a free induction decay proportional to the longitudinal magnetization flipped into the x-y plane.

When we compare the mean SI between the lesion and WM at the same TI, the mean SI of the lesion is greater than WM. Most pathological lesions have slower T1 recovery curves than those of WM because of their vasogenic edema (which contains H_2O) and also have a longer T_2 than that WM (13). Then after the lesions and WM have flipped 180^0, the T_1 recovery curve for the lesion begins lower that is more negatives along the Z axis than is WM. The longitudinal magnetization for the lesion grows along its T_1 recovery curve until it reaches its maximum. The T_1 growth curve for WM, because of its shorter T_1, it recovers more rapidly along its T_1 curve than does the lesion to reach its maximum. FLAIR sequence uses a long TE to enhance the T_2 effect, so at the time TI, a 90^0 excitation pulse is applied. The lesion and WM will have longitudinal magnetization that will flip into the x-y plane and give off a signal according to their T_2 curves. The lesions have the lesser dephasing, and thus longer T_2 decay curve than WM (Figure 16). Therefore the lesions are brighter than WM and have SI more than WM. The relationship between increased inversion time and signal intensity is that when TI is increased, the SI of WM is less increased than SI of the lesion because WM has shorter T_1 and recovers more rapidly along its T_1 curve than lesions to reach its maximum (17).

The mean SI of CSF is minimum (near zero) in the fast FLAIR pulse sequence with TI 2100 msec. This TI valued is difference from the null TI of CSF in calculation in the equation (10) approximate 4%, these difference is not significant. However, when we consider the Figure 33, it shows the null SI of CSF is between TI 2100 and 2200 msec. So the next study should measurement the mean SI of CSF in FLAIR

pulse sequence with TI values between TI 2100 and 2200 msec to provide the null SI of CSF

6.2.2 CNR and CR

Our research showed that the fast FLAIR pulse sequence with optimal TI 2100 msec for optimal CSF suppression, provided the highest CNR and CR between lesions to CSF. While Signa Horizon 1.5 Tesla protocol guide recommend fast FLAIR sequence with TI 2200 msec for optimal CSF suppression. Comparing of both techniques, lesions to CSF contrast to noise ratio was greater for the fast FLAIR with TI 2100 msec than for the fast FLAIR sequence with TI 2200 msec, but this difference was not significant (p-value > 0.05). Lesions to CSF contrast ratio was significantly higher for the fast FLAIR with TI 2100 msec than for the fast FLAIR sequence with TI 2200 msec (p-value < 0.0005).

These difference may be because Signa Horizon 1.5 Tesla protocol guide is considered for theTI that is optimal suppression with good gray-white matter contrast (23). While this research is considered for the TI that is optimal CSF suppression with good lesion to CSF contrast.

The result shows the fast FLAIR with TI 2100 msec provides the optimal TI for CSF suppression with good periventricular lesions to CSF more than fast FLAIR with TI 2200 msec (Signa Horizon) and TI 2400 msec (Previous research). However, Figure 36 and 37, show that the fast FLAIR sequence with TI 2100 and 2200 msec provides the higher CNR and CR than another TI. Then further study should study the CNR and CR between the lesion to CSF in fast FLAIR sequence with

TI values between TI 2100 and 2200 msec to provide the best optimal TI for CSF suppression with good periventricular lesions to CSF.

6.3 Image assessments of the lesion to CSF contrast optimized of the fast FLAIR images and T_2-weighted FSE images.

The SNR of the lesion, CSF and WM on T_2-weighted FSE images were greater than on the fast FLAIR images with TI 2100 (Our research), TI 2200 (Signa Horizon), and TI 2400 msec (Previous research) (p-value < 0.0005). Low SNR of lesion and WM on fast FLAIR images with different TI because 90^0 RF exciting pulse is applied at a TI, after the 180^0 inverting pulse. This 90^0 RF exciting pulse flips the partially recovery of longitudinal magnetization into the transverse plane. So the signal of the lesion and WM on the fast FLAIR images decrease.

The CNR between the periventricular lesions to CSF on the fast FLAIR images with TI 2100 msec (Our research) was significantly superior to T_2-weighted FSE images (p-value < 0.05). The CNR values between the periventricular lesions to CSF depend on CR of the lesions to CSF, and SNR of both tissues. When we consider Fig.41, it shows our research technique provides the higher difference between the SNR of the lesions and CSF than T_2-weighted FSE sequence. Although the T_2-weighted FSE sequence provides the high SNR of both tissues more than our research techniques, but the effect of the difference between the SNR of the lesion and CSF is more than those of the SNR of both tissues.

In contrast, the CNR and CR between the periventricular lesion to WM on T_2-weighted FSE images was significantly superior to the fast FLAIR images with TI

2100 msec (p-value < 0.005). The data in appendix E and F show T_2-weighted FSE images provides the high difference between the SNR of the lesion and WM, and SNR of both tissues more than fast FLAIR images with TI 2100 msec.

These result; are consistent with previous research, T OKUDA and Y KOROGI (24) that evaluate the usefulness of FLAIR techniques comparing with T_2-weighted FSE techniques in patients with periventricular leukomalacia (PVL) .

However, because the pathology of periventricular lesions in our study was not obtained which may effect our image assessment, further study of selected pathology should be performed.

CHAPTER VII

CONCLUSION

This study demonstrates that the optimal inversion time for optimum CSF suppression with good periventricular lesions to CSF for fast fluid-attenuated inversion recovery (FLAIR) pulse sequence is 2100 msec. We found the fast FLAIR pulse sequence with TI 2100 msec was superior to T_2-weighed fast spin echo pulse sequence in demonstrating periventricular lesions located near the interfaces of CSF.

The limitation of this study are small sample size and nonselected pathologies lesion which may have effect upon the image assessments. Further study with larger sample size and base on selected pathologies lesion may be needed for better analysis of the accuracy of the optimization of the periventricular lesions to CSF contrast for the FLAIR technique compare to T_2-weighed spin echo technique.

REFERENCE

1. Rydberg JN, Hammond CA, Grimm RC, Erickson BJ, Jack CR, Huston J, et.al. Initial clinical experience in MR imaging of the Brain with a fast fluid-attenuated inversion recovery pulse sequence. Radiology Am J Neuroradiol 1994; 193:173-80.
2. Kates R, Atkinson D, Zawadzki MB. Fluid-attenuated inversion recovery (FLAIR)clinical prospectus of current and future applications. Magnetic Resonance Imaging 1996; 8(6): 389-95.
3. Coene BD, Hajnal JV, Gatehouse P, Longmore DB, White SJ, Oatridge A, et.al. MR of the brain using fluid-attenuated inversion recovery (FLAIR) pulse sequence. AJNR Am J Neuroradiol 1992 Nov-Dec; 13:1555-64.
4. Mathews VP, Greenspan SL, Caldemeyer KS, Patel MR. FLAIR and HASE imaging in neurologic diseases. MRI CLINICS OF NORTH AMERICA 1998 Feb; 6(1): 53-62.
5. Rydberg JN, Riederer SJ, Rydberg CH, Jack RC. Contrast optimization of fluid-attenuated inversion recovery (FLAIR) imaging. Magn. Reson. Med. 1995; 34: 868-77.
6. Listerud J, Mitchell J, Bagley L, Grossman R. Optimized Interleaved fluid-attenuated inversion recovery in 2D fast spin echo. Magn. Reson. Med. 1996; 36: 320-25.

7. Alexander JA, Sheppard S, Davis PC, Salverda. Role of modified rapid fluid-attenuated inversion- recovery sequences. AJNR Am J Neuroradiol 1996 Sep; 17: 1507-13.

8. Steen RG, Gronemeyer SA, Kingsley PB, Reddick WE, Langston JS, Taylor JS. Precise and accurate measurement of proton T1 in human brain in vivo: validation and preliminary clinical application. JMRI 1994; 4: 681-91.

9. Thurnher MM, Thurn SA, Fleischmann D, Steuer A, Rieger A, Helbich T. Comparison of T2-weighted and fluid-attenuated inversion- recovery fast spin-echo MR sequences in intracerebral AIDS-associated disease. AJNR Am J Neuroradiol 1997 Oct; 18: 1601-09.

10. มีชัย ศรีใส. ประสาทกายวิภาคศาสตร์. ครั้งที่ 2. กรุงเทพมหานคร: โรงพิมพ์ A.A; 2524 หน้า 575-598.

11. Lee SH, Rao KC, Zimmerman RA, editors. Cranial MRI and CT. 3rd ed. United States of America: Arcata Graphics; 1992. p. 63.

12. Basic principles of MR imaging. Philips Medical systems Nederland B.V., 1997. p. 19-30.

13. Mitchell CW, editor. MRI the basics. United States of America: Williams&Wilkins; 1997. p.18-167.

14. Marcus ML, Schelbert HR, Skorton DJ, Wolf GL, editors. Piladephia: W.B Saunders company; 1991. p. 733-42.

15. Price RR. The basic physics of MR imaging. In: Riederer SJ, Wood ML, editors. Radiological Society of North America; 83rd. 1997 Nov 30-Dec 5; The Radiological Society of North America, Inc.; 1997. p. 7-27.

16. Woodward P, Freimarck RD, editors. MRI for technologists. United States of America: McGraw-Hill, Inc.; 1995. p. 13-105.

17. Budinger TF, Cullander C. Health hazards in nuclear magnetic resonance in vivo studieds. In: Radiological Society of North America; 68th. 1984 Jan; Chicago: The Radiological Society of North America, Inc.; 1984. p. 18-35.

18. Signa Applications Guide 4.0 Signa Advantage volume two. GE Medical Systems, General Electric Company, 1990.

19. Application Guide Gyroscan NT Release 5 volume 2. Philips Medical systems Nederland B.V., 1997.

20. Hashemi RH, Bradley WG, Chen DY, Jordan JE, Queralt JA, Cheng AE, et.al. Suspected multiple sclerosis: MR imaging with a thin-section fast FLAIR pulse sequence. Radiology 1995; 196: 505-10.

21. สุชาย ธนวเสถียร, นิรยุทธ วันเพ็ญ, ประสาร ไตรรัตน์วรกุล, ฉัตรชัย พงศ์ไทย. Theory & Worked Examples in Calculus: part II Integral Calculus. กรุงเทพมหานคร: บริษัทโรงพิมพ์ไทยวัฒนาพานิช จำกัด; 2520.

22. Signa Applications Guide 4.0 Signa Advantage volume one. GE Medical Systems, General Electric Company, 1990.

23. Signa Horizon 1.5T & 1.0T Protocal Guide. GE Medical System, General Electric Company, 1990.

24. Okuda T, Korogi Y, Ikushima I, Murakami R, Nakashima K, Yasunaga T, et.al. Use of fluid-attenuated inversion recovery (FLAIR) pulse sequences in perinatal hypoxic-ischaemia encephalopathy. Radiology March 1998; 71: 282-290.

APPENDIX A

THE EXAMPLE OF T_1 CALCULATION.

Table A. SI of CSF was measured on each of three IR images of a single volunteer.

TI (msec)	SI	Area (mm^2)
1500	-273.2	3
2000	-71.2	3
2600	124.1	3

The values SI acquired from the measurement were plotted versus TI by using the program package SPSS 7.5 for window (Fig.42). This program will show logarithmic curve, variables and constant of logarithmic curve. We can determine TI (null) by using constants of logarithmic curve in the equation (16) :

$$Y\ (SI) = B \ln TI + C$$

Where, B (722.869) and C (-5581.75) are constants that show in Figure 47.

Dependent variable.. SI Method.. LOGARITH
Multiple R .99986
R Square .99972
Adjusted R Square .99943
Standard Error 4.72875

Analysis of Variance:

	DF	Sum of Squares	Mean Square
Regression	1	78908.766	78908.766
Residuals	1	22.361	22.361

F = 3528.83902 Signif F = .0107

---------- Variables in the Equation ----------

Variable	B	SE B	Beta	T	Sig T
TI	721.979803	12.153717	.999858	59.404	.0107
(Constant)	-5555.038414	92.317029		-60.173	.0106

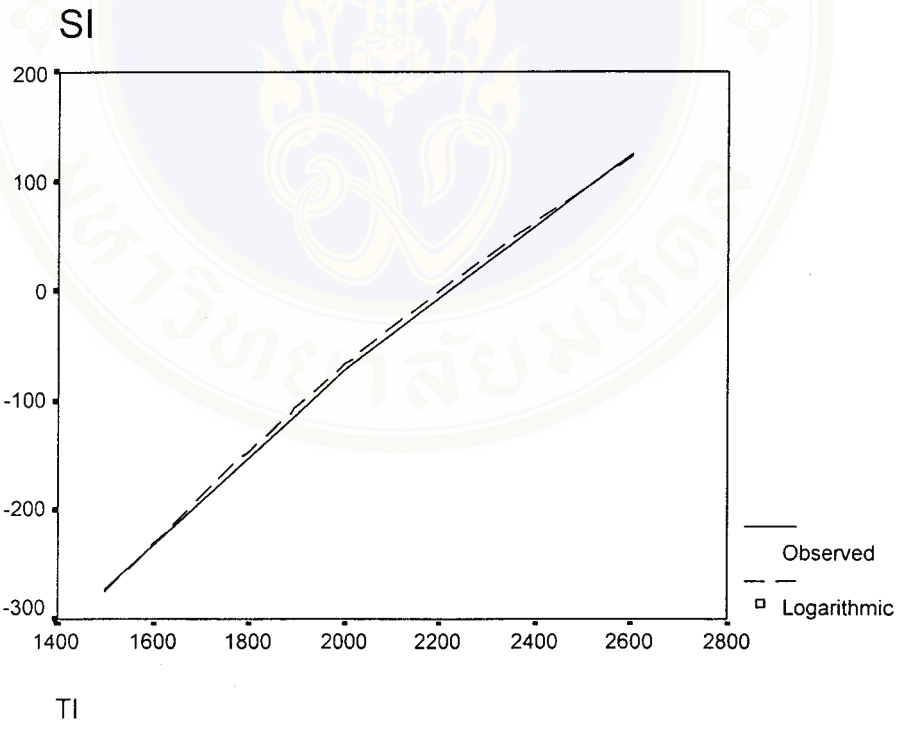

Fig. 47 Showing logarithmic curve and its constant of data in Table A that is estimated by SPSS programfor window.

At null point, the SI is zero,then

$$0 = 722.869 \ln TI_{null} + (-5581.75)$$

$$TI_{null} = 2313.69 \text{ msec}$$

We calculate T_1 of CSF in the equation (10) :

$$TI_{null\ of\ CSF} = 0.693 \text{ X } T_{1\ of\ CSF}$$

$$T_{1\ of\ CSF} = 2313.69 / 0.693 \text{ msec}$$

$$T_{1\ of\ CSF} = 3338.66 \text{ msec.}$$

Therefore $T_{1\ of\ CSF}$ of a single volunteer is 3338.66 msec.

APPENDIX B

SCAN PARAMETERS WHICH AFFECT SNR

The important scan parameters in MR. imaging that control and adjust SNR were voxel volume, NEX, number of phase encoding steps (N_y), bandwidth (BW). SNR is given by equation (18):

$$SNR \propto (\text{voxel volume})\sqrt{(N_y)\,(NEX) / BW} \qquad (18)$$

Where, voxel volume is $\Delta X \,.\, \Delta Y \,.\, \Delta Z$ that, ΔX is pixel size in the x direction.

ΔY is pixel size in the y direction.

ΔZ is slice thickness.

N_y is number of phase-encoding steps

NEX is number of excitation

BW is bandwidth

The pixel size along x-direction (ΔX) is given by equation (13):

$$FOV = (\text{pixel size}) \times (\text{number of pixels})$$

Therefore, the pixel size along x-direction (ΔX) is given by equation (20):

$$\Delta X = FOV_x / N_x \quad (20)$$

Where, FOV_x is field of view along x-direction

N_x is number of frequency-encoding steps

The pixel size along y-direction (ΔY) is given by equation (21): (13)

$$\Delta Y = FOV_y / N_y \quad (21)$$

Where, FOV_y is field of view along y-direction

Incorporating equations (20) and (21) into equation (17) gives us another way of expressing SNR:

$$SNR = (FOV_x / N_x) \cdot (FOV_y) \cdot \Delta Z \sqrt{(NEX) / (N_y) \cdot (BW)} \quad (22)$$

Difference of scanning parameters between fast FLAIR pulse sequence and T_2-weighted FSE pulse sequence were NEX and N_y.

Then, $SNR = K \sqrt{(NEX) / (N_y)}$

Where, K is constant that is $[(FOV_x / N_x) \cdot (FOV_y)] / \sqrt{(BW)}$

So, SNR(3NEX, 256x256) of T_2-weighted FSE pulse sequence must transfer to SNR at same NEX and N_y with fast FLAIR pulse sequence (1 NEX, 256 x 192) as follow:

$$\frac{\text{SNR of } T_2\text{-weighted images }_{(1NEX,\ 256x192)}}{\text{SNR of } T_2\text{-weighted images }_{(3NEX,\ 256x256)}} = \frac{K\sqrt{(NEX=1)/(N_{y(192)})}}{K\sqrt{(NEX=3)/(N_{y(256)})}}$$

$$\frac{\text{SNR of } T_2\text{-weighted images }_{(1NEX,\ 256x192)}}{\text{SNR of } T_2\text{-weighted images }_{(3NEX,\ 256x256)}} = \frac{\sqrt{(1)/(192)}}{\sqrt{(3)/(256)}}$$

$$\frac{\text{SNR of and } T_2\text{-weighted images }_{(1NEX,\ 256x192)}}{\text{SNR of and } T_2\text{-weighted images }_{(3NEX,\ 256x256)}} = 0.666667$$

SNR of and T_2-weighted images $_{(1NEX,\ 256x192)}$ = (0.666667) x SNR of and T_2-T_2-weighted images $_{(3NEX,\ 256x256)}$

APPENDIX C

THE PRECISION OF THE RANDOM SAMPLING FOR SIGNAL INTENSITY MEASUREMENTS.

The data of the precision of random sampling for SI measurement in the lesions of the fast FLAIR pulse sequence with TI 2000 msec

No.	SI_1	SI_2	SI_3	SI	Area (mm^2)	S.D	CV (%)
1	194.7	181.5	190.5	188.9	10.0	6.7	3.57
2	265.0	272.5	264.5	267.3	10.0	4.5	1.68
3	239.1	239.7	242.5	240.4	10.0	1.8	0.75
4	239.6	237.1	239.2	238.6	10.0	1.3	0.56
5	241.7	251.8	253.0	248.8	10.0	6.2	2.49
6	288.0	290.5	288.9	289.1	10.0	1.3	0.44
7	281.4	286.5	288.9	285.6	10.0	3.8	1.34
					Mean ± S.D		1.55 ± 1.146

The data of the precision of random sampling for SI measurement in the lesions of the fast FLAIR pulse sequence with TI 2100 msec

No.	SI_1	SI_2	SI_3	SI	Area (mm^2)	S.D	CV(%)
1	288.6	286.6	289.2	288.1	10.0	1.4	0.47
2	255.2	259.6	252.8	255.9	10.0	3.4	1.35
3	252.4	245.2	248.3	248.6	10.0	3.6	1.45
4	267.4	268.8	257.3	264.5	10.0	6.3	2.37
5	301.8	311.6	308.0	307.1	10.0	5.0	1.61
6	304.6	311.9	306.0	307.5	10.0	3.9	1.26
7	295.4	307.0	297.0	299.8	10.0	6.3	2.10
					Mean ± S.D		1.52 ± 0.615

The data of the precision of random sampling for SI measurements in the lesions of the fast FLAIR pulse sequence with TI 2200 msec

No.	SI_1	SI_2	SI_3	SI	Area (mm^2)	S.D	CV(%)
1	225.2	212.1	210.9	216.1	10.0	6.5	3.00
2	307.5	289.8	304.6	300.6	10.0	7.8	2.58
3	258.1	268.2	271.9	266.1	10.0	5.8	2.19
4	259.5	248.2	254.2	254.0	10.0	4.6	1.82
5	318.8	327.6	325.2	323.9	10.0	3.7	1.15
6	340.1	349.2	331.6	340.3	10.0	7.2	2.11
7	302.1	308.0	322.9	311.0	10.0	8.8	2.81
					Mean ± S.D		2.24 ± 0.634

The data of the precision of random sampling for SI measurements in the lesions of the fast FLAIR pulse sequence with TI 2300 msec

No.	SI_1	SI_2	SI_3	SI	Area (mm^2)	S.D	CV(%)
1	320.1	313.4	317.5	317.0	10.0	3.4	1.07
2	279.8	277.9	277.5	278.4	10.0	1.2	0.44
3	277.2	263.7	266.6	269.2	10.0	7.1	2.64
4	294.0	300.5	296.8	297.1	10.0	3.3	1.10
5	329.6	343.6	339.9	337.7	10.0	7.3	2.15
6	359.4	363.4	340.0	354.3	10.0	12.5	3.53
7	341.4	357.3	340.2	346.3	10.0	9.5	2.76
					Mean ± S.D		1.95 ± 1.1

The data of the precision of random sampling for SI measurements in the lesions of the fast FLAIR pulse sequence with TI 2400 msec

No.	SI_1	SI_2	SI_3	SI	Area (mm^2)	S.D	CV(%)
2	259.1	243.8	249.1	250.7	10.0	7.8	3.10
3	339.3	319.8	326.5	328.5	10.0	9.9	3.02
4	293.6	288.7	291.5	291.3	10.0	2.5	0.84
5	281.4	275.6	270.1	275.7	10.0	5.7	2.05
6	308.7	313.8	301.1	307.9	10.0	6.4	2.08
8	373.8	374.8	376.8	375.1	10.0	1.5	0.41
10	341.1	371.1	356.9	356.4	10.0	15.0	4.21
					Mean ± S.D		2.24 ± 1.3

The data of the precision of random sampling for SI measurements in WM of the fast FLAIR pulse sequence with TI 2000 msec

No.	SI_1	SI_2	SI_3	SI	Area (mm^2)	S.D	CV(%)
1	87.7	88.7	81.5	86.0	7	3.2	3.70
2	77.7	80.6	82.8	80.4	7	2.1	2.60
3	88.5	96.6	90.9	92.0	7	3.4	3.69
4	82.4	87.5	81.3	83.7	7	2.7	3.23
5	85.4	80.9	89.3	85.2	7	3.4	4.03
6	99.0	106.4	99.4	101.6	7	3.4	3.34
7	99.9	105.9	106.8	104.2	7	3.1	2.94
					Mean ± S.D		3.36 ± 0.492

The data of the precision of random sampling for SI measurements in WM of the fast FLAIR pulse sequence with TI 2100 msec

No.	SI_1	SI_2	SI_3	SI	Area (mm^2)	S.D	CV(%)
1	87.2	85.2	80.1	84.2	7	3.7	4.35
2	89.1	80.8	85.9	85.3	7	4.2	4.91
3	81.2	85.2	88.8	85.1	7	3.8	4.47
4	88.4	90.0	83.3	87.2	7	3.5	4.01
5	92.6	85.0	87.1	88.2	7	3.9	4.45
6	108.0	105.7	106.9	106.9	7	1.2	1.08
7	97.4	100.2	104.9	100.8	7	3.8	3.76
					Mean ± S.D		3.86 ± 1.281

The data of the precision of random sampling for SI measurements in WM of the fast FLAIR pulse sequence with TI 2200 msec

No.	SI_1	SI_2	SI_3	SI	Area (mm^2)	S.D	CV(%)
1	83.4	86.9	85.6	85.3	7	1.8	2.07
2	83.1	79.9	77.3	80.1	7	2.9	3.63
3	93.6	96.1	91.8	93.8	7	2.2	2.30
4	84.1	83.9	80.9	83.0	7	1.8	2.15
5	96.3	91.6	95.5	94.5	7	2.5	2.66
6	105	102.3	102.7	103.3	7	1.5	1.41
7	101.3	104.6	107.4	104.4	7	3.1	2.92
					Mean ± S.D		2.45 ± 0.706

The data of the precision of random sampling for SI measurements in WM of the fast FLAIR pulse sequence with TI 2300 msec

No.	SI_1	SI_2	SI_3	SI	Area (mm^2)	S.D	CV(%)
1	92.2	96.4	89.7	92.8	7	3.4	3.65
2	77.1	76.8	74.2	76.0	7	1.6	2.10
3	97.2	89.1	96.2	94.2	7	4.4	4.69
4	94.2	92.6	91.9	92.9	7	1.2	1.27
5	83.7	89.1	91.4	88.1	7	4.0	4.49
6	115.9	117.3	114.7	116.0	7	1.3	1.12
7	107.7	107.3	113.3	109.4	7	3.4	3.07
					Mean ± S.D		2.91 ± 1.459

The data of the precision of random sampling for SI measurements in WM of the fast FLAIR pulse sequence with TI 2400 msec

No.	SI_1	SI_2	SI_3	SI	Area (mm^2)	S.D	CV(%)
1	85.5	90.4	89.8	88.6	7	2.7	3.02
2	88.1	85.1	88.6	87.3	7	1.9	2.17
3	95.3	93.5	94.4	94.4	7	0.9	0.95
4	96.1	106.1	99.5	100.6	7	5.1	5.06
5	90.9	93.1	94.8	92.9	7	2.0	2.10
6	105.1	115.5	113.2	111.3	7	5.5	4.91
7	103.9	100.6	110.4	105.0	7	5.0	4.75
					Mean ± S.D		3.28 ± 1.637

The data of the precision of random sampling for SI measurements in CSF of the fast FLAIR pulse sequence with TI 2000 msec

No.	SI_1	SI_2	SI_3	SI	Area (mm^2)	S.D	CV(%)
1	48.6	44.5	37.1	43.4	7	4.8	10.97
2	41.7	38.0	43.0	40.9	7	2.1	5.18
3	34.7	36.6	40.1	37.1	7	2.2	6.02
4	33.0	33.9	40.6	35.8	7	3.4	9.46
5	45.5	42.6	40.1	42.7	7	2.2	5.16
6	40.6	34.0	35.6	36.7	7	2.8	7.65
7	18.6	20.9	19.8	19.8	7	0.9	4.75
					Mean ± S.D		7.03 ± 2.412

The data of the precision of random sampling for SI measurements in CSF of the fast FLAIR pulse sequence with TI 2100 msec

No.	SI_1	SI_2	SI_3	SI	Area (mm^2)	S.D	CV(%)
1	16.1	16.9	15.5	16.2	7.0	0.7	4.34
2	9.9	12.4	11.2	11.2	7.0	1.3	11.20
3	18.9	22.5	20.2	20.5	7.0	1.8	8.88
4	13.2	9.9	10.7	11.3	7.0	1.7	15.28
5	36.0	35.0	32.5	34.5	7.0	1.8	5.23
6	21.2	19.2	24.0	21.5	7.0	2.4	11.23
7	13.8	14.0	15.2	14.3	7.0	0.8	5.28
					Mean ± S.D		8.78 ± 4.054

The data of the precision of random sampling for SI measurements in CSF of the fast FLAIR pulse sequence with TI 2200 msec

No.	SI_1	SI_2	SI_3	SI	Area (mm^2)	S.D	CV(%)
1	40.3	38.3	39.6	39.4	7	1.0	2.58
2	27.3	24.7	30.9	27.6	7	3.1	11.27
3	38.3	35.1	38.3	37.2	7	1.8	4.96
4	33.6	37.4	32.2	34.4	7	2.7	7.82
5	25.1	23.9	28.3	25.8	7	2.3	8.83
6	36.9	42.5	46.7	42.0	7	4.9	11.70
7	54.3	56.8	51.8	54.3	7	2.5	4.60
					Mean ± S.D		7.39 ± 3.48

The data of the precision of random sampling for SI measurements in CSF of the fast FLAIR pulse sequence with TI 2300 msec

No.	SI_1	SI_2	SI_3	SI	Area (mm^2)	S.D	CV(%)
1	75.5	70.8	80.5	75.6	7	4.9	6.42
2	67.3	60.1	53.1	60.2	7	7.1	11.80
3	77.0	86.2	85.3	82.8	7	5.1	6.12
4	73.7	78.6	82.5	78.3	7	4.4	5.63
5	58.2	64.9	65.3	62.8	7	4.0	6.35
6	74.1	71.1	71.1	72.1	7	1.7	2.40
7	36.6	41.8	41.8	40.1	7	3.0	7.49
					Mean ± S.D		6.60 ± 2.791

The data of the precision of random sampling for SI measurements in CSF of the fast FLAIR pulse sequence with TI 2400 msec

No.	SI_1	SI_2	SI_3	SI	Area (mm^2)	S.D	CV(%)
1	104.3	101.2	104.7	103.4	7	1.9	1.85
2	107.5	100.1	106.4	104.7	7	4.0	3.81
3	105.9	111.9	110.3	109.4	7	3.1	2.84
4	84.8	79.1	80.3	81.4	7	3.0	3.69
5	97.3	105.5	98.1	100.3	7	4.5	4.51
6	75.2	72.3	68.8	72.1	7	3.2	4.44
7	96.3	97.0	92.4	95.2	7	2.5	2.60
					Mean ± S.D		3.39 ± 0.993

APPENDIX D

THE DATA MEASUREMENTS OF SI

OF fast FLAIR PULSE SEQUENCE.

The data measurements of SI of fast FLAIR pulse sequence with TI 2000 msec

No.	SEX	SI of lesion	SI of WM.	SI of CSF	SDair
1	F	224.6	96.2	32.2	8.2
2	F	208.7	80.4	34.2	8.2
3	M	223.8	85.3	37.2	8.1
4	F	206.4	87.5	38.2	7.4
5	F	188.0	90.1	17.1	8.1
6	F	230.0	89.3	29.2	8.1
7	M	220.6	92.1	31.5	8.2
8	M	183.1	81.5	18.2	8.2
9	M	199.5	70.2	23.4	8.2
10	M	199.4	86.7	13.1	8.2
11	M	207.0	94.9	30.9	8.5
12	M	181.1	92.8	30.3	8.5
13	M	220.8	78.2	16.8	8.5
14	M	202.3	78.5	35.0	10.6
15	M	144.6	69.6	44.6	10.6
16	F	245.2	93.0	13.0	7.6
17	F	244.6	121.1	17.8	7.8
18	M	237.5	99.9	50.0	8.9
19	M	242.5	102.6	30.5	8.9
20	M	190.8	91.0	48.8	9.8
21	M	190.1	79.3	44.3	9.8
22	F	185.2	107.0	51.4	7.5

The data measurements of SI of fast FLAIR pulse sequence with TI 2000 msec (Continued).

No.	SEX	SI of lesion	SI of WM.	SI of CSF	SDair
23	F	280.9	102.1	45.3	7.5
24	F	281.6	112.7	45.3	7.5
25	F	264.1	99.9	40.8	7.5
26	F	281.8	98.2	31.4	7.5
27	F	209.6	80.5	26.6	9.1
28	M	126.1	65.9	30.0	6.8
29	M	151.6	69.6	26.2	6.8
30	F	189.8	91.0	41.8	8.1
31	F	190.0	82.6	57.5	8.1
32	F	228.7	106.1	30.6	8.2
33	F	220.9	115.6	24.9	8.2
34	F	298.9	93.1	44.5	8.2
35	F	227.9	97.8	44.5	8.2
36	F	191.8	97.8	44.5	8.2
37	M	200.0	-	21.0	9.8
38	F	257.4	-	35.8	8.9
39	F	265.8	-	54.3	8.9
40	F	273.6	-	46.2	8.9
41	F	270.6	-	44.0	8.9

The data measurements of SI of fast FLAIR pulse sequence with TI 2100 msec

No.	SEX	SI of lesion	SI of WM.	SI of CSF	SDair
1	F	200.7	99.8	13.9	8.8
2	F	215.0	99.8	16.0	8.8
3	M	248.7	86.6	12.6	7.6
4	F	220.6	79.4	17.2	7.7
5	F	188.6	89.8	19.2	8.1
6	F	241.2	89.2	12.7	8.1
7	M	231.5	89.4	12.1	8.5
8	M	190.9	84.0	18.5	8.5
9	M	197.7	78.5	15.5	8.5
10	M	228.1	83.0	27.7	8.5
11	M	213.9	92.6	9.3	8.2
12	M	199.9	88.5	12.5	8.2
13	M	222.6	93.4	28.2	8.2
14	M	195.6	68.4	28.6	9.5
15	M	171.0	87.2	18.5	9.5
16	F	258.2	96.6	39.5	8.2
17	F	268.2	132.8	37.7	8.2
18	M	257.4	103.7	26.3	8.5
19	M	255.8	115.8	18.5	8.5
20	M	212.3	82.6	24.2	8.2
21	M	205.5	75.9	20.5	8.2
22	F	190.6	103.1	22.4	8.6
23	F	291.7	99.9	14.7	8.6
24	F	301.9	112.9	14.7	8.6
25	F	283.9	102.2	27.4	8.6
26	F	295.0	102.6	39.3	8.6
27	F	224.2	82.6	14.5	8.8
28	M	132.1	69.5	14.0	7.4
29	M	152.0	72.2	9.0	7.4
30	F	191.8	95.8	17.2	7.7
31	F	217.3	87.7	24.8	7.7

The data measurements of SI of fast FLAIR pulse sequence with 2100 msec (Continued).

No.	SEX	SI of lesion	SI of WM.	SI of CSF	SDair
32	F	274.0	109.1	18.4	8.2
33	F	241.9	103.8	17.8	8.2
34	F	307.4	95.0	15.9	8.2
35	F	252.0	110.2	15.9	8.2
36	F	234.8	110.2	15.9	8.2
37	M	211.7	-	31.5	8.2
38	F	270.2	-	18.9	9.0
39	F	291.0	-	28.4	9.0
40	F	301.6	-	16.2	9.0
41	F	280.9	-	25.1	9.0

The data measurements of SI of fast FLAIR pulse sequence with TI 2200 msec.

No.	SEX	SI of lesion	SI of WM.	SI of CSF	SDair
1	F	217.1	94.2	41.6	9.0
2	F	225.1	89.9	38.8	9.0
3	M	261.9	96.3	28.7	7.8
4	F	224.6	82.0	29.8	7.3
5	F	189.4	94.8	53.2	8.1
6	F	271.3	92.7	37.8	8.1
7	M	238.6	91.1	22.4	9.4
8	M	190.3	71.5	36.8	9.4
9	M	211.1	75.5	32.2	9.4
10	M	215.2	77.5	40.0	9.4
11	M	228.1	98.9	28.0	8.8
12	M	211.1	96.6	24.8	8.8
13	M	243.8	84.1	54.2	8.8
14	M	242.6	72.7	7.0	9.4
15	M	175.8	92.5	14.7	9.4
16	F	270.0	103.5	74.9	7.8
17	F	292.4	142.1	64.8	8.2
18	M	261.8	107.9	15.2	9.1
19	M	262.8	109.7	29.9	9.1
20	M	203.7	86.1	25.8	8.2
21	M	217.0	75.3	19.0	8.2
22	F	204.7	106.6	24.6	7.9
23	F	310.4	105.2	35.8	7.9
24	F	320.8	119.9	35.8	7.9
25	F	310.3	106.5	39.8	7.9
26	F	316.6	103.5	55.8	7.9
27	F	239.2	82.4	24.1	8.3
28	M	179.3	75.2	13.6	7.0
29	M	162.8	70.6	26.8	7.0
30	F	192.5	92.4	25.9	7.5
31	F	225.6	88.7	16.2	7.5

The data measurements of SI of fast FLAIR pulse sequence with TI 2200 msec (Continued).

No.	SEX	SI of lesion	SI of WM.	SI of CSF	SDair
32	F	268.1	116.3	35.7	8.1
33	F	274.5	110.3	46.8	8.1
34	F	324.3	101.1	18.7	8.1
35	F	264.0	106.3	18.7	8.1
36	F	239.6	106.3	18.7	8.1
37	M	223.7	-	48.8	8.2
38	F	297.8	-	41.7	11.5
39	F	275.4	-	20.2	11.5
40	F	282.1	-	23.1	11.5
41	F	316.4	-	26.8	11.5

The data measurements of SI of fast FLAIR pulse sequence with TI 2300 msec.

No.	SEX	SI of lesion	SI of WM.	SI of CSF	SDair
1	F	204.9	97.9	72.0	8.8
2	F	213.2	100.9	73.2	8.8
3	M	265.4	87.0	63.2	7.9
4	F	226.9	85.9	59.1	7.2
5	F	187.0	96.2	82.5	8.7
6	F	269.8	90.6	69.3	8.7
7	M	222.5	106.6	50.1	8.8
8	M	189.4	82.5	67.4	8.8
9	M	215.0	94.3	67.4	8.8
10	M	212.2	79.5	78.0	8.8
11	M	247.4	99.6	61.7	8.9
12	M	229.7	99.8	47.6	8.9
13	M	234.8	94.9	91.5	8.9
14	M	266.8	76.3	38.6	9.4
15	M	179.4	88.1	28.0	9.4
16	F	289.2	105.5	110.4	8.0
17	F	321.2	140.6	105.1	8.2
18	M	285.1	111.7	36.2	8.6
19	M	279.3	111.2	68.6	8.6
20	M	204.9	86.9	66.7	9.3
21	M	222.7	72.5	49.6	9.3
22	F	207.2	112.1	59.9	7.8
23	F	323.5	102.6	74.2	7.8
24	F	341.6	118.2	74.2	7.8
25	F	327.7	111.4	86.4	7.8
26	F	322.2	101.2	80.3	7.8
27	F	247.6	91.2	50.9	9.1
28	M	179.6	72.8	35.8	7.3
29	M	165.8	66.9	44.0	7.3
30	F	226.9	94.0	51.8	8.4
31	F	230.6	87.2	41.6	8.4

The data measurements of SI of fast FLAIR pulse sequence with TI 2300 msec (Continued).

No.	SEX	SI of lesion	SI of WM.	SI of CSF	SDair
32	F	270.6	110.9	58.7	8.3
33	F	291.0	113.5	72.8	8.3
34	F	330.7	100.9	60.1	8.3
35	F	275.8	106.2	60.1	8.3
36	F	244.0	106.2	60.1	8.3
37	M	217.9	-	63.6	9.3
38	F	289.3	-	48.2	9.3
39	F	318.2	-	49.6	9.3
40	F	341.3	-	56.7	9.3
41	F	305.4	-	62.1	9.3

The data measurements of SI of fast FLAIR pulse sequence with TI 2400 msec .

No.	SEX	SI of lesion	SI of WM.	SI of CSF	SDair
1	F	225.5	94.2	108.1	8.8
2	F	240.3	95.9	109.6	8.8
3	M	269.5	88.6	83.1	7.5
4	F	241.4	90.4	83.9	7.4
5	F	203.2	92.0	106.9	8.6
6	F	281.8	88.5	97.4	8.6
7	M	242.4	110.5	72.6	9.5
8	M	205.1	74.5	97.9	9.5
9	M	222.8	105.9	90.6	9.5
10	M	243.8	82.8	103.4	9.5
11	M	241.4	97.8	79.1	8.0
12	M	245.4	93.7	77.4	8.0
13	M	244.1	92.2	118.8	8.0
14	M	270.8	89.0	64.9	9.6
15	M	161.2	99.9	66.4	9.6
16	F	303.6	107.6	142.0	7.4
17	F	341.0	145.5	135.6	7.9
18	M	288.9	113.8	57.8	8.4
19	M	295.8	114.3	85.1	8.4
20	M	214.4	88.6	74.3	8.5
21	M	230.9	71.1	63.8	8.5
22	F	215.4	115.6	62.7	8.6
23	F	321.8	92.7	86.3	8.6
24	F	311.0	120.1	86.3	8.6
25	F	336.8	116.6	96.1	8.6
26	F	333.7	111.1	97.9	8.6
27	F	260.8	90.4	78.0	7.7
28	M	156.9	70.5	61.8	7.5
29	M	162.4	78.1	66.9	7.5
30	F	234.8	92.1	84.8	8.8
31	F	245.7	94.6	72.8	8.8

The data measurements of SI of fast FLAIR pulse sequence with TI 2400 msec (Continued).

No.	SEX	SI of lesion	SI of WM.	SI of CSF	SDair
32	F	313.3	106.9	85.2	8.3
33	F	313.5	123.0	100.8	8.3
34	F	334.6	103.8	90.6	8.3
35	F	291.7	110.1	90.6	8.3
36	F	235.3	110.1	90.6	8.3
37	M	220.8	-	71.9	8.5
38	F	289.1	-	95.7	8.9
39	F	342.4	-	71.9	8.9
40	F	367.7	-	101.1	8.9
41	F	342.6	-	91.4	8.9

APPENDIX E

THE DATA OF SNR, CR, AND CNR OF fast FLAIR PULSE SEQUENCE.

The data of SNR, CR, and CNR of fast FLAIR pulse sequence with TI 2000 msec.

No.	SD_{air}	$CR_{lesion,CSF}$	$CNR_{lesion,CSF}$	$CR_{lesion,WM}$	$CNR_{lesion,WM}$	SNR_{lesion}	SNR_{WM}	SNR_{CSF}
1	8.20	0.749	23.46	0.400	15.66	27.39	11.73	3.93
2	8.20	0.718	21.28	0.444	15.65	25.45	9.80	4.17
3	8.10	0.715	23.04	0.448	17.10	27.63	10.53	4.59
4	7.40	0.688	22.73	0.405	16.07	27.89	11.82	5.16
5	8.10	0.833	21.10	0.352	12.09	23.21	11.12	2.11
6	8.10	0.775	24.79	0.441	17.37	28.40	11.02	3.60
7	8.20	0.750	23.06	0.411	15.67	26.90	11.23	3.84
8	8.20	0.819	20.11	0.384	12.39	22.33	9.94	2.22
9	8.20	0.790	21.48	0.479	15.77	24.33	8.56	2.85
10	8.20	0.877	22.72	0.394	13.74	24.32	10.57	1.60
11	8.50	0.740	20.72	0.371	13.19	24.35	11.16	3.64

The data of SNR, CR, and CNR of fast FLAIR pulse sequence with TI 2000 msec (Continued).

No.	SD_{air}	$CR_{lesion,CSF}$	$CNR_{lesion,CSF}$	$CR_{lesion,WM}$	$CNR_{lesion,WM}$	SNR_{lesion}	SNR_{WM}	SNR_{CSF}
12	8.50	0.713	17.74	0.322	10.39	21.31	10.92	3.56
13	8.50	0.859	24.00	0.477	16.78	25.98	9.20	1.98
14	10.60	0.705	15.78	0.441	11.68	19.08	7.41	3.30
15	10.60	0.529	9.43	0.350	7.08	13.64	6.57	4.21
16	7.60	0.899	30.55	0.450	20.03	32.26	12.24	1.71
17	7.80	0.864	29.08	0.338	15.83	31.36	15.53	2.28
18	8.90	0.652	21.07	0.408	15.46	26.69	11.22	5.62
19	8.90	0.777	23.82	0.405	15.72	27.25	11.53	3.43
20	9.80	0.593	14.49	0.354	10.18	19.47	9.29	4.98
21	9.80	0.622	14.88	0.411	11.31	19.40	8.09	4.52
22	7.50	0.566	17.84	0.268	10.43	24.69	14.27	6.85
23	7.50	0.722	31.41	0.467	23.84	37.45	13.61	6.04
24	7.50	0.723	31.51	0.428	22.52	37.55	15.03	6.04
25	7.50	0.732	29.77	0.451	21.89	35.21	13.32	5.44
26	7.50	0.799	33.39	0.483	24.48	37.57	13.09	4.19
27	9.10	0.775	20.11	0.445	14.19	23.03	8.85	2.92
28	6.80	0.616	14.13	0.314	8.85	18.54	9.69	4.41
29	6.80	0.705	18.44	0.371	12.06	22.29	10.24	3.85

The data of SNR, CR, and CNR of fast FLAIR pulse sequence with TI 2000 msec (Continued).

No.	SD_{air}	$CR_{lesion,CSF}$	$CNR_{lesion,CSF}$	$CR_{lesion,WM}$	$CNR_{lesion,WM}$	SNR_{lesion}	SNR_{WM}	SNR_{CSF}
30	8.10	0.639	18.27	0.352	12.20	23.43	11.23	5.16
31	8.10	0.535	16.36	0.394	13.26	23.46	10.20	7.10
32	8.20	0.764	24.16	0.366	14.95	27.89	12.94	3.73
33	8.20	0.797	23.90	0.313	12.84	26.94	14.10	3.04
34	8.20	0.741	31.02	0.525	25.10	36.45	11.35	5.43
35	8.20	0.673	22.37	0.399	15.87	27.79	11.93	5.43
36	8.20	0.623	17.96	0.325	11.46	23.39	11.93	5.43
37	9.80	0.810	18.27	-	-	20.41	-	2.14
38	8.90	0.756	24.90	-	-	28.92	-	4.02
39	8.90	0.661	23.76	-	-	29.87	-	6.10
40	8.90	0.711	25.55	-	-	30.74	-	5.19
41	8.90	0.720	25.46	-	-	30.40	-	4.94
Mean		0.73	22.29	0.40	15.09	26.46	11.15	4.16
S.D		0.09	5.33	0.06	4.36	5.50	2.04	1.42
$S.D^2$		0.01	28.41	0.00	19.02	30.29	4.15	2.00
C.V		12.3%	23.9%	14.4%	28.9%	20.8%	18.3%	34.0%

The data of SNR, CR, and CNR of fast FLAIR pulse sequence with TI 2100 msec.

No.	SD_{air}	$CR_{lesion,CSF}$	$CNR_{lesion,CSF}$	$CR_{lesion,WM}$	$CNR_{lesion,WM}$	SNR_{lesion}	SNR_{WM}	SNR_{CSF}
1	8.80	0.870	21.23	0.336	11.47	22.81	11.34	1.58
2	8.80	0.861	22.61	0.366	13.09	24.43	11.34	1.82
3	7.60	0.904	31.07	0.483	21.33	32.72	11.39	1.66
4	7.70	0.855	26.42	0.471	18.34	28.65	10.31	2.23
5	8.10	0.815	20.91	0.355	12.20	23.28	11.09	2.37
6	8.10	0.900	28.21	0.460	18.77	29.78	11.01	1.57
7	8.50	0.901	25.81	0.443	16.72	27.24	10.52	1.42
8	8.50	0.823	20.28	0.389	12.58	22.46	9.88	2.18
9	8.50	0.855	21.44	0.432	14.02	23.26	9.24	1.82
10	8.50	0.783	23.58	0.466	17.07	26.84	9.76	3.26
11	8.20	0.917	24.95	0.396	14.79	26.09	11.29	1.13
12	8.20	0.882	22.85	0.386	13.59	24.38	10.79	1.52
13	8.20	0.775	23.71	0.409	15.76	27.15	11.39	3.44
14	9.50	0.745	17.58	0.482	13.39	20.59	7.20	3.01
15	9.50	0.805	16.05	0.325	8.82	18.00	9.18	1.95
16	8.20	0.735	26.67	0.455	19.71	31.49	11.78	4.82
17	8.20	0.754	28.11	0.338	16.51	32.71	16.20	4.60
18	8.50	0.815	27.19	0.426	18.08	30.28	12.20	3.09

The data of SNR, CR, and CNR of fast FLAIR pulse sequence with TI 2100 msec (Continued).

No.	SD_{air}	$CR_{lesion,CSF}$	$CNR_{lesion,CSF}$	$CR_{lesion,WM}$	$CNR_{lesion,WM}$	SNR_{lesion}	SNR_{WM}	SNR_{CSF}
19	8.50	0.865	27.92	0.377	16.47	30.09	13.62	2.18
20	8.20	0.795	22.94	0.440	15.82	25.89	10.07	2.95
21	8.20	0.819	22.56	0.461	15.80	25.06	9.26	2.50
22	8.60	0.790	19.56	0.298	10.17	22.16	11.99	2.60
23	8.60	0.904	32.21	0.490	22.30	33.92	11.62	1.71
24	8.60	0.907	33.40	0.456	21.98	35.10	13.13	1.71
25	8.60	0.824	29.83	0.471	21.13	33.01	11.88	3.19
26	8.60	0.765	29.73	0.484	22.37	34.30	11.93	4.57
27	8.80	0.879	23.83	0.462	16.09	25.48	9.39	1.65
28	7.40	0.808	15.96	0.311	8.46	17.85	9.39	1.89
29	7.40	0.888	19.32	0.356	10.78	20.54	9.76	1.22
30	7.70	0.835	22.68	0.334	12.47	24.91	12.44	2.23
31	7.70	0.795	25.00	0.425	16.83	28.22	11.39	3.22
32	8.20	0.874	31.17	0.430	20.11	33.41	13.30	2.24
33	8.20	0.863	27.33	0.399	16.84	29.50	12.66	2.17
34	8.20	0.902	35.55	0.528	25.90	37.49	11.59	1.94
35	8.20	0.881	28.79	0.391	17.29	30.73	13.44	1.94
36	8.20	0.873	26.70	0.361	15.20	28.63	13.44	1.94

The data of SNR, CR, and CNR of fast FLAIR pulse sequence with TI 2100 msec (Continued).

No.	SD_{air}	$CR_{lesion,CSF}$	$CNR_{lesion,CSF}$	$CR_{lesion,WM}$	$CNR_{lesion,WM}$	SNR_{lesion}	SNR_{WM}	SNR_{CSF}
37	8.20	0.741	21.98	-	-	25.82	-	3.84
38	9.00	0.869	27.92	-	-	30.02	-	2.10
39	9.00	0.822	29.18	-	-	32.33	-	3.16
40	9.00	0.898	31.71	-	-	33.51	-	1.80
41	9.00	0.836	28.42	-	-	31.21	-	2.79
Mean		0.84	25.42	0.41	16.17	27.84	11.28	2.41
S.D		0.05	4.68	0.06	4.06	4.82	1.68	0.91
$S.D^2$		0.00	21.90	0.00	16.49	23.20	2.82	0.83
C.V		6.2%	18.4%	14.2%	25.1%	17.3%	14.9%	37.7%

The data of SNR, CR, and CNR of fast FLAIR pulse sequence with TI 2200 msec .

No.	SD_{air}	$CR_{lesion,CSF}$	$CNR_{lesion,CSF}$	$CR_{lesion,WM}$	$CNR_{lesion,WM}$	SNR_{lesion}	SNR_{WM}	SNR_{CSF}
1	9.00	0.678	19.50	0.395	13.66	24.12	10.47	4.62
2	9.00	0.706	20.70	0.429	15.02	25.01	9.99	4.31
3	7.80	0.802	29.90	0.462	21.23	33.58	12.35	3.68
4	7.30	0.766	26.68	0.465	19.53	30.77	11.23	4.08
5	8.10	0.561	16.81	0.333	11.68	23.38	11.70	6.57
6	8.10	0.755	28.83	0.491	22.05	33.49	11.44	4.67
7	9.40	0.828	23.00	0.447	15.69	25.38	9.69	2.38
8	9.40	0.676	16.33	0.454	12.64	20.24	7.61	3.91
9	9.40	0.735	19.03	0.473	14.43	22.46	8.03	3.43
10	9.40	0.687	18.64	0.470	14.65	22.89	8.24	4.26
11	8.80	0.781	22.74	0.395	14.68	25.92	11.24	3.18
12	8.80	0.790	21.17	0.372	13.01	23.99	10.98	2.82
13	8.80	0.636	21.55	0.487	18.15	27.70	9.56	6.16
14	9.40	0.944	25.06	0.539	18.07	25.81	7.73	0.74
15	9.40	0.846	17.14	0.310	8.86	18.70	9.84	1.56
16	7.80	0.566	25.01	0.446	21.35	34.62	13.27	9.60
17	8.20	0.637	27.76	0.346	18.33	35.66	17.33	7.90
18	9.10	0.890	27.10	0.416	16.91	28.77	11.86	1.67

The data of SNR, CR, and CNR of fast FLAIR pulse sequence with TI 2200 msec (Continued).

No.	SD_{air}	$CR_{lesion,CSF}$	$CNR_{lesion,CSF}$	$CR_{lesion,WM}$	$CNR_{lesion,WM}$	SNR_{lesion}	SNR_{WM}	SNR_{CSF}
19	9.10	0.796	25.59	0.411	16.82	28.88	12.05	3.29
20	8.20	0.775	21.70	0.406	14.34	24.84	10.50	3.15
21	8.20	0.839	24.15	0.485	17.28	26.46	9.18	2.32
22	7.90	0.785	22.80	0.315	12.42	25.91	13.49	3.11
23	7.90	0.793	34.76	0.494	25.97	39.29	13.32	4.53
24	7.90	0.799	36.08	0.456	25.43	40.61	15.18	4.53
25	7.90	0.773	34.24	0.489	25.80	39.28	13.48	5.04
26	7.90	0.700	33.01	0.507	26.97	40.08	13.10	7.06
27	8.30	0.817	25.92	0.488	18.89	28.82	9.93	2.90
28	7.00	0.859	23.67	0.409	14.87	25.61	10.74	1.94
29	7.00	0.717	19.43	0.395	13.17	23.26	10.09	3.83
30	7.50	0.763	22.21	0.351	13.35	25.67	12.32	3.45
31	7.50	0.866	27.92	0.436	18.25	30.08	11.83	2.16
32	8.10	0.765	28.69	0.395	18.74	33.10	14.36	4.41
33	8.10	0.709	28.11	0.427	20.27	33.89	13.62	5.78
34	8.10	0.891	37.73	0.525	27.56	40.04	12.48	2.31
35	8.10	0.868	30.28	0.426	19.47	32.59	13.12	2.31
36	8.10	0.855	27.27	0.385	16.46	29.58	13.12	2.31

The data of SNR, CR, and CNR of fast FLAIR pulse sequence with TI 2200 msec (Continued).

No.	SD_{air}	$CR_{lesion,CSF}$	$CNR_{lesion,CSF}$	$CR_{lesion,WM}$	$CNR_{lesion,WM}$	SNR_{lesion}	SNR_{WM}	SNR_{CSF}
37	8.20	0.642	21.33	-	-	27.28	-	5.95
38	11.50	0.754	22.27	-	-	25.90	-	3.63
39	11.50	0.863	22.19	-	-	23.95	-	1.76
40	11.50	0.849	22.52	-	-	24.53	-	2.01
41	11.50	0.844	25.18	-	-	27.51	-	2.33
Mean		0.77	24.98	0.43	17.67	28.77	11.51	3.80
S.D		0.09	5.26	0.06	4.62	5.72	2.15	1.85
$S.D^2$		0.01	27.64	0.00	21.33	32.67	4.63	3.42
C.V		11.5%	21.1%	13.4%	26.1%	19.9%	18.7%	48.7%

The data of SNR, CR, and CNR of fast FLAIR pulse sequence with TI 2300 msec .

No.	SD_{air}	$CR_{lesion,CSF}$	$CNR_{lesion,CSF}$	$CR_{lesion,WM}$	$CNR_{lesion,WM}$	SNR_{lesion}	SNR_{WM}	SNR_{CSF}
1	8.80	0.480	15.10	0.353	12.16	23.28	11.13	8.18
2	8.80	0.489	15.91	0.358	12.76	24.23	11.47	8.32
3	7.90	0.615	25.59	0.506	22.58	33.59	11.01	8.00
4	7.20	0.587	23.31	0.451	19.58	31.51	11.93	8.21
5	8.70	0.388	12.01	0.321	10.44	21.49	11.06	9.48
6	8.70	0.591	23.05	0.497	20.60	31.01	10.41	7.97
7	8.80	0.632	19.59	0.352	13.17	25.28	12.11	5.69
8	8.80	0.475	13.86	0.393	12.15	21.52	9.38	7.66
9	8.80	0.523	16.77	0.390	13.72	24.43	10.72	7.66
10	8.80	0.462	15.25	0.455	15.08	24.11	9.03	8.86
11	8.90	0.601	20.87	0.426	16.61	27.80	11.19	6.93
12	8.90	0.657	20.46	0.394	14.60	25.81	11.21	5.35
13	8.90	0.439	16.10	0.424	15.72	26.38	10.66	10.28
14	9.40	0.747	24.28	0.555	20.27	28.38	8.12	4.11
15	9.40	0.730	16.11	0.341	9.71	19.09	9.37	2.98
16	8.00	0.447	22.35	0.465	22.96	36.15	13.19	13.80
17	8.20	0.507	26.35	0.391	22.02	39.17	17.15	12.82
18	8.60	0.775	28.94	0.437	20.16	33.15	12.99	4.21

The data of SNR, CR, and CNR of fast FLAIR pulse sequence with TI 2300 msec (Continued).

No.	SD_{air}	$CR_{lesion,CSF}$	$CNR_{lesion,CSF}$	$CR_{lesion,WM}$	$CNR_{lesion,WM}$	SNR_{lesion}	SNR_{WM}	SNR_{CSF}
19	8.60	0.606	24.50	0.430	19.55	32.48	12.93	7.98
20	9.30	0.509	14.86	0.404	12.69	22.03	9.34	7.17
21	9.30	0.636	18.61	0.509	16.15	23.95	7.80	5.33
22	7.80	0.551	18.88	0.298	12.19	26.56	14.37	7.68
23	7.80	0.627	31.96	0.518	28.32	41.47	13.15	9.51
24	7.80	0.643	34.28	0.486	28.64	43.79	15.15	9.51
25	7.80	0.583	30.94	0.493	27.73	42.01	14.28	11.08
26	7.80	0.601	31.01	0.522	28.33	41.31	12.97	10.29
27	9.10	0.659	21.62	0.462	17.19	27.21	10.02	5.59
28	7.30	0.668	19.70	0.423	14.63	24.60	9.97	4.90
29	7.30	0.581	16.68	0.425	13.55	22.71	9.16	6.03
30	8.40	0.628	20.85	0.414	15.82	27.01	11.19	6.17
31	8.40	0.694	22.50	0.451	17.07	27.45	10.38	4.95
32	8.30	0.643	25.53	0.419	19.24	32.60	13.36	7.07
33	8.30	0.600	26.29	0.439	21.39	35.06	13.67	8.77
34	8.30	0.692	32.60	0.532	27.69	39.84	12.16	7.24
35	8.30	0.642	25.99	0.444	20.43	33.23	12.80	7.24

The data of SNR, CR, and CNR of fast FLAIR pulse sequence with TI 2300 msec (Continued).

No.	SD_{air}	$CR_{lesion,CSF}$	$CNR_{lesion,CSF}$	$CR_{lesion,WM}$	$CNR_{lesion,WM}$	SNR_{lesion}	SNR_{WM}	SNR_{CSF}
36	8.30	0.605	22.16	0.393	16.60	29.40	12.80	7.24
37	9.30	0.548	16.59	-	-	23.43	-	6.84
38	9.30	0.714	25.92	-	-	31.11	-	5.18
39	9.30	0.730	28.88	-	-	34.22	-	5.33
40	9.30	0.715	30.60	-	-	36.70	-	6.10
41	9.30	0.662	26.16	-	-	32.84	-	6.68
Mean		0.59	22.51	0.43	18.10	29.94	11.60	7.42
S.D		0.09	5.80	0.06	5.38	6.50	2.03	2.26
$S.D^2$		0.01	33.68	0.0036	28.92	42.21	4.14	5.10
C.V		15.6%	2580.0%	14.0%	29.7%	21.7%	17.5%	30.4%

The data of SNR, CR, and CNR of fast FLAIR pulse sequence with TI 2400 msec .

No.	SD_{air}	$CR_{lesion,CSF}$	$CNR_{lesion,CSF}$	$CR_{lesion,WM}$	$CNR_{lesion,WM}$	SNR_{lesion}	SNR_{WM}	SNR_{CSF}
1	8.80	0.352	13.34	0.411	14.92	25.63	10.70	12.28
2	8.80	0.374	14.85	0.430	16.41	27.31	10.90	12.45
3	7.50	0.529	24.85	0.505	24.12	35.93	11.81	11.08
4	7.40	0.484	21.28	0.455	20.41	32.62	12.22	11.34
5	8.60	0.311	11.20	0.377	12.93	23.63	10.70	12.43
6	8.60	0.486	21.44	0.522	22.48	32.77	10.29	11.33
7	9.50	0.539	17.87	0.374	13.88	25.52	11.63	7.64
8	9.50	0.354	11.28	0.467	13.75	21.59	7.84	10.31
9	9.50	0.422	13.92	0.356	12.31	23.45	11.15	9.54
10	9.50	0.404	14.78	0.493	16.95	25.66	8.72	10.88
11	8.00	0.506	20.29	0.423	17.95	30.18	12.23	9.89
12	8.00	0.520	21.00	0.447	18.96	30.68	11.71	9.68
13	8.00	0.345	15.66	0.452	18.99	30.51	11.53	14.85
14	9.60	0.613	21.45	0.505	18.94	28.21	9.27	6.76
15	9.60	0.417	9.88	0.235	6.39	16.79	10.41	6.92
16	7.40	0.363	21.84	0.477	26.49	41.03	14.54	19.19
17	7.90	0.431	26.00	0.402	24.75	43.16	18.42	17.16
18	8.40	0.667	27.51	0.435	20.85	34.39	13.55	6.88

The data of SNR, CR, and CNR of fast FLAIR pulse sequence with TI 2400 msec (Continued).

No.	SD_{air}	$CR_{lesion,CSF}$	$CNR_{lesion,CSF}$	$CR_{lesion,WM}$	$CNR_{lesion,WM}$	SNR_{lesion}	SNR_{WM}	SNR_{CSF}
19	8.40	0.553	25.08	0.443	21.61	35.21	13.61	10.13
20	8.50	0.485	16.48	0.415	14.80	25.22	10.42	8.74
21	8.50	0.567	19.66	0.529	18.80	27.16	8.36	7.51
22	8.60	0.549	17.76	0.302	11.60	25.05	13.44	7.29
23	8.60	0.577	27.38	0.553	26.64	37.42	10.78	10.03
24	8.60	0.566	26.13	0.443	22.20	36.16	13.97	10.03
25	8.60	0.556	27.99	0.486	25.60	39.16	13.56	11.17
26	8.60	0.546	27.42	0.500	25.88	38.80	12.92	11.38
27	7.70	0.540	23.74	0.485	22.13	33.87	11.74	10.13
28	7.50	0.435	12.68	0.380	11.52	20.92	9.40	8.24
29	7.50	0.416	12.73	0.351	11.24	21.65	10.41	8.92
30	8.80	0.469	17.05	0.437	16.22	26.68	10.47	9.64
31	8.80	0.543	19.65	0.444	17.17	27.92	10.75	8.27
32	8.30	0.572	27.48	0.491	24.87	37.75	12.88	10.27
33	8.30	0.513	25.63	0.436	22.95	37.77	14.82	12.14
34	8.30	0.574	29.40	0.526	27.81	40.31	12.51	10.92
35	8.30	0.526	24.23	0.452	21.88	35.14	13.27	10.92
36	8.30	0.444	17.43	0.362	15.08	28.35	13.27	10.92

The data of SNR, CR, and CNR of fast FLAIR pulse sequence with TI 2400 msec (Continued).

No.	SD_{air}	$CR_{lesion,CSF}$	$CNR_{lesion,CSF}$	$CR_{lesion,WM}$	$CNR_{lesion,WM}$	SNR_{lesion}	SNR_{WM}	SNR_{CSF}
37	8.50	0.509	17.52	-	-	25.98	-	8.46
38	8.90	0.503	21.73	-	-	32.48	-	10.75
39	8.90	0.653	30.39	-	-	38.47	-	8.08
40	8.90	0.569	29.96	-	-	41.31	-	11.36
41	8.90	0.579	28.22	-	-	38.49	-	10.27
Mean		0.50	20.83	0.44	18.87	31.23	11.78	10.39
S.D		0.09	5.87	0.07	5.30	6.65	2.07	2.51
$S.D^2$		0.01	34.50	0.00	28.07	44.24	4.28	6.32
C.V		17.4%	28.2%	15.3%	28.1%	21.3%	17.5%	24.2%

APPENDIX F

THE DATA OF SNR, CR, AND CNR FOR T_2-WEIGHTED FSE PULSE SEQUENCE.

The data of SNR of individual type tissue , CR, and CNR between lesions to CSF and white matter for T_2-weighted FSE pulse sequence.

No.	SD_{air}	SNR_{lesion}	SNR_{WM}	SNR_{CSF}	SNR_{lesion}	SNR_{WM}	SNR_{CSF}	$CNR_{lesion,csf}$	$CR_{lesion,CSF}$	$CNR_{lesion,wm}$	$CR_{lesion,WM}$
1	8.0	*51.7*	*21.2*	*96.7*	34.442	14.150	64.450	30.008	0.303	20.292	0.418
2	8.0	*44.7*	*21.4*	*97.8*	29.767	14.267	65.225	35.458	0.373	15.500	0.352
3	7.6	*61.2*	*22.7*	*105.7*	40.798	15.132	70.456	29.658	0.267	25.667	0.459
4	7.5	*57.7*	*24.8*	*96.7*	38.444	16.533	64.489	26.044	0.253	21.911	0.399
5	8.1	*46.2*	*21.7*	*103.8*	30.782	14.444	69.210	38.428	0.384	16.337	0.361
6	8.1	*58.6*	*21.5*	*102.0*	39.095	14.329	67.992	28.897	0.270	24.765	0.464
7	8.2	*47.6*	*20.3*	*85.5*	31.756	13.553	57.008	25.252	0.284	18.203	0.402
8	8.2	*51.7*	*21.0*	*83.1*	34.472	14.033	55.415	20.943	0.233	20.439	0.421
9	8.2	*46.7*	*20.2*	*81.5*	31.138	13.488	54.317	23.179	0.271	17.650	0.396
10	8.2	*48.7*	*23.2*	*85.2*	32.472	15.463	56.772	24.301	0.272	17.008	0.355
11	8.2	*48.8*	*20.0*	*90.8*	32.545	13.366	60.504	27.959	0.300	19.179	0.418
12	8.2	*62.4*	*23.0*	*89.2*	41.610	15.333	59.488	17.878	0.177	26.276	0.461

The data of SNR of individual type tissue , CR, and CNR between lesions to CSF and white matter for T_2-weighted FSE pulse sequence.

No.	SD_{air}	SNR_{lesion}	SNR_{WM}	SNR_{CSF}	SNR_{lesion}	SNR_{WM}	SNR_{CSF}	$CNR_{lesion,csf}$	$CR_{lesion,CSF}$	$CNR_{lesion,wm}$	$CR_{lesion,WM}$
13	8.2	*45.7*	*20.1*	*93.2*	30.488	13.390	62.106	31.618	0.341	17.098	0.390
14	9.4	*59.8*	*17.5*	*79.0*	39.894	11.652	52.681	12.787	0.138	28.241	0.548
15	9.4	*32.9*	*15.2*	*75.4*	21.950	10.142	50.270	28.319	0.392	11.809	0.368
16	7.7	*64.9*	*28.2*	*111.6*	43.238	18.779	74.433	31.195	0.265	24.459	0.394
17	8.7	*75.3*	*25.2*	*101.1*	50.230	16.797	67.402	17.172	0.146	33.433	0.499
18	7.7	*58.9*	*25.0*	*77.8*	39.255	16.649	51.853	12.597	0.138	22.606	0.404
19	7.7	*61.3*	*26.0*	*75.7*	40.866	17.342	50.459	9.593	0.105	23.524	0.404
20	7.5	*68.3*	*19.8*	*85.6*	45.564	13.173	57.084	11.520	0.112	32.391	0.551
21	7.5	*64.1*	*18.0*	*78.7*	42.729	11.973	52.436	9.707	0.102	30.756	0.562
22	8.1	*101.7*	*24.6*	*104.7*	67.770	16.428	69.819	2.049	0.015	51.342	0.610
23	8.1	*69.6*	*25.8*	*106.6*	46.420	17.177	71.086	24.667	0.210	29.243	0.460
24	8.1	*76.4*	*23.7*	*103.4*	50.947	15.802	68.963	18.016	0.150	35.144	0.527
25	8.1	*79.4*	*27.5*	*107.4*	52.963	18.354	71.572	18.609	0.149	34.609	0.485
26	8.1	*51.7*	*22.9*	*103.2*	34.444	15.292	68.774	34.329	0.333	19.152	0.385
27	8.1	*58.8*	*19.5*	*85.0*	39.185	12.979	56.658	17.473	0.182	26.206	0.502
28	6.4	*50.9*	*21.9*	*86.8*	33.927	14.625	57.875	23.948	0.261	19.302	0.398
29	6.4	*50.8*	*21.5*	*85.9*	33.854	14.365	57.292	23.438	0.257	19.490	0.404
30	8.5	*46.4*	*20.7*	*89.2*	30.949	13.780	59.459	28.510	0.315	17.169	0.384

The data of SNR of individual type tissue , CR, and CNR between lesions to CSF and white matter for T_2-weighted FSE pulse sequence.

No.	SD_{air}	*SNR lesion*	*SNR WM*	*SNR CSF*	SNR_{lesion}	SNR_{WM}	SNR_{CSF}	$CNR_{lesion,csf}$	$CR_{lesion,CSF}$	$CNR_{lesion,wm}$	$CR_{lesion,WM}$
31	8.5	*50.6*	*19.0*	*87.7*	33.757	12.667	58.478	24.722	0.268	21.090	0.454
32	10.8	*68.8*	*18.5*	*74.6*	45.883	12.352	49.765	3.883	0.041	33.531	0.576
33	10.8	*57.3*	*19.0*	*75.1*	38.173	12.673	50.068	11.895	0.135	25.500	0.502
34	10.8	*47.8*	*20.3*	*76.2*	31.846	13.525	50.827	18.981	0.230	18.321	0.404
35	10.8	*45.4*	*17.0*	*73.4*	30.253	11.364	48.951	18.698	0.236	18.889	0.454
36	10.8	*47.0*	*21.5*	*75.9*	31.321	14.352	50.617	19.296	0.235	16.969	0.372
37	7.5	*60.6*	-	*84.0*	40.373	-	55.991	15.618	0.162	-	-
38	8.5	*73.5*	-	*98.5*	48.996	-	65.647	16.651	0.145	-	-
39	8.5	*70.2*	-	*97.1*	46.831	-	64.761	17.929	0.161	-	-
40	8.5	*68.2*	-	*98.6*	45.459	-	65.718	20.259	0.182	-	-
41	8.5	*68.7*	-	*97.8*	45.796	-	65.184	19.388	0.175	-	-
			Mean		39.041	14.437	60.282	21.241	0.219	23.708	0.443
			S.D		8.431	1.967	7.413	8.258	0.090	7.697	0.068

Note. *SNR* is signal to noise ratio at 3 NEX, 256 x 256

SNR is signalto noise ratio at 1 NEX,256 x 192

BIOGRAPHY

NAME Captain Pathchraporn Saengruang-orn

DATE OF BIRTH 23 December 1966.

PLACE OF BIRTH Bangkok, Thailand

INSTITUTIONS ATTENDED

Mahidol University, 1985-1988.

Bachelor of Science

(Radiological technology)

Mahidol University, 1998-2000.

Master of Science (Medical Physics)

Position & OFFICE

1997-Present, MRI, Dept. of Radiology,

Royal Thai Army Hospital, Bangkok,

Thailand.

Position: MRI technician.